ULTRASONIC HEALING OF STRUCTURAL THERMOPLASTICS

by

Vincent Steffan Francischetti

A thesis submitted in partial fulfillment
of the requirements for the degree

of

Master of Science

in

Mechanical Engineering

MONTANA STATE UNIVERSITY
Bozeman, Montana

May 2011

©COPYRIGHT

by

Vincent Steffan Francischetti

2011

All Rights Reserved

APPROVAL

of a thesis submitted by

Vincent Steffan Francischetti

This thesis has been read by each member of the thesis committee and has been found to be satisfactory regarding content, English usage, format, citation, bibliographic style, and consistency and is ready for submission to The Graduate School.

Dr. Christopher H. Jenkins

Approved for the Department of Mechanical and Industrial Engineering

Dr. Christopher H. Jenkins

Approved for The Graduate School

Dr. Carl A. Fox

STATEMENT OF PERMISSION TO USE

In presenting this thesis in partial fulfillment of the requirements for a master's degree at Montana State University, I agree that the Library shall make it available to borrowers under rules of the Library.

If I have indicated my intention to copyright this thesis by including a copyright notice page, copying is allowable only for scholarly purposes, consistent with "fair use" as prescribed in the U.S. Copyright Law. Requests for permission for extended quotation from or reproduction of this thesis in whole or in parts may be granted only by the copyright holder.

Vincent Steffan Francischetti

May 2011

ACKNOWLEDGEMENTS

Thank you to my committee chair and advisor Dr. Christopher Jenkins whose tireless direction, guidance, and patience made this thesis a reality. Without his direction on research methods along with suggestions on experiments to run nothing would ever have gotten accomplished. Thank you to my committee members Dr. Stephen Sofie and Dr. David Miller for taking time to make comment and suggestions on how to improve this work. Thank you also to Matt Peterson and Donny Zignego, my research partners, who were there to offer advice and support whenever it was needed.

Thank you to my family who helped support me and encouraged me to keep pursuing my education, especially my Grandfather Vincent Francischetti Sr. who was the inspiration to keep going when the work seemed like it would never end. There were times when I was tired of school and wanted to slow down but he encouraged me to keep going because he wanted to see me get the degree. I would like to say a big thank you to my mother and father who were kind enough to help me out through a few extra years of school when they were ready to boot me out the door after the first degree. To all of my family I would like to say that I love you all and thank you for the support and encouragement that you always gave when I needed it most.

TABLE OF CONTENTES

1. INTRODUCTION 1

2. LITERATURE REVIEW 6

Healing in Nature 6

Self Healing Materials and Structures 9

Ultrasonic Damage Detection and Healing 12

Time Reversed Acoustics 16

Advanced Methods of Damage Detection 20

Ultrasonic waves (applications in Biology) 21

Ultrasonic Welding; Methods Relevant to Ultrasonic Self Healing 23

3. EXPERIMENTAL DESIGN 28

Summary of Experiments 28

Thermal Process Experiment 30

Nylon Tensile Test 38

Four Point Bend Configuration 42

Bending Apparatus Design: 42

T-slot Four Point Bend Design 44

Single Notch Four Point Bend Design 48

Short Single Notch Four Point Bend Design: 51

4. FINITE ELEMENT ANALYSES OF MECHANICAL TESTING 54

FEA Analysis of T-Slot Four Point Bend Specimens: 56

FEA Analysis of Mode-One Four Point Bend Specimens: 59

FEA Analysis of Mode-One Four Point Bend Specimens: 62

TABLE OF CONTENTS-CONTINUED

5. RESULTS OF TESTING 65

Results of Thermal Experiment 65

Tensile Specimen Results 76

Transition to Transverse Wave Propagation 82

Results of Four Point Bend Configuration 84

T-slot Four Point Bend Configuration 84

Results of Single Notch four Point Bend Specimens: 98

Results of Short Single Notch four Point Bend Specimens: 104

6. CONCLUSIONS 108

7. FUTURE WORK 112

REFERENCES CITED 113

APPENDICES 118

APPENDIX A: Ansys Input Files 1189

APPENDIX B: Braonson Power Level Calorimetry 11828

LIST OF TABLES

Table: Page

1: Summary of all experiments conducted and the purpose of each experiment for demonstrating healing. 29

2: Weight of components used to vary the contact pressure between the ultrasonic probe and the nylon specimen. No coupling was used besides contact pressure.....34

3: List of physical and acoustic properties of plastics used for testing as well as properties for other relevant materials needed for calculations.....37

4: Mechanical Properties of plastics used for ANSYS Finite Element Analysis.....55

5: Working temperature limits of plastics taken from various sources.....72

6: Comparison of damaged and ultrasonically healed Nylon dog bone tensile samples. The three specimens from each group with the highest strain to failure are chosen as a basis for comparison of average strain to failure between the two groups. F: Research/Nylon Damaged.....79

7: Summary of Rate and Temperature effects on PVC T-slot four point bend specimens.....86

8: Summary of sample maximum strain performance compared to the average maximum strain of the unhealed samples. 88

9: performance of Healed Cold temperature samples compared to average of unhealed samples. 91

10: Summary of performance of Single notch bend healed samples compared to average performance of unhealed samples. 101

11: Summary of performance of Short Single notch bend healed samples compared to average performance of unhealed samples. 106

12: Summary of ultrasonic power settings and percent increase in the mechanical performance of the healed specimens for each test. 109

LIST OF FIGURES

Figure: Page

1: Slit fracture in plastic piping caused by a stress rupture test. Ultrasonic damage detection could detect and mitigate similar damage before it becomes s a problem [5]. 2

2: Biological inspiration for ultrasonic damage healing. Shown are modeling, testing, and connectivity of experiments conducted to determine if ultrasonic healing is a viable damage repair method for thermoplastics.....4

3: Ultrasonic system detailing how all the processes of a healing system can be accomplished with the same wave field.....5

4: Stages of salamander limb regeneration. 6

5: Phases of wound healing in organisms [13]. 7

6: Wound Healing in two different strains of Hybrid Poplar trees. Slow re-growth from inside exhibited on the left, and quick healing and scabbing over exhibited on the right [14]. 8

7: Imbedded Healing Agents imbedded in Material Image from University of Illinois [17].....10

8: Hollow Fibers Containing Healing agent imbedded in composite, method pioneered by University of Bristol, I.P. Bond [19].....11

9: Amplitude change of sound wave due to an impedance difference between two materials [23]. 13

10: Diagram of reflection of ultrasonic energy upon encountering material boundaries or defects and oscilloscope display of detected surfaces[24]. (Note: transmitted energy not shown. 14

11: Pulse echo technique of ultrasonic testing [25] 16

12: Schematic of time reversed acoustic algorithm. A: initial pulse sent through media. B: reflection of initial pulse by target and propagation of reflected signal back through media where it is recorded by transducers. C: time reversed signal sent back through media converges back onto target. [29].....18

13: Schematic of time reversed acoustic system used for kidney stone ablation [26]. 19

LIST OF FIGURES-CONTINUED

Figure: Page

14: model of pelvis bone structure and ligaments that are modeled as spring mass systems for in vivo ultrasound testing of mechanical properties. Left: Front view or pelvis, Right: back view [33]. 22

15: Method of disrupting the blood brain barrier (BBB) with focused ultrasonic energy. A: intact BBB. B: temporary disruption of BBB with focused ultrasonic energy. C: Introduction of magnetic nanoparticles with chemotherapeutic agent [37].....23

16: Schematic of components of an ultrasonic welding system. Electrical energy is converted into a mechanical vibration by the transducer and amplified by the booster [43].....24

17: Amorphous (Left) vs. crystalline (Right) polymer structures; note the highly organized regions in the crystalline structure [45] 26

18: SEM image of two dissimilar plastics joined by vibratory welding. Left: looking down the direction of vibration (note the line near the top where the refractive index changes). Right, transverse to the direction of vibration (mixing of the two materials is evident) [46].....27

19: Solid works drawing of Imbedded Thermocouple location through the thickness of Sample specimen and ultrasonic probe location. Thermocouples are staggered with 1mm spacing down through the thickness of the sample. 32

20: Comparison of old ultrasonic probe stand and the new stand machined for more precise alignment between probe and specimen.....33

21: Picture of the Nylon dog bone sample with thermocouples imbedded and ultrasonic probe applied.....35

22: Conductive thermal analysis configuration. Bottom side of specimen is in direct contact with the aluminum holder which is considered a large heat sink.....36

23: Convective thermal analysis configuration. Quarter inch spacers are inserted between the bottom of the sample and the aluminum holder exposing the bottom of the sample to a boundary of air.....37

24: Dog Bone sample with razor damage on edge used for initial testing [21].....39

LIST OF FIGURES-CONTINUED

Figure: Page

25: Orientation of ultrasonic probe on tensile dog bone specimens. 40

26: Four point bend apparatus in Instron 5882 frame. The bottom supports can be moved in an array of holes in the base plate to change the support span. 43

27: Diagram of the initial four point bend specimens. Note the "T-slot" machined into the sample has razor cuts at both ends. The razor cut is aligned with the outer most wall of the band saw cut so the bending strain can be maximized. 45

28: Application of ultrasonic energy to the four point bend "T-slot" sample. The probe is slowly moved across the width of the entire sample above either one or both of the razor cuts. 47

29: Single notch four point bend specimen with crack orientated to take advantage of maximum principle stress direction so that the crack will propagate easier. 49

30: Application of ultrasonic energy to the four point bend "single notch bend" sample. The probe is slowly moved across the width of the entire sample above razor cut.....50

31: Short single notch bending specimen designed to allow failure within the limits of the bending apparatus. The sample is half the length of the previous single notch bend sample. 53

32: Finite Element analyses of Von Mises stress concentrations in T-slot bending specimens. The picture is zoomed in on the end of the band saw slot. The obvious concentration is the crack tip, but the corner of the band saw slot is only 20% less stress.....56

33: Stress distribution with singularity at the crack tip removed. Not that the highest stress concentration is shifted toward the.....58

34: Stress field ahead of the crack tip in the single notch four point bend specimen calculated at 44.5mm displacement. This stress field is calculated using classical LEFM stress intensity functions built into ANSYS. 60

LIST OF FIGURES-CONTINUED

Figure: Page

35: Stress field of healed single notch bending specimen at 50.8 mm displacement. Notice that the stress is transferred away from the crack tip and is supported by the ligament of material. 61

36: Stress distribution in short single notch bend specimen. Displacement is 6.53 mm which is the average displacement to failure of the damaged samples. 63

37: Temperature distribution through the thickness of a nylon sample with conductive back surface. 66

38: Temperature profile through the thickness of a nylon dog bone specimen with a convective back surface. 68

39: Temperature distribution in a nylon dog bone specimen with a 0.847Kg weight added to the ultrasonic probe to increase the contact pressure between the probe and the specimen. The bottom surface of the dog bone is subjected to a conductive boundary condition because it is in contact with the aluminum holder. 71

40: Temperature distribution in a nylon dog bone specimen a contact pressure of 480 kPa. Again, the bottom surface of the dog bone is subjected to a conductive boundary condition. 73

41: Temperature distribution in a nylon dog bone specimen with a 1.25 Kg weight added to the ultrasonic probe to increase the contact pressure between the probe and the specimen. The bottom surface of the dog bone is subjected to a convective boundary condition because it is suspended above the aluminum holder. 75

42: Results of tensile test specimens Two of the ultrasonically treated samples failed early, but the remainder of the ultrasonically treated samples outperformed the damaged samples (from F:Research/Nylon Damaged). 78

43: Failure surface of tensile specimens. Left: Untreated specimen, note the razor ct on the left side of the specimen and the plastic failure zone which is the white region. Right: Ultrasonically healed sample, note the large ductile fracture zone compared to the unhealed sample. 81

LIST OF FIGURES-CONTINUED

Figure: Page

44: Side of initial Nylon transverse ultrasonic wave specimen. Left: Crack tip before ultrasonic treatment. Right: crack after ultrasonic treatment, note that the crack is closed and it appears some material may have melted and bridged the sample. Picture at 200X magnification. 83

45: Front of initial Nylon transverse ultrasonic wave specimen. Left: Crack tip before ultrasonic treatment. Right: crack after ultrasonic treatment; note that the crack is closed no apparent flashing due to melted material has exited the razor crack. 50X magnification 84

46: Load displacement curves for PVC T-Slot samples. The ultimate load and thus the stress in the samples increases as the displacement rate increases and the temperature decreases. 85

47: Cold Temperature trials of PVC. Solid lines Indicate damaged but unhealed samples. Dotted lines are samples with healing on only one side at power levels 4 and 5(160W and 200W respectively). Dashed Lines are samples with healing on both sides at power levels 4 and 5. 87

48: Cold temperature performance of samples treated at high power level settings. Samples with two numbers after the name indicate the two power settings used, one on each of the damage locations. 90

49: Damage caused by ultrasonic probe operating at various power levels. Left: Power Level 4 (160 W) generally localized damage not always over crack location. Right: Power Level 8 (320 W), higher power settings cause more wide spread damage. 92

50: Failure surfaces of low power treatment. Left: power level 4 (160 W), notice that the sample failed at the razor cut which is the flat surface at the bottom of the sample. Right: power level 5 (200 W), also failed at the razor cut location although it is difficult to tell because of the way the failure surface is angled. 93

51: Failure surfaces of high power treatment. Left: power level 6 (240 W), notice that the sample failed at the razor cut which is the flat surface at the bottom of the sample. Right: power level 9 (360 W), did not fail at the razor cut; there may is likely some amount of healing that occurred at the crack tip. 94

LIST OF FIGURES-CONTINUED

Figure: Page

52: Failure surfaces of PL9R1(360 W). Left: original failure side, notice the ductile failure zone above the razor cut, the failure does not start at the razor. Right, secondary failure side cause by brittleness of material. Notice that the secondary failure does not follow the razor cut the whole way across. 95

53: SEM images of an unhealed specimen. Notice the clearly defined crack with a sharp tip. 96

54: Ultrasonically healed PVC specimen treated with power level 9 (360 W). notice that the crack tip appears to be blunted slightly. The 3000x image (bottom) shows a slightly rounded tip when compared to the unhealed images. 97

55: Single notch bend sample test results. Solid lines are virgin specimens with no damage. Dashed lines are damaged samples. Dotted lines are ultrasonically healed samples. The majority of healed samples outperformed the damaged samples 100

56: Failure surfaces of polycarbonate specimens. Left: Unhealed specimen with clean razor cut on the top of the sample. Right: Ultrasonically healed specimen, where the razor cut is no longer clean because the material has melted. and bridged the damaged section. 103

57: Bend Test results of Short Single notch bend samples. Solid line represents virgin specimens with no damage. Dashed lines are damaged samples with 1.27 mm razor cut in beam. Dotted lines are ultrasonically healed samples. 105

LIST OF EQUATIONS

Equation: Page

1: Attenuation of a plane wave in a dissipative material 12

2: Portion of ultrasonic energy reflected at material interface.....14

3: Fourier transformation from spatial domain to frequency domain.....17

4: ASTM equation for calculating displacement rate for four point bend testing with an apparatus with the load span one third the support span.....44

5: Trapezoidal rule for numerical integration of discrete data sets.....79

ABSTRACT

This thesis is a preliminary investigation into the effectiveness of ultrasonic damage healing in thermoplastic materials. The work was based on the proposition that ultrasonics can form the basis of a damage detection and healing system that draws inspiration from the systems-level approach to wound healing seen in living organisms. Ultrasonic inspection has been well established as a method of nondestructive damage location. Testing includes tensile testing and investigation of the temperature distribution in specimens in response to ultrasonic energy input. Additionally, bending tests following the guidelines of ASTM 6272-02, to investigate healing were performed. Healing with ultrasonics is realized through focusing ultrasonic energy into the damage site, which results in a thermal process that occurs in the vicinity of the damaged area. Healing was defined as an increase in the mechanical performance of the healed specimens over the unhealed samples.

Tensile specimens exhibited a 9% increase in displacement to failure. T-slot bending specimens used to investigate cross crack wave propagation showed that high power treated samples were able to withstand up to 14% more displacement than the unhealed samples. The preliminary “single notch bend” samples showed a minimum of 12% increase in displacement to failure but the bending apparatus geometry limited complete investigation. Further investigation into single notch bend samples using short specimens showed an increase in displacement of over 30%. Microscopic inspection revealed that ultrasonic treatment causes melting. The melted material bridges the crack opening which transfers stress away from the crack tip. Microscopic evidence does not suggest that crack blunting is a prevalent form of damage healing.

Ultrasonic energy is shown to be a viable energy source for both damage detection and healing. The process still needs refinement, but even with limited material and equipment an approximate increase in displacement to failure of 30% and an increase in fracture energy of over 70% are demonstrated. Future testing can use the information about healing gleaned from this thesis in a time reversed acoustics system to heal remotely deployed structures on satellites or other equipment that cannot easily be repaired.

1. INTRODUCTION

The goal of this work was to investigate the effectiveness of ultrasonic energy for healing polymer structures. This work draws inspiration from healing mechanisms that occur in nature. By and large, all healing in nature is associated with generation of new material. Material generation, one way or the other, requires external energy input. Hence, healing in nature is an active process, one that can be intrinsic (autonomous) or conscious (semi-autonomous).

Ultrasonic damage detection is a well established field with many techniques for sub-surface damage detection near the ultrasonic transducer. There are currently many researchers investigating advanced techniques for structural health monitoring over large areas such as plates [1, 2] with the idea being to be able to monitor large structures such as aircraft structural wing spars, wing surfaces, or wind turbine blades. Time reversed acoustics has the potential to automatically steer ultrasonic energy back into the damage location regardless of whether the material is very homogeneous or highly dispersive [3]. If the material is a thermoplastic or other material that can be melted at a relatively low temperature, ultrasonic energy can be steered into the damage location and locally melt the plate to facilitate healing. This time reversed healing scheme draws on the biological idea of organisms being able to self-monitor and transport healing agents from remote parts of the body to heal the damaged area. Healing in this thesis is defined as an increase in mechanical performance of samples which is determined by an increase in displacement to failure and fracture energy of the samples.

The financial savings from development of a time reversed acoustic healing system could be potentially very large. It could be possible to treat a small area of a structural component and restore the strength and integrity of the system instead of having to replace an entire large structural component. There is no way to put an exact number on the potential financial savings but the U.S. Department of Commerce, which published a report in 1983 that places the economic cost of replacing failed components and the cost of repairs for the United States annually at around $119 billion dollars, which was 4% of the gross national product [4]. If even a small fraction of the components made of thermoplastics could benefit from the development of such a system the savings would be significant.

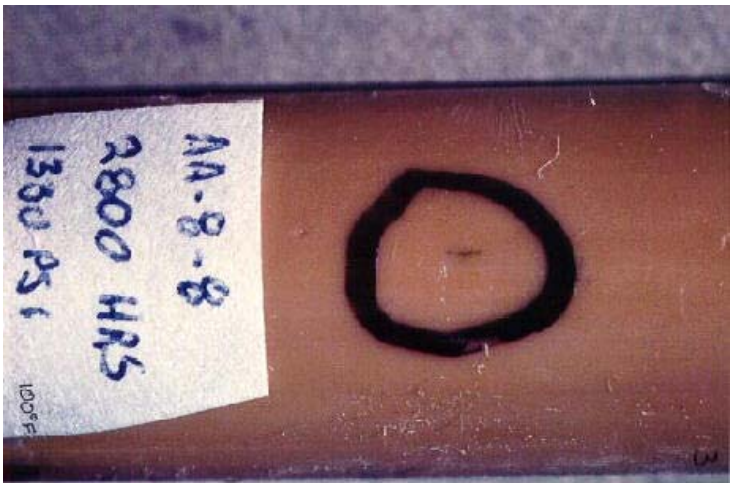

Figure 1: Slit fracture in plastic piping caused by a stress rupture test. Ultrasonic damage detection could detect and mitigate similar damage before it becomes s a problem [5].

Some examples of where the ultrasonic healing system could be deployed to monitor the structural integrity of critical components could include satellites or rovers deployed to remote locations where sending a person to perform repairs would be

prohibitively expensive or impossible. More and more, components of automobiles, aircraft and spacecraft are being made of either thermoplastic materials or carbon fiber reinforced plastics (CFRP), both of which could benefit from the damage detection and healing possibilities of ultrasonic systems.

This thesis is a preliminary investigation into the effectiveness of ultrasonic damage healing in thermoplastic materials. Testing includes tensile testing and investigation of the temperature distribution in the tensile specimens in response to ultrasonic energy input to determine if sufficient heating is caused by the ultrasonic energy. Additionally, bending test specimens were designed to further investigate modes of healing such as cross crack wave propagation and crack tip blunting as well as melting of the crack surfaces back together. Healing was determined by an increase in the mechanical performance of the healed specimens over the unhealed samples. Finite Element Analyses (FEA) will be utilized to guide decisions about sample geometry and damage placement and orientation in the bending specimens. Additionally, FEA was used to investigate possible modes of healing that are seen in some of the samples. **Figure 2** shows the biological inspiration for development of the ultrasonic healing system, and the relatedness of the experiments conducted to demonstrate the healing potential of the system.

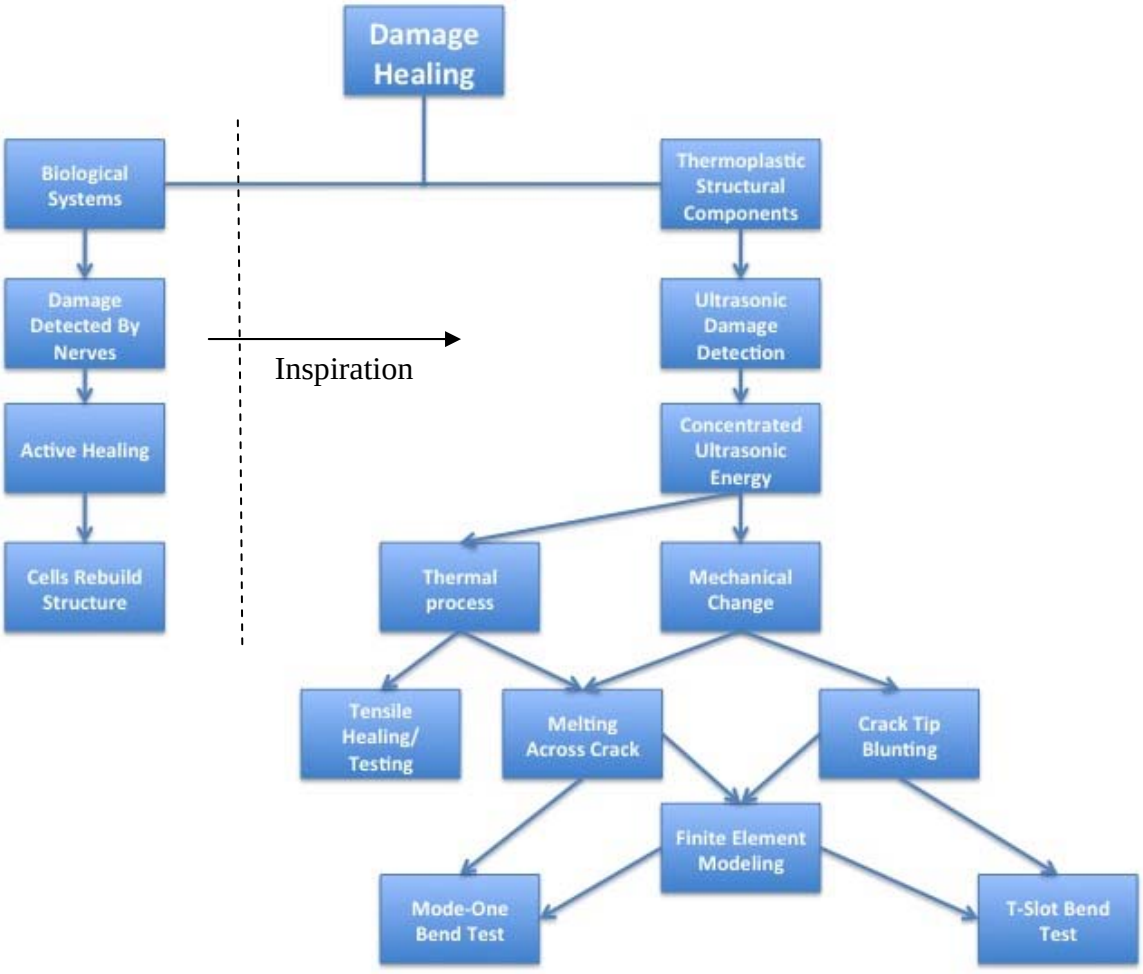

Figure 2: Biological inspiration for ultrasonic damage healing. Shown are modeling, testing, and connectivity of experiments conducted to determine if ultrasonic healing is a viable damage repair method for thermoplastics.

The ultimate goal of this research is to demonstrate that ultrasonic energy is a viable method of healing damage in thermoplastic materials, and hopefully the research will lead to the development of full damage detection and healing ultrasonic systems that can be integrated into structural components deployed on remote structures. The development of a time reversed acoustic system that could monitor a structural component for damage and, if damage is detected, be able to focus ultrasonic energy into

the damage site thereby healing the damage through a localized thermal process is the end game of this research. **Figure 3** shows a schematic of how the ultrasonic energy can be used for multiple purposes.

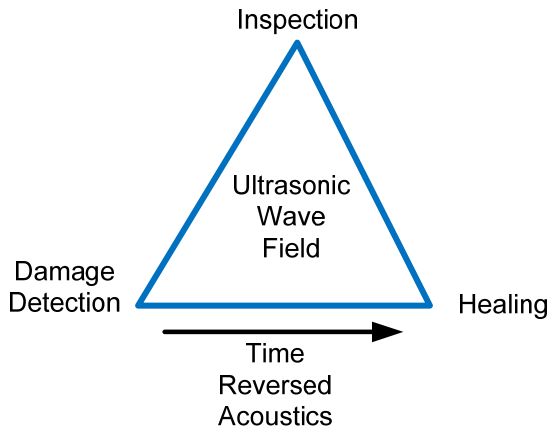

Figure 3: Ultrasonic system detailing how all the processes of a healing system can be accomplished with the same wave field.

The ultrasonic damage detection and healing system uses a systems level approach that mirrors the self healing approach done in nature. Using damage detection and healing system that uses the same wave field would save weight in satellites or other structures where weight is a major concern. Piezoelectric transducers cold be adhered to the edges of a structural components and be controlled by a central computer processor that contains the time reversed acoustic algorithm. Development and integration of the full system would take several more years of research and development, so this work simply aims to demonstrate that ultrasonic energy is a viable wave form for the eventual development of the system.

2. LITERATURE REVIEW

Healing in Nature

Nature has developed a healing mechanism for organisms ranging in complexity from an amoeba [6], to lizards and starfish which are able to regenerate entire appendages [7]. Nature's most advanced organisms, including humans and other mammals, are able to utilize large vascular networks and bring in platelets from other parts of the body to help combat wounds but generally lack the ability to regenerate entire limbs [8]. Self-healing in biological systems is almost always an active system level process where the organism's body detects damage and routs healing agents to the damaged area.

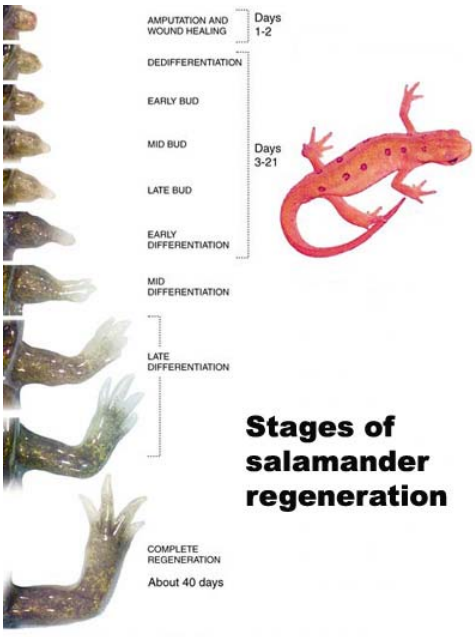

Figure 4: Stages of salamander limb regeneration.

There seems to be an inverse relationship between ability to heal large sections of an organism and the biological complexity of the organism. Newts have the ability to re-grow appendages multiple times if amputations of a limb occur. This ability is possible because the specialized muscle and bone cells are able to "de-differentiate" back to a mass of stem cells which regenerate the limb [9]. Teleost zebra fish are able to regenerate large amounts of cardiac muscle when damage occurs[10].

Four stages of biological healing are: *hemostasis*, which is the stopping of a flow of blood; *inflammation*, where the body swells due to increased blood flow to an area necessary to transport immune system components to a wound site [11]; *proliferation*, the formation of new cells in the wound area; and *remodeling* the organization of new cells in the wound area into the structure that preceded the wound event [12]. **Figure 5** shows a time scale of the healing processes that occur in response to damage.

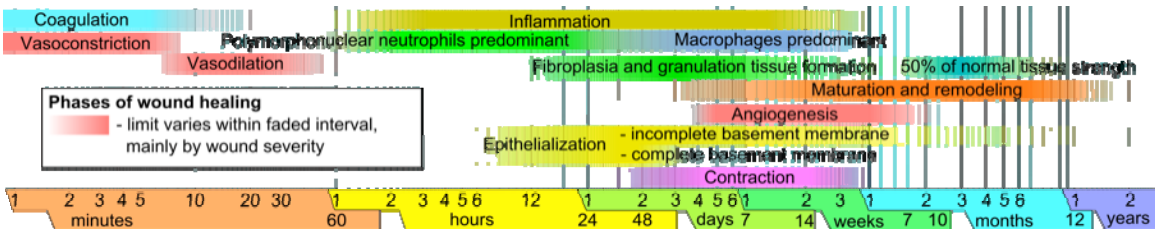

Figure 5: Phases of wound healing in organisms [13].

The three predominant modes of healing found in nature are *contraction*, which commonly occurs in an amputation scenario [12]; *epithelialization*, is the process of healing by scabbing and covering the wound with a new layer of material; and *connective tissue deposition*, which occurs when a deep wound is stitched closed. Healing may use one or a combination of all three of the processed described above. All these processes

are characterized by external energy being required in order to facilitate the healing process.

When a tree is damaged, sap will flow into the wound area forming a type of scab that will harden and protect the tree from further damage or infection at the site; this is an example of healing by the process of epithelialization. It could be argued that the sap flowing into the wound area is due to gravity and there solely a passive process, but a study conducted by the United States Forest Service examined several different strains of hybrid poplar trees and found different forms of healing [14]. Some species of trees never closed the wound and instead healed from slowly from the inside by walling off the wound from the rest of the tree. Other species closed over the hole quickly and exhibited quick re-growth of material indicating active wound healing mechanisms more substantial than gravitational flow of sap.

Figure 6: Wound Healing in two different strains of Hybrid Poplar trees. Slow re-growth from inside exhibited on the left, and quick healing and scabbing over exhibited on the right [14].

Self Healing Materials and Structures

Many structural self-healing materials have been developed which heal by passive processes. Passive processes are characterized by all the healing elements being located within a structure ready to be deployed when damage occurs. No external energy is required to deploy the healing agents other than the damage event itself. This design works well but it requires healing cells to be located throughout the structure, which is fine in bulk polymeric material but has the possibility of significantly changing the strength and mechanical response of a composite structure.

There are currently two main paradigms for passive structural self-healing. The first is to use imbedded micro-spheres distributed throughout an epoxy resin. The spheres contain a catalyst to stimulate additional bonding when the micro spheres are broken by damage propagating through their casing [15] (see **Figure 7**). The microspheres are reported to increase the toughness of the epoxy, but one potential problem is that material property characterization will need to be done for each different epoxy, capsule size, and capsule volume fraction combination. This process can be extremely time consuming and costly. Additionally, healing efficiency decreases with the number of times damage occurs in an area; with a maximum of three to five healing cycles possible [16]. Finally, if the spheres are attached at the fiber matrix interface of the composite in effect a void is formed that has significant consequences for composite performance.

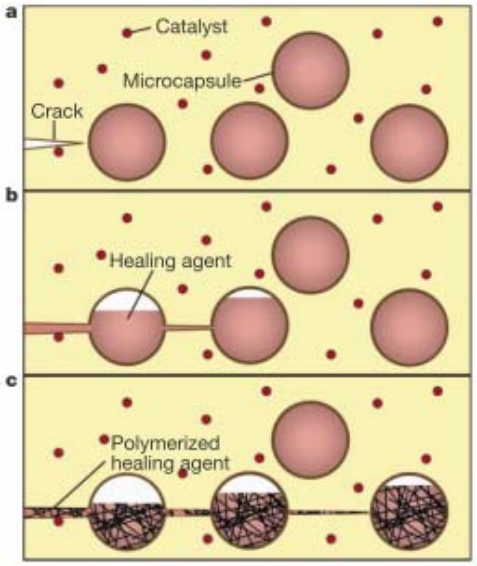

Figure 7: Imbedded Healing Agents imbedded in Material Image from University of Illinois [17].

The second main paradigm draws inspiration from vascular networks found in all complex organisms. The idea is being pioneered by researchers at the University of Bristol. Both glass fiber reinforced polymers (GFRP) and carbon fiber reinforced polymers (CFRP) permeated with hollow glass fibers containing healing agents, see **Figure 8**, have been shown to be viable self healing composite structures with the ability to recover approximately 90% of undamaged strength with a slightly higher standard deviation [18]. Recent studies regarding implementing simple vascular networks inspired by hard woods in carbon fiber composites without adversely effecting weight and material performance have shown promise and investigation is ongoing [19].

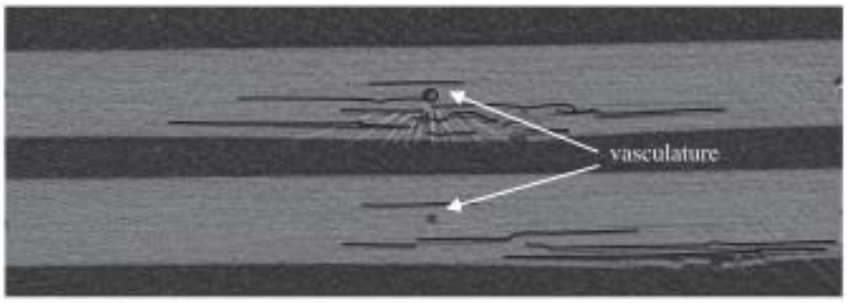

Figure 8: Hollow Fibers Containing Healing agent imbedded in composite, method pioneered by University of Bristol, I.P. Bond [19]

There are a few forms of structural healing that can be classified as active healing, because it is necessary for the structure to realize that there is damage then perform a response to the damage. Researchers at the University of Pittsburgh and the University of Massachusetts have drawn inspiration from white blood cells moving throughout the body to heal wounds to develop a system of flowing hydrophobic micro spheres filled with nano-particles over a body with surface damage. The spheres find the cracks which are also hydrophobic and release the nano-particles by entropy forces to fill the crack and heal the material [20].

At Montana State University, a healing concept is being investigated using ultrasonic energy to both detect and heal damage in a polymeric material. Ultrasonic energy will be concentrated at the damage site in order to locally heat the material in the vicinity of the damage to heal the material. This concept utilizes the healing schemes of connective tissue deposition and epithelialization defined earlier in this chapter, when the polymer is heated to the point where it can begin to viscously flow, intermolecular diffusion of polymer chains can occur to facilitate some amount of crack closing. Cody

Sarrazin performed initial research and modeling of these phenomena in his Master's thesis published in 2009 [21].

Ultrasonic Damage Detection and Healing

The field of nondestructive testing (NDT) has used ultrasonic waves to detect subsurface damage for a long time. The waves emitted from an ultrasonic transducer will propagate by vibratory motion of many particles in unison causing a mechanical wave [22]. There are several different modes of propagation but the two simplest wave forms are longitudinal waves, where the particle motion is in the direction of the strain wave, and shear waves, which occur when the particle motion is transverse to the direction of wave propagation.

Mechanical waves will propagate largely unhindered through a material with no flaws other than the attenuation caused by the natural damping of the material, where the strain energy of the ultrasonic wave is converted into various other forms of energy such as heat and sound. The attenuation of a plane wave can be described by a decaying exponential shown below in **(1** [23]. In **(1** A_0 is the original strain wave amplitude, α is the experimentally obtained attenuation coefficient, and x is the distance that the wave has traveled from the transducer.

$$A = A_0 e^{-\propto x} \tag{1}$$

When an internal flaw or change in material is encountered by the ultrasonic wave the impedance difference between the two materials reflects a portion of the wave back to the transducer. The acoustic impedance of a material is simply calculated by the product of the density of the material and the speed of sound in the material. A wave that experiences an acoustic impedance change because of a change in material will undergo a change in the amplitude of the wave that propagates into the second material as seen in **Figure 9**.

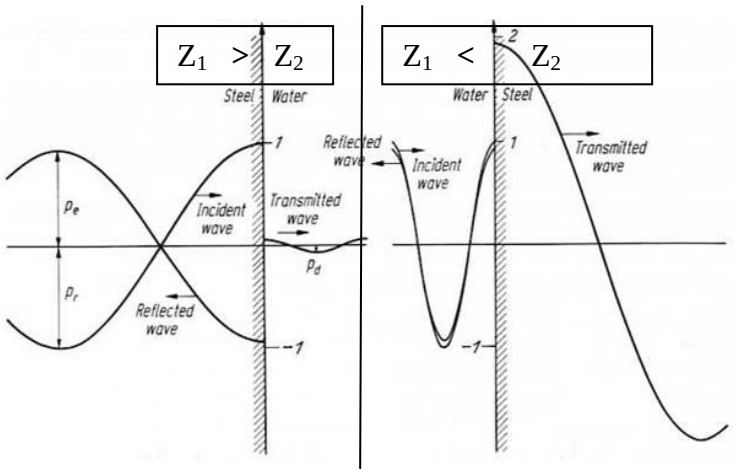

Figure 9: Amplitude change of sound wave due to an impedance difference between two materials [23].

Additionally, the portion of the energy reflected and transmitted is determined by the change in impedance. **(2** describes the fraction of incident wave intensity that is reflected back from a material interface where the materials have different acoustic impedances where Z_1 and Z_2 are the

acoustic impedances of the initial material and the material into which the ultrasonic wave is moving respectively [23].

$$R = \left(\frac{Z_2 - Z_1}{Z_2 + Z_1}\right)^2 \quad (2)$$

The simplest setup for an ultrasonic damage detection system is a single transducer pulse-echo technique which can be implemented using an oscilloscope and a piezoelectric transducer as seen in **Figure 10**. The transducer first pings the material when a voltage is applied to the piezoelectric material causing the transducer to undergo a strain that is imparted to the material. The wave then propagates through the material until it either hits the back surface of the material or it encounters an internal flaw. The internal flaw will show up sooner on the time scale than the back surface of the material because the wave has to travel less distance to the crack and back than to the back surface of the material.

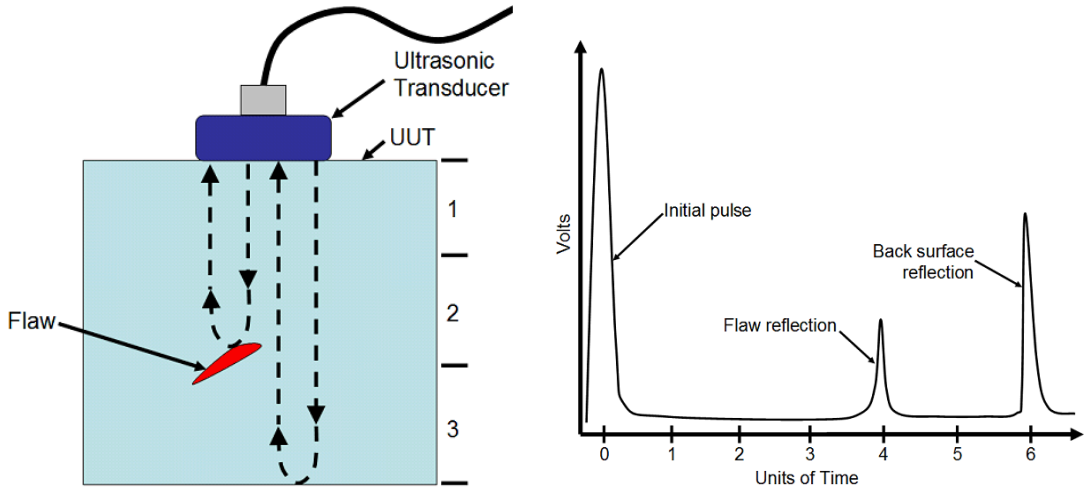

Figure 10: Diagram of reflection of ultrasonic energy upon encountering material boundaries or defects and oscilloscope display of detected surfaces[24]. (Note: transmitted energy not shown.

The frequency of an ultrasonic transducer is an important factor in ultrasonic NDT because it determines the wavelength of the strain wave and thus determines the size of the defect that can be detected. It is recommended that the wave length be at least half of the size of the expected flaw [22]. Frequency also affects the speed of wave propagation in the material which can affect the spatial resolution of detecting two separate cracks that are close together. Higher frequencies will allow the detection of smaller cracks but there will also be more attenuation and noise due to scattering of the wave [25].

There are many more sophisticated schemes that utilize multiple transducers such as the through transmission technique and the pitch catch scheme that is shown in **Figure 11**. In the pitch-catch technique, the ultrasonic wave is sent into the material on an angle which converts part of the wave into a shear wave that vibrates the material molecules transversely to the direction of wave propagation. The angle of reflectance is equal to the angle of incidence as described by Snell's law. The pitch catch method is useful for non linear parallel-sided geometries, where it is not practical to have a transducer on the inside of the test specimen [25].

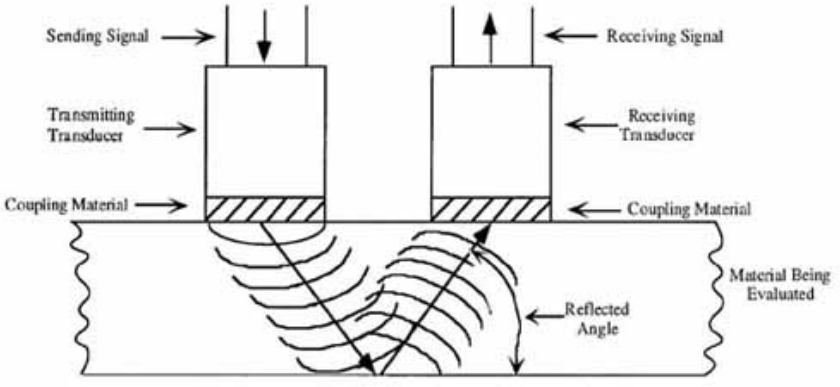

Figure 11: Pulse echo technique of ultrasonic testing [25]

The ultrasonic damage detection techniques discussed thus far are useful for detecting damage over a limited range from the transducer. In order to detect damage further from the transducer over large structural components, different forms of waves with much lower attenuation coefficients must be examined. Wave forms with low attenuation coefficients are generally complex combinations of shear and longitudinal waves that have a coupling property that allows the wave to propagate further into the material with sufficient strength to detect damage.

Time Reversed Acoustics

Time reversed acoustics is a very important field in both damage detection and target destruction in biomedical applications. It is based on the principle that if a sound wave propagating forward from a source is a solution to the wave equation, then a wave propagating in the reverse direction beginning with a complex wave state and converging back to the source of the forward propagating wave is also a solution to the wave equation [26]. This is known as the invariance of the wave equation during time reversal

or reversal invariance. Methias Fink of Université Denis Diderot in Paris France is one of the leading figures in the field of time reversed acoustics [27].

The reversibility of time waves is only strictly true for non dissipative media, but if the loss coefficient is small over the frequency of waves used for ultrasonic testing then the reversal invariance is roughly preserved [3]. The idea is similar to Fourier transformations in optics where an image in the spatial domain can be transformed to the frequency domain by an infinite summation over the frequencies of light or sound that compose the object[28] as seen in **(3**.

$$f(\omega) = \frac{1}{\sqrt{2\pi}} \int_{-\infty}^{+\infty} f(x) e^{-i\omega x} dx \quad (3)$$

It is not computationally efficient or practical to carry all of the frequencies in the calculations, so after a certain point, a sufficient representation of the object can be recreated using a finite number of frequencies. Dropping the high order frequencies in the Fourier transformation will result in losing very little information, and when the image is reconstructed the vast majority of the image will be preserved, but the sharp lines will be slightly blurred because the high frequency information that allows the construction of sharp edges has been dropped. The effect of a dissipative medium on time reversed acoustics is to create a convergence point of the time reversed wave of finite size (no longer a point source)[26].

The time reversal process is quite simple to understand and would not be overly complicated to implement with a computer program that is able to perform simple signal manipulation. The first step of the process is for an array of transducers to send a signal

into the test media. The pulse propagates through the media until it encounters an acoustically reflective target. The target then reflects the sound wave back through the media where it is recorded by the transducers. A computer program is then used to select the portion of the recorded signal that was from the reflective target and reverse the signal in time where the beginning of the recorded signal becomes the end of the signal. The reversed signal is then emitted by the transducers and propagates back through the sample and converges on the reflective target. A schematic of the time reversal process is shown in **Figure 12.**

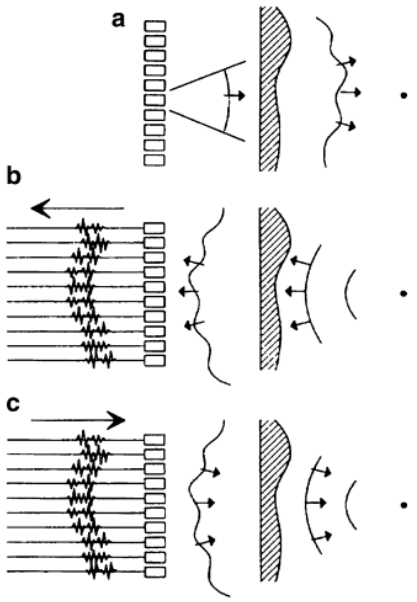

Figure 12: Schematic of time reversed acoustic algorithm. A: initial pulse sent through media. B: reflection of initial pulse by target and propagation of reflected signal back through media where it is recorded by transducers. C: time reversed signal sent back through media converges back onto target. [29]

One of the benefits of time reversed acoustics is that the process can be repeated several times with each iteration improving the amount of acoustic energy focused onto

the target area. The ultrasonic energy can be steered to converge onto any acoustically reflective target in the sample by selecting the portion of the return signal that corresponds to the desired target. When the ultrasonic energy from each of the transducers arrives at the damage site, the waves interfere constructively and large mechanical strains are generated [29] in the sample which can allow for heating of target areas for healing of damage in plastics or even for mechanical destruction of targets such as kidney stones in patients see **Figure 13**.

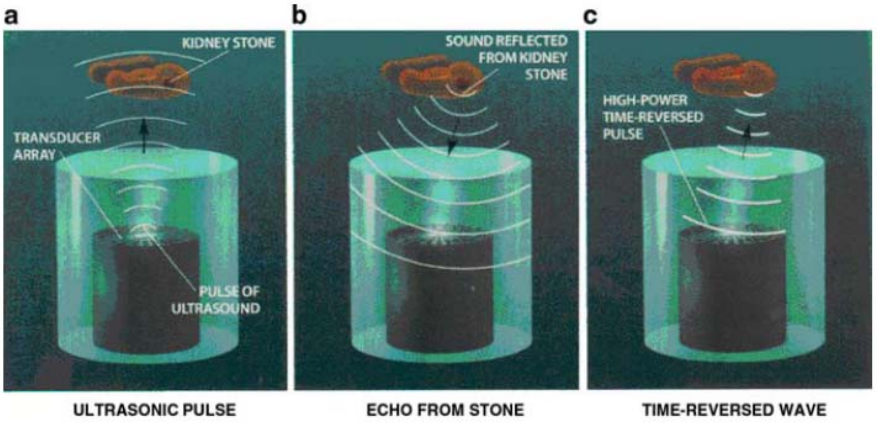

Figure 13: Schematic of time reversed acoustic system used for kidney stone ablation [26].

Ultrasonic energy can be locked onto the kidney stone and can be kept on target even while the target is moving due to patient breathing because of the auto focusing aspect of time reversed acoustics[26]. Additionally, because the speed of sound is high in biological material, the time reversal algorithm can be performed several hundred times a second so that the ultrasonic energy can remain locked onto the target and destruction of surrounding tissues can be avoided.

Advanced Methods of Damage Detection

One wave form that has been of interest for structural health monitoring of thin plates is the Lamb wave, which is generated by a coupling of the shear and longitudinal waves reflected at the upper and lower boundaries of the plate [30]. The Lamb wave is ideal because of its low attenuation coefficient allows it to effectively monitor large plate like structures such as the wings of an aircraft. Lamb waves are difficult to use because they have multiple dispersive modes and high wave speeds. Additionally the baseline signal used for damage detection will be modified throughout the life of the plate by thermal and mechanical loads which affect how the strain wave propagates [31].

Researchers at the Indian Institute of Technology Mumbai India propose the use of a time reversal process with Lamb waves for structural health monitoring to eliminate the need for a baseline signal, because when damage occurs the time reversibility property is no longer preserved, the input wave and the returned time reversed signal will be significantly different [1]. After careful selection of the excitation frequencies, pulse shape (modulated sine wave), and Lamb wave modes, they were able to detect the presence of a penny glued to the surface and a 3mm hole drilled in an isotropic plate of aluminum at several distances between the transducers.

Armen Sarvazyan and colleagues showed that it is possible to have a high degree of spatial convergence using relatively few piezoelectric transducers and a time reversed acoustics process to create a virtual phased array [32]. Sarvazyan demonstrated that with time reversed acoustics a time reversed acoustic array with four transducers was able to

have nearly the same spatial convergence as a phased array with the same effective area but having 128 channels.

Ultrasonic Waves (Applications in Biology)

To date, doctors do not have reliable and objective methods to diagnose pain caused by disorders at the skeletal interfaces in the lower back, which is a frequent health problem experienced by many people. Lower back pain generally originates in the linkages between the bones in the pelvis, which is one of the most important load bearing structures of the human body. Researchers are developing dynamic models of the human pelvis which they will use to diagnose the mechanical properties of ligaments using Doppler Ultrasound [33]. The skeletal components and the ligaments that connect the skeletal components are being modeled as a spring-mass system so that unobtrusive in-vivo diagnosis of disorders can be possible. The model is quite complicated because of the natural variation of human bone structure, but the researchers at Erasmus University in Rotterdam are determined to develop a model for objective diagnosis of the mechanical properties of a complex biological structure.

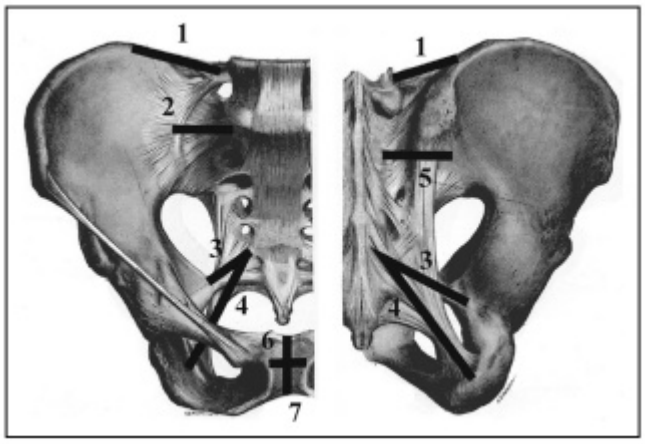

Figure 14: model of pelvis bone structure and ligaments that are modeled as spring mass systems for in vivo ultrasound testing of mechanical properties. Left: Front view or pelvis, Right: back view [33].

Ultrasonic waves have been shown to be effective in both speeding recovery time for broken bones [34]. Doctors can issue portable low intensity ultrasonic devices that have been shown to reduce recovery time by up to 40 percent. Additionally studies have been conducted on rats with broken bones, in which the rats were exposed to low intensity mechanical pulses for twenty minutes daily over the course of several weeks. Not only did the bone heal faster, they also showed an increased second moment of inertia which corresponds to more bone mass, and a 100% increase in fatigue resistance [35].

Medical research from China has investigated the uses of high powered concentrated ultrasonic waves as a noninvasive method to treat various types of osteosarcoma (malignant bone tumors). Typical treatments are either amputation of the limb entirely, or removing and replacing large sections of bone with a custom made prosthesis. Results showed an increase in long term survival rates in the group that received ultrasonic ablation in addition to chemotherapy, over groups that only received

partial chemo or partial ablation. Of the 69 patients that received full ablation only 7% had a recurrence [36]. The ultrasonic ablation procedure is intended to reduce the need for amputation or invasive surgery of the diseased limb.

Chang-Guan University (Taiwan) researchers are pioneering a noninvasive method to deliver cancer treating magnetic nanoparticles to brain tumors using a combination of focused ultrasound and magnetic fields. The focused ultrasonic waves and locally introduced micro air bubbles are used to temporarily disrupt the blood brain barrier and allow chemotherapeutic agents contained in the nanoparticles to pass into the brain [37]. The researchers report a 15 fold increase in the drug delivery concentration compared to other in-vivo methods, and a 66% increase in survival time in the rat test subjects.

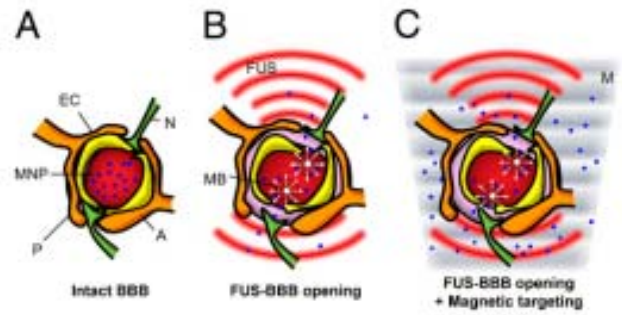

Figure 15: Method of disrupting the blood brain barrier (BBB) with focused ultrasonic energy. A: intact BBB. B: temporary disruption of BBB with focused ultrasonic energy. C: Introduction of magnetic nanoparticles with chemotherapeutic agent [37].

Ultrasonic Welding; Methods Relevant to Ultrasonic Self Healing

Ultrasonic welding is a process where plastics are clamped between a piezoelectric transducer and an anvil. The piezoelectric transducer then receives an

electrical signal that is converted to mechanical vibrations of the same frequency [38]. Heat is generated within the plastics by internal damping and energy dissipation is concentrated in the weld zone by a wave guide that provides a line contact between the two parts, the concentrated energy caused heating along the line contact point and welds the two parts together [39]. A schematic of an ultrasonic welding system can be seen in **Figure 16.** Ultrasonic welding of thermoplastics is quick and efficient and has become an extremely important industry as society moves toward using more and more plastics. Much research has been done over the years to identify the combination of parameters that will yield the strongest welds [40-42].

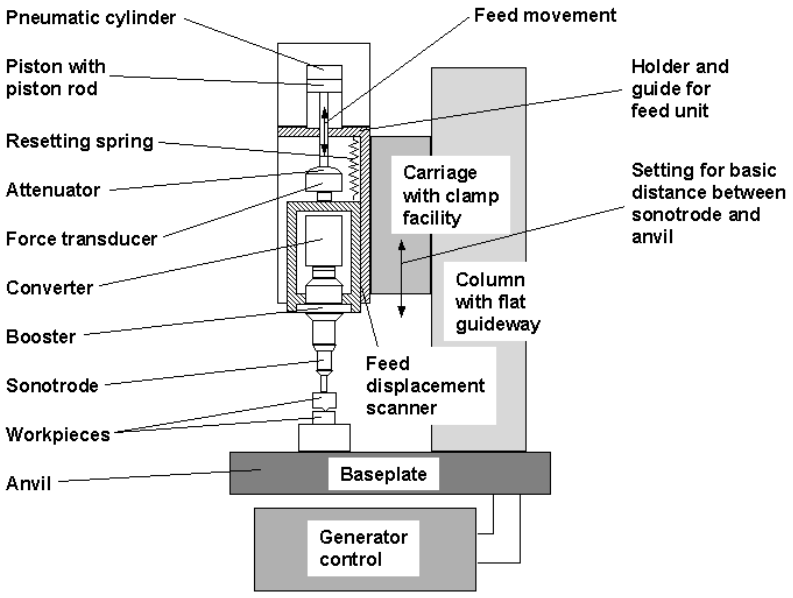

Figure 16: Schematic of components of an ultrasonic welding system. Electrical energy is converted into a mechanical vibration by the transducer and amplified by the booster [43]

There are 5 main processes that occur during ultrasonic welding: dynamics and vibration, viscoelastic heating, heat transfer, flow and diffusion, and cooling [40]. the

most relevant welding parameters have been identified weld time, weld pressure which keeps the parts in contact and provides friction for heating, and amplitude of vibration [41]. Amplitude of vibration may be the most significant because power dissipated is proportional to the square of the amplitude.

The reaction of thermoplastics to ultrasonic welding is dependent on the crystalline structure of the material, amorphous polymers tend to react elastically, and crystalline polymers react viscously. In a purely elastic material the driving force causes deformation rates in the part that are in phase with the force so there is no energy dissipation, in a purely viscous material the deformation rate is proportional to the input force but out of phase by ninety degrees, in this case the dissipated energy is proportional to the square of the local strain [39].

Amorphous polymers are easy to weld because once the polymer reaches the glass transition temperature, the modulus softens and the polymer is free to flow and diffuse. The problem with amorphous polymers is that they are soft and not always useful for structural applications. Stronger thermoplastics are called semi-crystalline because they have areas of ordered repeating microstructure that form areas of folded chains held together by crystal bonds which are local bonds formed in the tightly packed crystalline areas [44]. Semi-crystalline polymers are generally more useful for structural applications and therefore it is important to understand material response to the welding process.

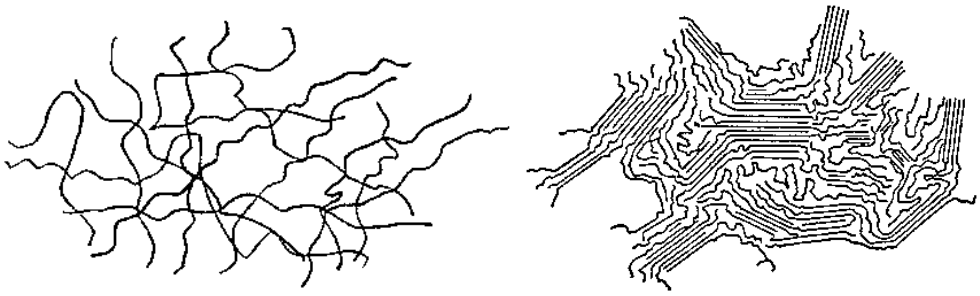

Figure 17: Amorphous (Left) vs. crystalline (Right) polymer structures; note the highly organized regions in the crystalline structure [45]

Semi-crystalline plastics are characterized by areas of order and disorder; the ordered areas of the material act as energy absorbing components because they vibrate in unison and consume a large amount of ultrasonic energy because they vibrate out of phase with the input signal and rapidly attenuate the signal. Because of the crystalline regions, the plastics characterized as semi crystalline require more energy input to achieve a weld because the modulus does not drop significantly until near the melt temperature [42, 44]. Examples of semi-crystalline thermoplastics include polyethylene PE, Polybutylene Terephthalate PBT, polyethelene Terepthalate PET, and Nylon6-6.

The main method of welding, or in the case of this study ‘healing’, in thermoplastics is when viscoelastic heating raises the temperature of the thermoplastic to the point where viscous flow can occur and inter chain diffusion occurs at the elevated temperatures. A postulate put forth by V.K. Stokes that states that additional strength is imparted to the polymer structure during welding by stress relaxation, which will occur when thermoplastics approach their glass transition temperature [46]. Stokes postulation arose when, upon viewing vibration welded polymers using polarized light imaging, he noticed areas around the weld with a different refractive index.

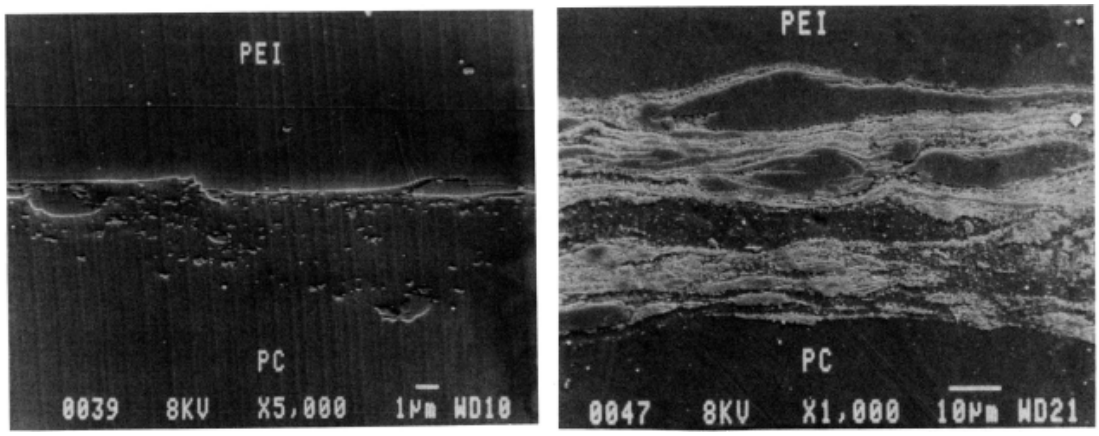

Figure 18: SEM image of two dissimilar plastics joined by vibratory welding. Left: looking down the direction of vibration (note the line near the top where the refractive index changes). Right, transverse to the direction of vibration (mixing of the two materials is evident) [46]

Weld strength is a function of temperature and strength increases until the maximum use temperature is reached. The maximum use temperature is defined as the lowest temperature at which change in the plastic material occurs that would be detrimental to the particular application [44]. According to K.S. Suresh, in order to achieve a strong weld without altering the properties of the polymer the weld temperature for a semi-crystalline polymer should not exceed 75% of melt temp [44, 47].

The efficiency of ultrasonic welding method is substantially improved if the vibration energy is concentrated into a small region rather than across the entire surface to be welded. By concentrating the energy, the small region melts and spreads over the entire bonding area, thus creating the bond desired and doing it with less energy [44].

3. EXPERIMENTAL DESIGN

Summary of Experiments

A quick summary of all of the experiments and their purposes is compiled in the beginning of this section before delving into the details of the setup of each experiment in later sections of this chapter. **Table 1** shows all of the experiments and the areas that each was designed to investigate and attempts to show the relationship of each of the experiments and the logical progression in sample design.

The thermal experiment was conducted first as a follow on to work done previously [21]. The thermal experiment was intended to investigate the temperature profile inside the nylon dog bone test specimens that were used in [21] additionally, the effects of varying the contact pressure between the samples and the ultrasonic probe was investigated. The ideal power level, contact pressure, and length of treatment found from the thermal experiment were used for the healing parameters in the tensile testing. There was hope that by optimizing the treatment, a larger amount of healing could be demonstrated beyond the marginal improvement shown in [21].

Finally, additional testing in the form of bending tests were performed in an effort to investigate different wave propagation orientations and demonstrate higher levels of healing than achievable in tensile testing. The T-Slot samples were designed to show cross crack wave propagation, but the PVC samples were tough and could not be broken at room temperature. Cooling was expensive because dry ice was needed to shift the samples into a brittle regime. The single notch bend samples were designed to have a

more sensitive crack orientation so they did not require cooling and also they demonstrated crack closure by material melting across the crack.

Table 1: Summary of all experiments conducted and the purpose of each experiment for demonstrating healing.

EXPERIMENTS		
Experiment Name	**Material**	**Purpose**
Thermal Process Experiment	Nylon 66	• Investigate the temperature profile in Nylon 66 tensile specimens used in [21]. • Additionally investigate effects of varying contact pressure between probe and sample. • Demonstrate depth to which probe can raise temperature to above 80% melting temp.
Tensile Test	Nylon 66	• Follow up Thermal process experiment using the Idealized power setting, contact pressure, and application time • Try to recreate and reinforce the results shown previously by [21]. • See if additional improvement gained by optimization found in thermal experiment
T-Slot Bend Test	PVC	• Investigate Cross Crack strain wave propagation • Demonstrate healing of samples by shifting damage initiation point from razor cut to groove corner deeper in the sample
Single Notch Bend Test	Polycarbonate	• More sensitive crack direction than T-Slot Samples, eliminate sample cooling • Demonstrate bridging of crack with melted material
Short Single Botch Bend Test	Polycarbonate	• Improve Single Notch Bend samples • Fail healed samples within stroke of bender for better comparison to damaged samples

Thermal Process Experiment

Investigation into the healing effectiveness of ultrasonic energy applied to damaged areas of thermoplastics continued from the work performed by Sarrazin [21]. The hypothesis was developed that regardless of what healing mechanism is actually occurring in the plastic at the crack tip—of which there could be several—the healing mechanism is due to a thermal process occurring in the damage zone. The vibration is dissipated through the sample in the form of friction between molecules and thus generating heat.

The ultrasonic probe used in this experiment is a Branson sonifier 450 with a maximum output of 400 W of energy. The probe was designed for mixing ceramic slurries rather than for welding. The Branson sonifier does not have any automated pressure or application time controls, so it makes treating the samples difficult at times because it is being used in a manner in which it was never intended. The Branson sonifier has a power adjustment that ranges from 0 to 10 with a linear output of energy from 0 W to 400 W, (See **Appendix B** for the calorimetry experiment to determine that the power is linear). The thermal process occurs because of the strain wave imparted to the sample by the probe tip vibrating at 20kHz where the amplitude of vibration is governed by the power setting.

According to research done R.M. Rani of PSG College of Technology in Coimbatore India on optimizing ultrasonic welding parameters it was demonstrated that the temperature for semi-crystalline plastics has to be very near the melting temperature and for amorphous solids the temperature needs to be approximately 80% of the melting

temperature [41]. With these benchmarks for temperature in mind it was desirable to know what the temperature inside of the sample so that the amount of healing, if any, could be ascertained given the specimen geometry and orientation.

An experiment was designed that used an Agilent 34970A data logging system and a 20 channel multiplexer to monitor the temperature profile through the thickness of the specimen while the probe was operating. The sample rate of the data logger was set to half second increments in an attempt to capture the transient thermal processes. Small holes were drilled at various depths through the sample in a staggered configuration with one-millimeter increments in depth below the probe.

The staggered pattern was used so that the ultrasonic energy and heat would be interfered with as little as possible as they propagated through the sample. K-type thermocouples were imbedded into the sample and secured with a small drop of epoxy compound so that the thermocouples would not come loose under the potentially high temperatures caused by the ultrasonic energy. A Solid Works schematic of the staggered thermocouple array and the orientation of the ultrasonic probe above the thermocouples are shown in **Figure 19.**

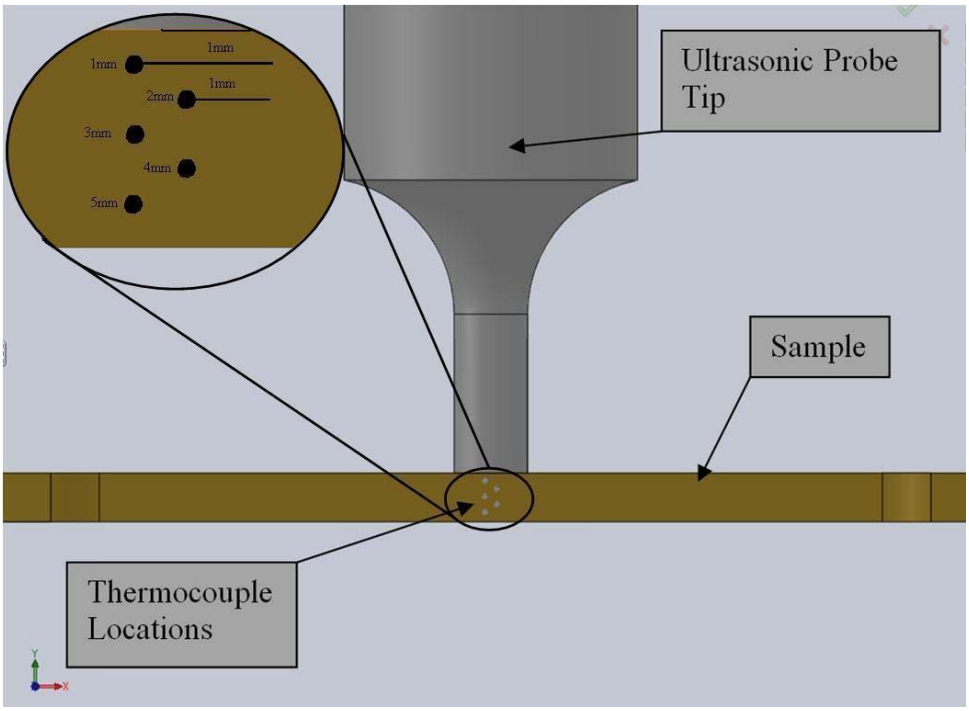

Figure 19: Solid works drawing of Imbedded Thermocouple location through the thickness of Sample specimen and ultrasonic probe location. Thermocouples are staggered with 1mm spacing down through the thickness of the sample.

A new probe holder was machined out of a piece of PVC pipe with the inside bored out to have only a few thousandths clearance between itself and the probe so that the probe was allowed to press down with on samples with its full weight and also minimize wobble when operating at high power levels. Furthermore the probe can be much more closely and repeatedly aligned on the sample specimens than previously possible. Pictures of the early probe stand compared to the new setup are seen in **Figure 20.**

Figure 20: Comparison of old ultrasonic probe stand and the new stand machined for more precise alignment between probe and specimen.

Adding weights to the top of the ultrasonic probe could vary the contact pressure between the probe tip and the nylon specimen. The weights were short sections of steel pipe that fit securely onto the top of the ultrasonic probe. The probe itself was 1.4kg and each of the sections of pipe were 0.847kg. The contact pressure between the probe and the specimen can be quickly calculated by dividing the weight of the probe by the area of the half inch diameter probe tip that is in contact with the nylon specimen. In the tensile testing only half of the probe is on the samples so that the through thickness edge notch crack is centered under the probe tip. The contact pressures for the three different probe weights used in the experiment are calculated in **Table 2.**

Table 2: Mass of components used to vary the contact pressure between the ultrasonic probe and the nylon specimen. No coupling was used besides contact pressure.

Component Name	Mass kg	**Pressure applied (KPa)**
Ultrasonic Probe	1.403	218
Probe + one weight	1.403+0.847	348
Probe + two weight	1.403+0.847*2	480

The contact pressure used during experimentation is similar to what is used in welding processes. Both experiments by conducted by R.M. Rani and Avraham Benatar on optimizing welding parameters use contact pressures ranging between 200kPa and 800kPa [41, 48]. The healing process is not entirely akin to the welding process because in welding there is an energy-directing component between the two pieces that are to be joined. The energy director concentrates the strain energy causing melting and thus joining the parts together. In the thermal experiment and healing trials, there is no energy director to cause a concentration of energy and rapid melting. Instead it is desirable to monitor the temperature inside the specimens to determine the best combination of power settings, contact pressure, and length of application time to best heal the specimens.

The thermal experiment went through several iterations in order to refine the process so that clean data could be recorded from the thermocouples. Initially the thermocouples had too much exposed wire to accurately report the temperature at the desired sampling location because thermocouples average the temperature encountered across the exposed section of wire. Additionally, in the initial trials the old probe stand could allow the probe to move and cause inconsistencies, noise, and erroneous jumps in the temperatures reported by the thermocouples.

The noisy data from the experiments actually lead to the development of the new stand for the ultrasonic probe mentioned earlier. Additionally a holder for the plastic specimens was machined out of aluminum to secure the samples in place because the samples had a tendency to jump around and vibrate out from underneath the probe if not secured. A picture of a Nylon dog bone sample with thermocouples imbedded and secured in the sample holder ready for testing can be seen in **Figure 21**.

Figure 21: Picture of the Nylon dog bone sample with thermocouples imbedded and ultrasonic probe applied.

The samples were secured to the aluminum holder in several different ways to try to look at the differences in the boundary conditions between an aluminum plate at the back surface of the nylon sample and an air boundary at the back surface. The first method of securing the sample was with the back of the sample directly touching the

aluminum as seen in **Figure 22**. In this configuration it was thought that the aluminum holder could act as a heat sink for the heat being generated in the sample because the conduction coefficient is much higher in the aluminum than in the nylon sample. In addition to being a heat sink for the transmitted portion of the ultrasonic energy, the aluminum has a different acoustic impedance than the nylon which will reflect some of the ultrasonic wave back into the nylon sample.

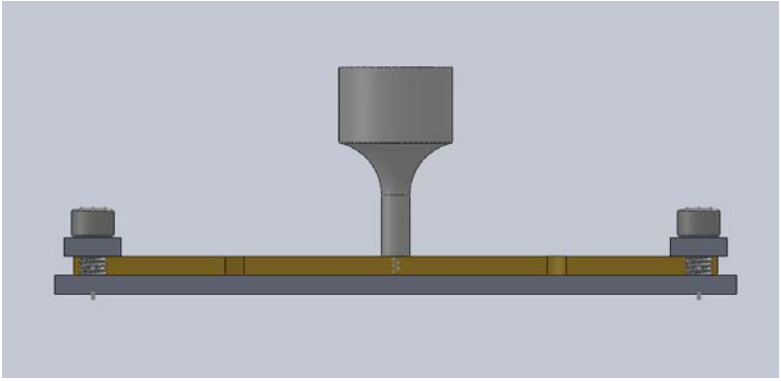

Figure 22: Conductive thermal analysis configuration. Bottom side of specimen is in direct contact with the aluminum holder which is considered a large heat sink.

The second method was to place spacers between the plastic and the aluminum holder on the ends where the plastic was secured as seen in **Figure 23**; this resulted in an air gap between the plastic and the holder effectively changing the boundary condition of the back surface of the plastic. The high conduction coefficient of the aluminum has been replaced by a convective boundary condition that, in a room where most of the air is stationary, generally transfers heat much more slowly. But, by changing the material interface at the back of the sample from aluminum to air the amount of energy reflected back into the sample may also be effected.

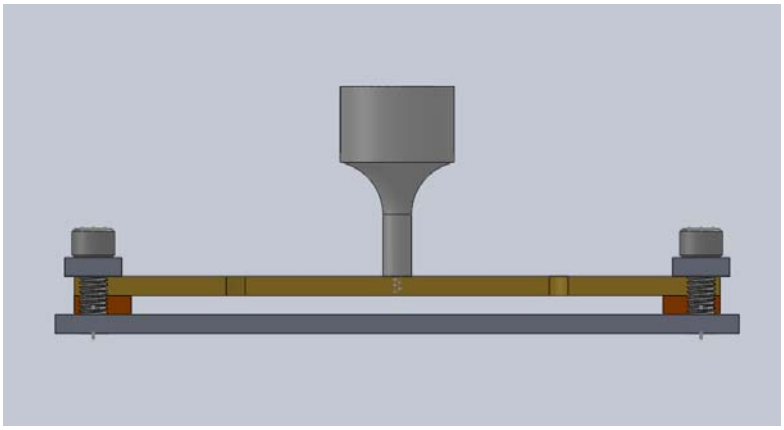

Figure 23: Convective thermal analysis configuration. Quarter inch spacers are inserted between the bottom of the sample and the aluminum holder exposing the bottom of the sample to a boundary of air.

It is important to have an idea of the amount of ultrasonic energy reflected back into the sample by the different material interfaces on the bottom side of the nylon dog bone. Several relevant acoustic and physical properties needed to perform calculations of the reflection coefficient and other important interactions are listed in **Table 3**. The acoustic impedance is calculated by simply a product of the density of the material and speed of sound in the material.

Table 3: List of physical and acoustic properties of plastics used for testing as well as properties for other relevant materials needed for calculations

Material	**Density (g/cm^3)**	**Thermal Conductivity (W/m-K)**	**Speed of Sound (cm/s)**	**Acoustic Impedance $kg/s\text{-}m^2$ (MRayl)**	**Loss (dB/cm)**
Air	$1.29x10^{-3}$	0.025	3.43	0.429	
Aluminum	2.73	237	64	17.41	
Nylon 6/6	1.12	0.23	26	2.9	2.9@5
Acrylic	1.19	0.19	27.5	3.26	6.4@5
Polycarbonate	1.18	0.20	22.7	2.77	24.9@5
PVC	1.38	0.16	23.8	3.27	11.2@5

Using **(2** it can quickly be determined that the percentage of ultrasonic energy reflected back into the sample when wave passes from the nylon sample to the aluminum base is 51%. If an ultrasonic wave passes through a boundary of nylon and air the calculation of the percentage of ultrasonic energy reflected back into the nylon is 55%. By changing the material from aluminum to air it does not significantly alter the amount of energy reflected back into the sample, so difference between the aluminum and air trials should mainly be caused by the change in the orientation of the reflected pressure wave. Referring back to **Figure 9** it can be seen that when the strain wave encounters a boundary with lower acoustic impedance the strain wave changes sign from positive to negative. If the wave encounters a material with greater acoustic impedance the sign of the strain wave will stay the same. The difference in boundary conditions will change the locations where constructive interference occurs, which should slightly change the temperature profile.

The thermal experiments were mostly used to gain insights into the correct power levels needed to reach temperatures near 75% of the melting point of the plastic specimens. With that knowledge, it was possible to apply a power setting that would raise the temperature of the sample sufficiently to promote healing but not degrade the structural integrity of the samples by burning holes in the plastic and inducing damage that decreases the structural properties of the sample.

Nylon Tensile Test

Previous testing had focused on using tensile specimens to demonstrate the effectiveness of ultrasonic healing in thermoplastic materials. The test specimens were

nylon dog bones 12.7 mm (0.5 in) wide by 6.35 mm (0.25 in) thick. The gage section of the dog bones was 70 mm (2.75 in) long. Nylon was chosen because it was the material used by one of the undergraduate classes for tensile testing experiments to there was plenty of baseline information for undamaged specimens.

A sharp edge through thickness crack 1.9 mm (0.075 in) was imparted to the dog bone samples using a razor blade and a drill press to press a razor into the sample as seen in **Figure 24**. The damaged samples were tested on an Instron 5882 tensile testing machine to determine their failure characteristics so that a baseline for comparison could be made to the ultrasonically healed samples.

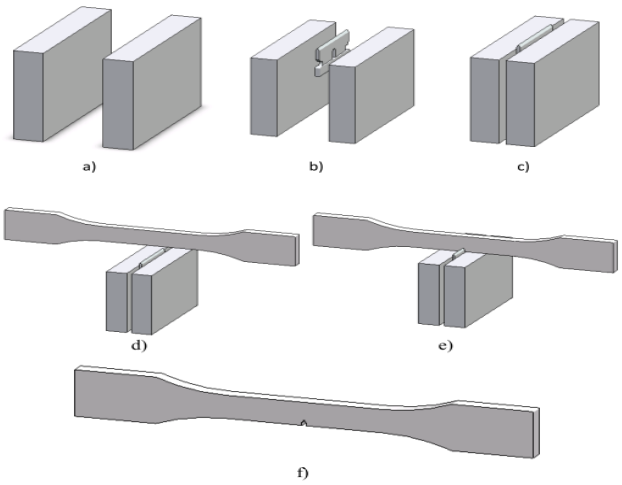

Figure 24: Dog Bone sample with razor damage on edge used for initial testing [21].

The ultrasonic probe was then applied to the flat side of the dog bone, as seen in **Figure 25**, at various power setting and lengths of time to find the best combination of variables for effective healing. The current work initially continued down the track of the previous thesis work of Sarrazin [21] with a focus on trying to improve the method and

further show that ultrasonic treatment is indeed a viable healing mechanism. The optimal set of healing parameters gleaned from the thermal testing were used in an attempt to optimize the amount of healing that could be imparted to the samples. In the end the ultrasonic probe was operated on power level 3 (120 W) with a contact pressure of 480 kPa and the application time was two minutes.

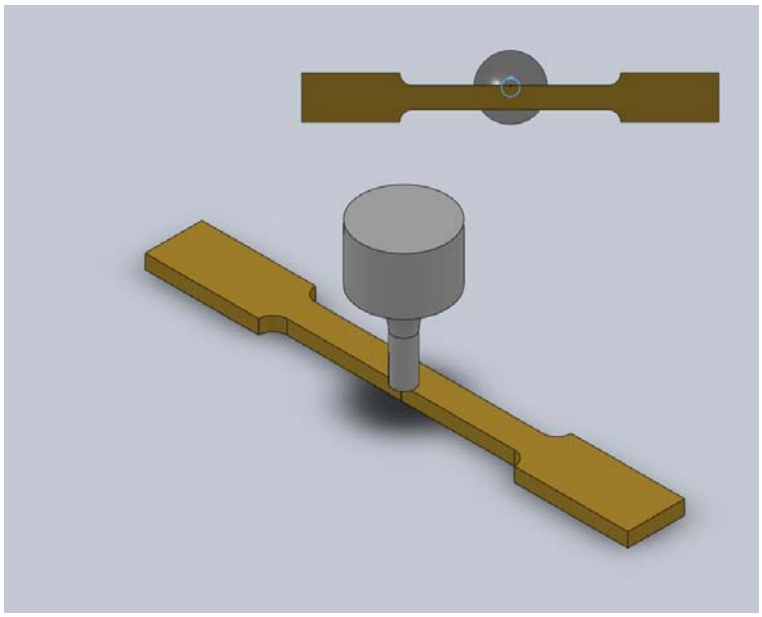

Figure 25: Orientation of ultrasonic probe on tensile dog bone specimens.

One of the problems with the initial ultrasonic probe holder and stand was that the setup lacked repeatability. It was extremely difficult to have the same amount of contact pressure and area between the probe and the sample applied consistently. Additionally, the probe would tend to shift mid treatment and affect the amount of energy being transferred to the sample.

Occasionally samples had little or no energy transferred to them because the probe was not sitting flush on the surface. Other samples incurred significant internal

damage from the probe transferring too much ultrasonic power and volatilizing some of the plastic molecules, which created gas pockets inside the specimen. Gas pockets and burned sections of samples take away from the load carrying area, thus degrading the performance of the specimen in the tensile test. It was determined that better process controls were needed to make treating the samples more consistent.

The hypothesis of initial testing was that the crack was closed by the ultrasonic treatment due to melting of the sample at the crack tip so that there was more load carrying area and the specimens were stronger accordingly. The previous work attempted to validate the hypothesis with a finite element model where the crack length was decreased and load displacement graphs of the samples were examined and compared to the finite element results.

The results of both the physical testing and the finite element modeling done in the previous work [21] indicated a slight increase in the strain to failure of the samples because the increased load carrying area prolongs reaching the ultimate failure stress criterion in the samples that had been subjected to the ultrasonic treatment. A slight trend appeared indicating that as the ultrasonic treatment power level increased the samples were able to sustain more strain to failure.

The present work sought to confirm this trend of increased strain to failure of samples subjected to ultrasonic treatment with more testing and also an examination of the samples with a microscope to try to find differences in the failure surfaces that might indicate that material had bridged the razor cut in some locations. Additionally, other microscopic evidence of healing mechanisms such as possible crack tip blunting, or some

form of material softening through an annealing process, was sought through microscopic examination.

Four Point Bend Configuration

After initial trials, we wanted to change the orientation in which the ultrasonic energy was applied to the sample because of inconclusive evidence of melting or crack tip blunting in the damage zone. It was thought that because the strain wave was propagating parallel to the crack it did not encounter the crack boundary as it propagated through the sample, and thus the strain did not close the crack. So melting of the crack surfaces back together may not have been the main mode of healing in the tensile samples. If the strain wave were to encounter the sides of the razor cut by changing the orientation of the ultrasonic wave to be perpendicular to the edge of the crack it may push the crack together and more effectively heat the area around the damage site.

Bending Apparatus Design

The four-point bend test procedure was based off of ASTM 6272-02 method for determining flexural properties of plastics. The standard was used as a guide for deciding on sample geometry, sample thickness to support span ratio, as well as the displacement rate to be used during testing. The tests do not completely follow the standard because of some equipment limitations but the majority of the test procedure is followed.

The apparatus used for testing was machined from AR44 hardened steel to ensure that there was no relevant amount of deflection in the fixture. The base plate of the apparatus had an array of holes so that the support arms could be moved to various spans

in increments of one inch. The ASTM 6272-02 standard states that for four-point bending of polymeric specimens, the support span must be at least 16 times the height of the sample. Given the available thicknesses of plastic sheeting and consideration for the geometries that needed to be machined into the samples a sample thickness of 9.53 mm (0.375 in) was chosen and the span that corresponds to a 1:16 ratio is 152.4 mm (6.0 in) but that span was incompatible with the pre-existing hole pattern machined into the base plate. ASTM specifically allows for some leeway in the ratio in order to accommodate testing a wide variety of materials so a support span of 177.8 mm (7.0 in) support span was used for testing. The height to support span ratio for all of the testing was 1:18.7, which conforms to the ASTM standards. A picture of the bending apparatus is shown in **Figure 26**.

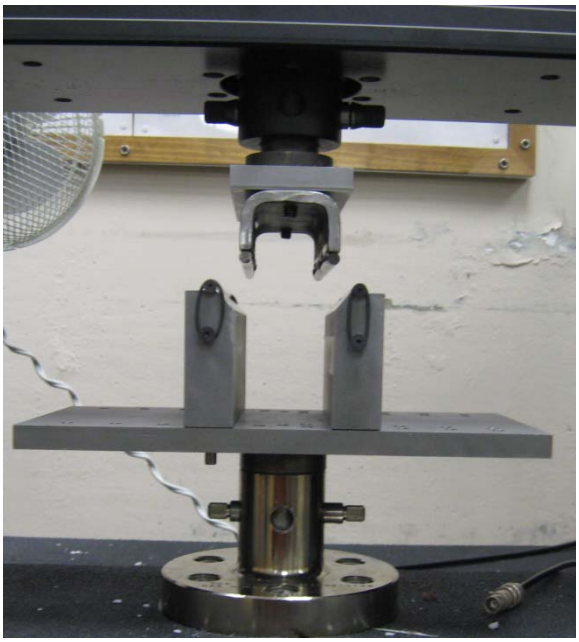

Figure 26: Four point bend apparatus in Instron 5882 frame. The bottom supports can be moved in an array of holes in the base plate to change the support span.

The Load Frame was machined from a 50.4 mm heavy walled square beam made of hardened steel. The beam was cut in half and the two arms were machined flat and 6.35 mm (0.25 in) steel dowels were carefully tack welded onto the ends of the U-shaped load frame. Ideally, the load frame would also have movable load arms, but the load frame was machined from available material to stay within a budget. The load frame dowels would also ideally be able to roll so that they would not provide any resistance to the sample moving during the bending process. Remedy the discrepancies of the geometry of the load frame to ASTM standard the dowels were lubricated with Vaseline so that friction could be minimized. Additionally, ASTM recommends a loading rate given in **(4**.

$$S = \frac{0.185PX^2}{d} \tag{4}$$

In **(4** P is the rate of straining in the outer fibers which ASTM says shall be equal to 0.01mm/mm [49], X is the width of the support span, d is the depth of the beam, and S is the calculated rate. Using the geometry of our bending apparatus the displacement rate for the tests can be calculated as 6.14 mm/min (0.242 in/min). The rate is slow so that the tests are quasi-static and the stresses are allowed to fully develop in the specimen.

T-slot Four Point Bend Design

Initially the four point bend specimen was designed along the lines of a double cantilever beam crack specimen. It was hoped that the crack could be located close to the

outer limits of the beam so that it would experience the greatest amount of strain causing the samples to fail within the limited 50 mm (2.0 in) stroke of the four point bend apparatus. In order to orient the crack to be perpendicular to the direction of the ultrasonic energy and have solid material beyond the crack tip a sample with a complex geometry was created as can be seen in **Figure 27**. A double cantilever beam specimen was not used because the specimen would be too thin to secure with grips if the damage was kept within the effective treatment depth of the ultrasonic probe (see D in below).

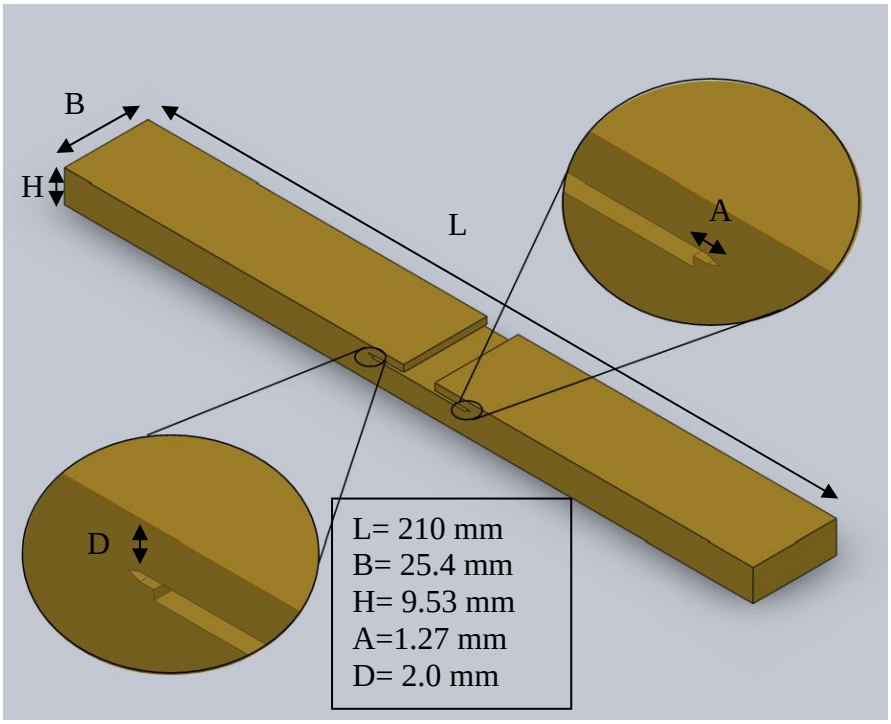

Figure 27: Diagram of the initial four point bend specimens. Note the "T-slot" machined into the sample has razor cuts at both ends. The razor cut is aligned with the outer most wall of the band saw cut so the bending strain can be maximized.

Specimens were cut out of solid sheet stock with a thickness of 9.53 mm (0.375 in) and were machined into rectangular samples with a width of 25.4mm (1 in) and a

length of 210 mm (8.25 in). An 7.94 mm (5/16 in) end mill was used to make a cut 2.92mm (0.115 in) deep in the center of the sample. A rip fence was then carefully aligned to a band saw so that the 0.812 mm (0.032 in) thick blade would cut a groove into the sample flush with the bottom of the end mill cut.

The samples were damaged using a special jig and a drill press to press a razor blade 1.27 mm (0.05 in) into the end of the band saw cut. The razor cut was placed on the outer most surface of the band saw cut which was 2.04 mm (0.08 in) below the top surface of the rectangular specimen. Trials using thin cuts of several types of scrap material showed that the Branson Sonifier was able to weld thin pieces up to roughly 2.54 mm (0.1 in) thick to a substrate of similar types of thermoplastics. Additionally, it also uses information from the thermal trials and tries to take advantage of the temperature profile seen in the samples.

The new crack orientation would allow the ultrasonic energy to propagate transverse to the crack in hopes that the strain wave would cause some amount of crack closure. Additionally, the weight of the ultrasonic probe should add to the crack closing pressure because the weight of the probe is oriented transversely to the crack direction as seen in **Figure 28**. This orientation is close to what is used in traditional ultrasonic welding when joining two sheets plastic together. It is also thought that there could be more significant crack tip blunting in this instance because the strain wave will encounter the side walls of the crack and possibly be able to cause enough molecular motion at the crack tip to be able to blunt the crack.

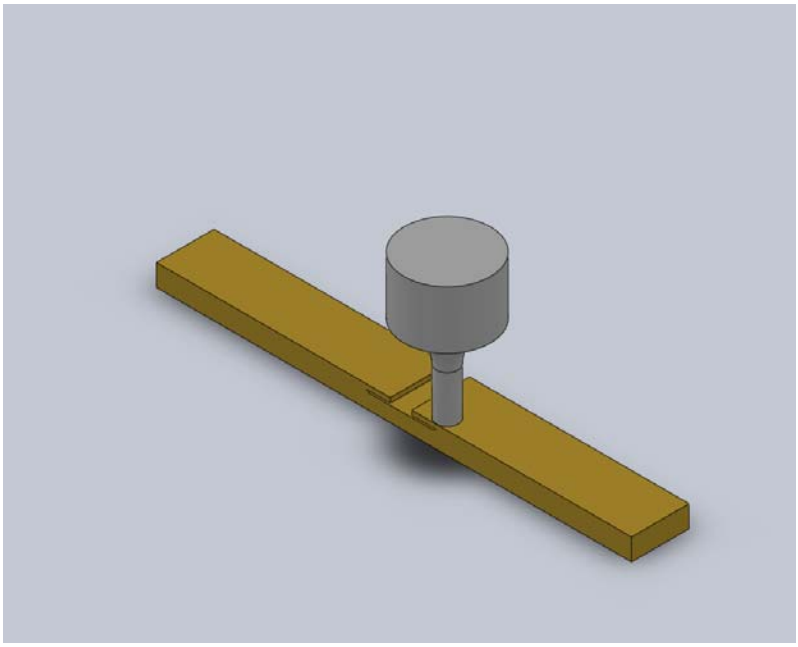

Figure 28: Application of ultrasonic energy to the four point bend "T-slot" sample. The probe is slowly moved across the width of the entire sample above either one or both of the razor cuts.

At room temperature it was found that the toughness of the PVC that was tested was too great, and none of the damaged samples failed. Several different parameters were changed in order to try to get the samples to fail within the limits of the bend apparatus starting with the displacement rate. The rate was greatly increased to 50.8 mm/min in a hope that the plastic molecules would not have time to align with the stress and the sample would fail quicker, but it had little effect. Secondly, the sample temperature was decreased using dry ice to drop the temperature of the samples to -78.5^{o} C and change the response of the plastic into a brittle regime.

The razor cut in the "T-slot" samples was not sensitive enough to fail the specimens at room temperature because the damage was not transverse to the major principle stress direction. A Finite Element Analysis (FEA) model was done to confirm the major principle stress direction around the T-slot. The model indicated that the major

principle stress does change direction around the tip of the t-slot but quickly resumes the normal orientation for a beam in bending. So a change in the razor cut orientation to be more sensitive to the principle stress directions was needed in order to fail the samples at room temperature.

Single Notch Four Point Bend Design

The single notch bend samples share the same rectangular geometry as the T-slot samples With a depth of 9.53 mm (0.375 in), a width of 25.4 mm (1.0 in), and a length of 210 mm (8.25 in). The difference is that the orientation of the crack was changed to be transverse to the major principle strain direction so that the crack was pulled apart by the bending process rather than relying on shear to cause failure as the T-slot samples did. A diagram of the specimen geometry and razor cut orientation can be seen in **Figure 29**.

This model is a hybrid of the tensile test specimens and the T-slot samples because the direction of the ultrasonic energy is not transverse to the crack direction which is the ideal orientation, but the crack is oriented so that the samples will reliably fail at room temperature. Having the samples fail at room temperature mitigates the need to cool the samples into a brittle regime.

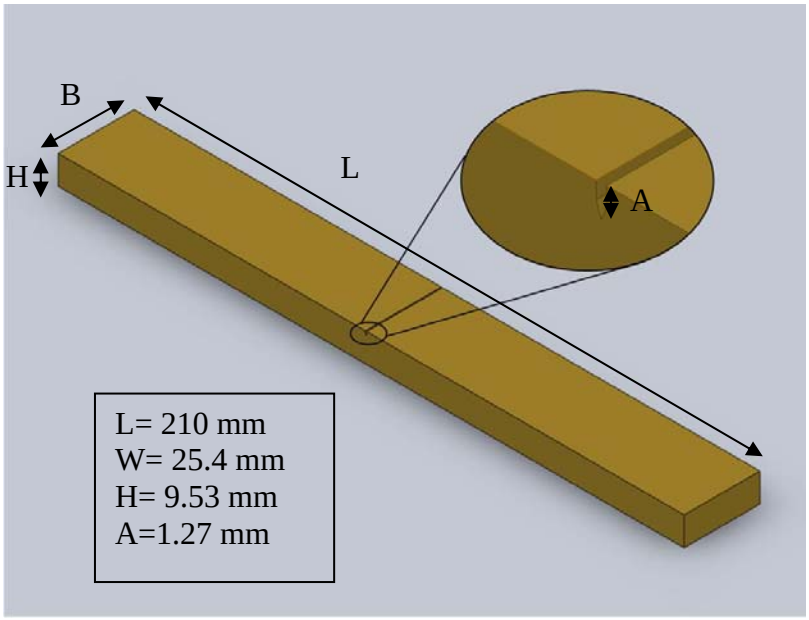

Figure 29: Single notch four point bend specimen with crack orientated to take advantage of maximum principle stress direction so that the crack will propagate easier.

Although the damage orientation and ultrasonic wave propagation direction is similar to the tensile specimen, the ultrasonic probe is applied in a fashion similar to the T-slot samples. The Ultrasonic probe is applied to the one-inch wide face of the beam and slowly moved across the entire length of the crack in order to heal the crack along the entire surface. The tensile specimen only has the probe applied to the narrow side of the specimen instead of the surface with the crack opening. A schematic of the orientation of the ultrasonic probe on the "single notch" four point bend specimen can be seen in **Figure 30**.

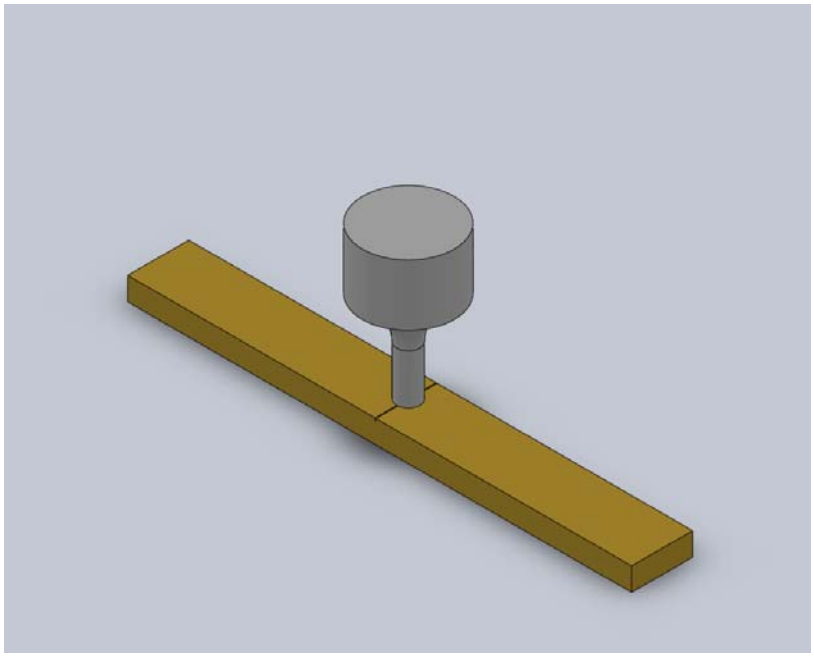

Figure 30: Application of ultrasonic energy to the four point bend “single notch bend” sample. The probe is slowly moved across the width of the entire sample above razor cut.

The damage is 1.27 mm (0.05 in) deep so the ultrasonic probe is able to heat up the area surrounding the crack. This allows the sample to heal by melting some of the material around the crack to the point where it is mobile and able to bridge the damage. This bridging of the crack should allow for the stress to be transferred away from the crack tip to the outside of the beam. This will decrease the stress at the crack tip and should allow the healed samples to outperform the damaged samples. Ideally, the material will fill the crack entirely, eliminating the damage all together.

The material used for the single notch bend testing was also changed in an attempt to find a more brittle plastic than PVC, which was used in the T-slot experiments. Additionally, a material that would respond well when heated with the ultrasonic probe was needed in order to minimize the internal damage caused when treating the samples.

Experimentation with polymeric materials available in the shop showed two promising candidates; acrylic and polycarbonate, both seemed to respond well to ultrasonic treatment. When the ultrasonic probe was applied, the material near the probe heated for a long time without much damage occurring sub surface in the samples where the mechanical performance could be affected. The other advantage of using acrylic and polycarbonate was that the samples were clear so any damage incurred by treating or testing the samples could easily be seen.

The acrylic was very hard and it was nearly impossible to press the razor into the samples. If the razor was pressed into the sample anywhere close to the 1.27 mm desired for testing, a crack would propagate from the razor tip through the sample destroying the sample before testing could take place. On this basis the acrylic was ruled out as a viable material. The polycarbonate was less brittle than the acrylic and it did not get damaged excessively by over exposure to ultrasonic energy. Instead of having large air pockets where the ultrasonic energy damaged the sample, it had smaller bubbles near the surface of the sample that caused fewer problems in specimen performance.

Short Single Notch Four Point Bend Design

This set of tests modifies the previous single notch bend test to be able to break the samples within the stroke of the bending apparatus. The damage orientation is identical to the previous section with the crack at the bottom of the beam opening in mode one. The problem with the previous single notch bend test is that the bending apparatus runs out of stroke before the healed samples fail. So, the samples needed to be

modified so that the true extent of the healing could be characterized. To accomplish this, the samples were shortened by a factor of two down to 105 mm (4.15 in) in length.

This test deviates considerably from what the ASTM 6272-02 standard recommends for load span to depth ratio because the samples are cut in half from the samples used in previous testing. This was done to increase the stiffness of the samples because the stiffness of a beam is inversely proportional to the cube of the length of the specimen. If the span of the beam is halved then the stiffness is increased by a factor of eight. In this configuration the load span is still the same 45.1 mm (1.78 in) and the support span is 76.2 mm (3.0 in). In this configuration, the maximum stroke available to the bending apparatus is 12.7 mm (0.5 in), beyond this point there is a risk of pushing the sample into the support frame causing potential damage to the bending apparatus. A schematic of the sample geometry is shown in **Figure 31**.

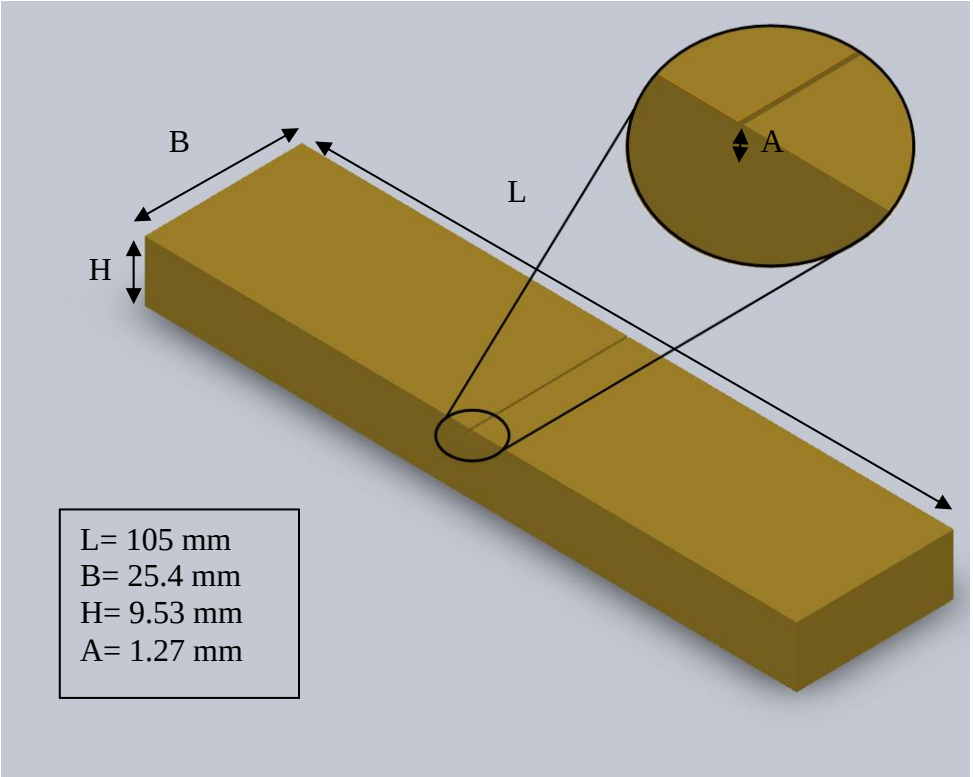

Figure 31: Short single notch bending specimen designed to allow failure within the limits of the bending apparatus. The sample is half the length of the previous single notch bend sample.

The bending apparatus is no longer close to the 1/3 load span to support span ratio recommended by ASTM specifications. It is possible that there will be end effects from the bending fixture because of the extremely short region between the load arms and the support arms in which the bending moment is generated. These possible end effects can be taken into account by only comparing the performance of the damaged and healed samples to other short specimens. It will not be possible to make any direct comparisons to other bending tests but the purpose of this round of testing is to try to determine the limits of mechanical performance improvement gained from ultrasonic healing of the damage site.

4. FINITE ELEMENT ANALYSES OF MECHANICAL TESTING

Finite element analyses were performed to try to predict the effects of ultrasonic healing on the bending specimens. Modeling efforts were directed to the bending specimens which is where the majority of testing in this work is concentrated. Modeling of the tensile specimens was done previously by Sarrazin in his master's thesis [21]; he postulated that ultrasonic treatment caused healing by crack closure, where the crack length decreased.

No significant modeling of the temperature distribution caused by ultrasonic treatment of the nylon dog-bone specimens because of the incredibly complex nature of the system. The main goal of this research is not to model the temperature profile in the specimens, but rather to use the results to help guide the processes used in the healing process for the mechanical specimens. Results of the temperature distribution in the nylon specimens presented in the next section cannot be modeled by a heat flux through the surface because the flux analysis simply yields a decaying temperature distribution as the distance from the probe increases. More complex analysis would be required to capture the physical processes that are occurring due to the application of ultrasonic treatment.

The software used for modeling of the bending specimens was ANSYS finite element package. All modeling was done in standard SI units (kg-m-s) and the beams were modeled as two-dimensional beams with a thickness. The plane183 2D, 6-node high order element with the plane strain option selected was used. The two dimensional model allowed for greater computational efficiency rather than analyzing full three-

dimensional models. The materials were characterized in ANSYS by their elastic modulus and Poisson's ratio, the properties are listed in **Table 4**. It can be seen that all of the materials tested have similar elastic moduli and Poisson's ratios; the only major differences are the ultimate strengths. Batch files for the finite element code are located in **APPENDIX A** for reference. Typical K_{IC} values for plastics are close to 2 text books list Acrylic at $1.8MPa\sqrt{m}$ and PVC at $2.4MPa\sqrt{m}$ [4].

Table 4: Mechanical Properties of plastics used for ANSYS Finite Element Analysis

Material	Elastic Modulus GPa	Poisson's Ratio	Tensile Yield Strength MPa	Flexural Yield Strength MPa	Ultimate Tensile Strength MPa
Nylon 6/6	2.34	0.37	84	141	99
Acrylic	2.88	0.402	73.7	99	100
Polycarbonate	2.39	0.37	64.1	91.2	72.4
PVC	2.45	0.38	28.4	80.6	55

The crack tip modeled in the unhealed models was modeled as a singularity and the stress intensity factor K_{IC} from Linear Elastic Fracture Mechanics (LEFM) was calculated by the ANSYS command KSCON. K_{IC} is a common way to treat crack tips in plane strain situations; the far field stress is multiplied by the intensity factor near the crack tip to find the stress just ahead of the crack. The calculation used by ANSYS for the crack tip is based off of the equation for a stress intensity factor due to the crack tip. The triangular elements surrounding the crack tip have a mid side nodes of the quadratic element moved to a quarter point location to effectively capture the stress around the crack tip.

FEA Analysis of T-Slot Four Point Bend Specimens:

Finite element analysis was used to try to better understand the failure path expected in the T-slot samples and also to try to determine what the effects of ultrasonic healing on the samples would be. The T-slot specimens were designed specifically to have the ultrasonic energy propagate transverse to the crack direction so that that the strain wave would tend to close the crack. Additionally when the strain wave encountered the free surface near the crack tip it was hoped that some amount of crack tip blunting would occur. The crack is defined with the KSCON command that assumes a singularity at the crack tip. **Figure 32** shows the stress distribution in the samples.

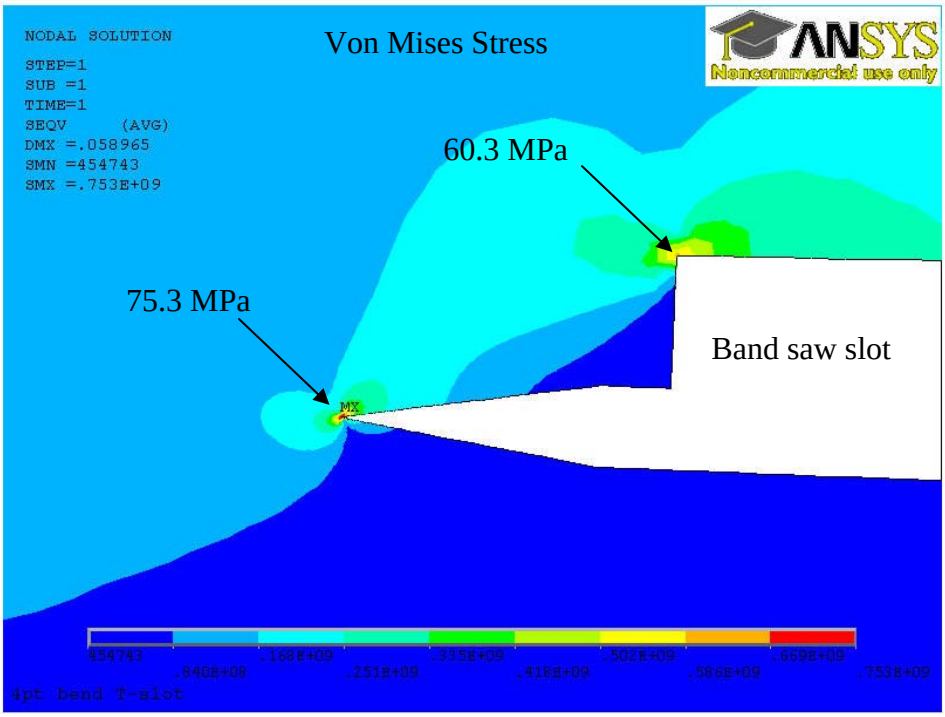

Figure 32: Finite Element analyses of Von Mises stress concentrations in T-slot bending specimens. The picture is zoomed in on the end of the band saw slot. The obvious concentration is the crack tip, but the corner of the band saw slot is only 20% less stress.

It is clear that the maximum stress is located at the crack tip, but there is a significant stress concentration at the corner of the band saw groove as well. This explains why the failure surface on the fracture plane sometimes changed from the crack tip to the corner of the band saw groove when the sample was brittle. Once the primary failure begins to occur the majority of the load is quickly transferred to the secondary damage location which causes rapid failure at the second location as well. The stress at the crack tip is recorded as 75.3 MPa, and at the corner of the band saw cut the node records 60.3 MPa. The corner of the band saw groove is about 20% less stress than the razor cut. The ultimate stress reported in the model is approximately at the bending yield stress listed for PVC (80.6 MPa)

If the crack tip singularity is removed to model a blunted crack tip, which is the hypothesized damage healing mode for this orientation, the stress at the crack tip is significantly reduced and the maximum stress in the T-slot specimen is shifted to the corner of the band saw groove deeper into the sample. So, if the samples are healed by the ultrasonic energy, the samples should not longer fail at the crack tip and they should instead fail at the corner of the band saw groove. A model of this situation is shown in **Figure 33.**

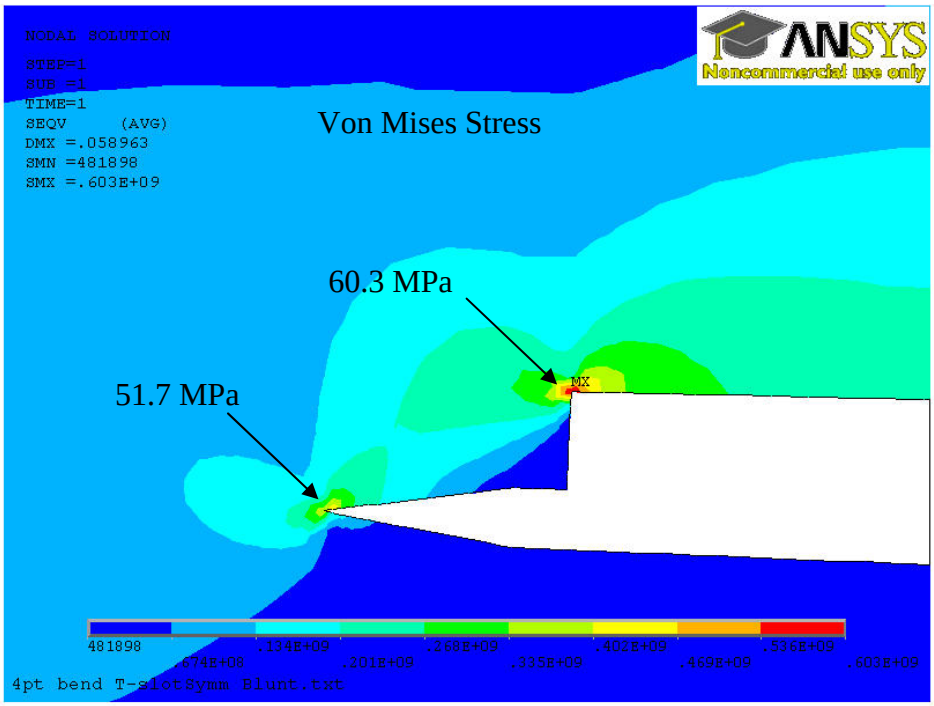

Figure 33: Stress distribution with singularity at the crack tip removed. Not that the highest stress concentration is shifted toward the

Removing the singularity at the crack tip by removing the stress concentration command (KSCON) makes the crack have a finite radius. The mesh density at the crack tip is increased so that the crack will have an approximate radius of 0.005 mm. It would be nearly impossible to characterize the exact diameter of the crack tip at all locations across the sample without taking many sections of the healed sample and examining them with a scanning electron microscope or another instrument with similar resolution. The finite element analyses presented here simply assumes that the crack tip is blunted and the singularity can therefore be eliminated. The lines in the model still converge to a point in the model and therefore the radius at the crack tip, but with the mesh density around the crack the radius is approximately 0.005 mm because of the finite size of the

elements. The mesh was refined further until the stress field showed convergence and the stress at the crack tip only increased slightly to 53.7MPa.

FEA Analysis of Mode-One Four Point Bend Specimens:

Analysis of the single notch bend specimens also used the same plane strain formulation and element type for the 25.4 mm thick beams. In this instance healing would most likely be caused by material melting across the crack near the surface of the sample. This mode of healing is most likely because the strain wave will not see the crack because it is propagating parallel to the crack direction and will only effect area of the sample near the probe tip. The Probe is moved across the sample face until the entire surface of the beam has been treated and the crack is melted across the whole width of the beam. The more heating that occurs near the vicinity of the damage, the greater the extent of the material the bridges the crack and can hold the two sides of the crack together.

Without the ability to direct energy to the crack tip it is difficult to melt at the depth of the crack tip without causing damage to the surface of the sample. The sample is considered healed when the material on the top surface begins to flow and bridges the crack tip. The material surrounding the damage does melt part way down into the razor crack and the material mobilizes and flows into the crack, although testing showed that it never penetrated all the way to the razor tip.

The crack tip modeled with the K_{IC} intensity factor can be seen in **Figure 34**. The figure focuses on the area immediately ahead of the crack and shows the classical stress

field at the crack tip. The model shows the beam displaced 44.5 mm (1.75 in) which is the displacement at which the single notch bend samples failed. The stress field at the crack tip is the classical LEFM stress field about a crack tip in plane strain. The maximum stress reported by the finite element analysis at the average displacement to failure of the unhealed samples (44.5 mm) is 76.4 MPa which is close to the failure stress of Polycarbonate. Matweb reports the ultimate stress of polycarbonate is 72.4 MPa, so the finite element model can accurately calculate the failure stress for this test.

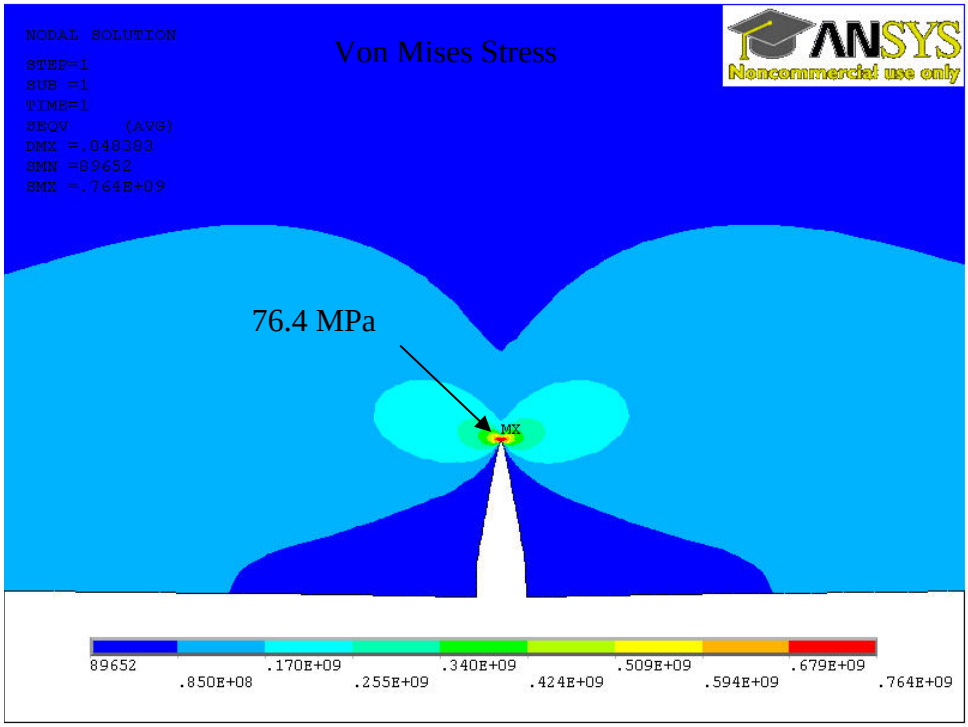

Figure 34: Stress field ahead of the crack tip in the single notch four point bend specimen calculated at 44.5mm displacement. This stress field is calculated using classical LEFM stress intensity functions built into ANSYS.

To model the effect of healing on the specimen another model is built with a piece of continuous material 0.27 mm (0.011 in) thick bridging the gap in the material. This

depth corresponds to one fifth of the razor crack being bridged by melted material; this is generally less than what is seen in the healed specimens, but it is done to keep the geometry of the crack the same and to demonstrate how the stress is transferred away from the crack tip. The stress field of the healed specimen is shown in **Figure 35**, notice that the maximum stress is now in the ligament of healed material.

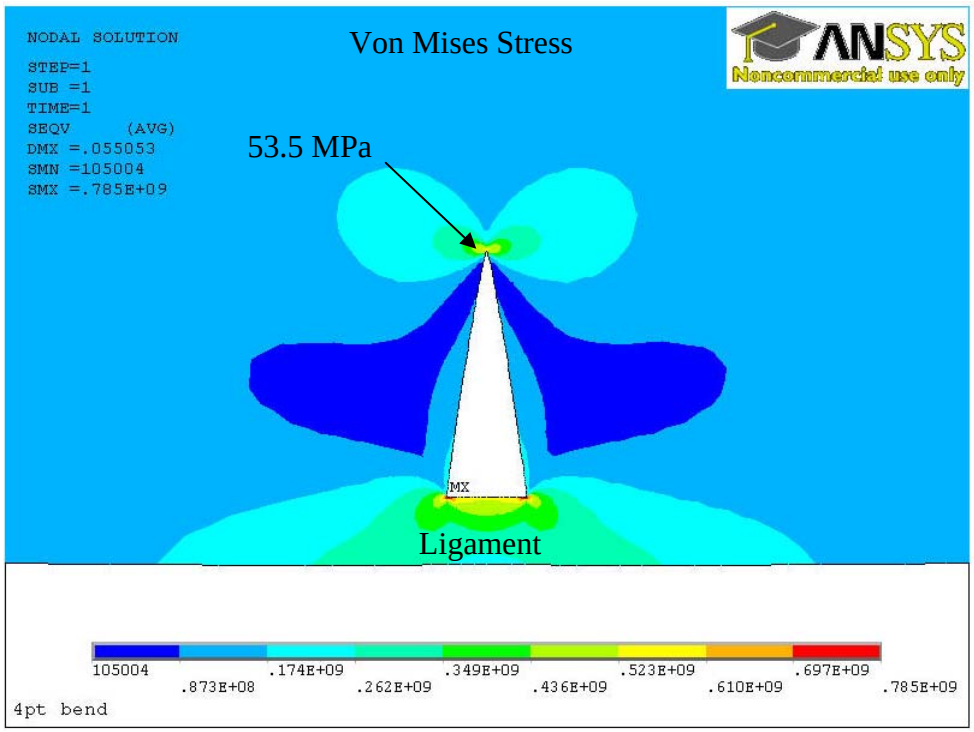

Figure 35: Stress field of healed single notch bending specimen at 50.8 mm displacement. Notice that the stress is transferred away from the crack tip and is supported by the ligament of material.

The stress field computed in **Figure 35** is computed at 50.8 mm displacement which is the maximum extent of the bending fixture for the specimen geometry. The concentration of the stress field at the corners of the razor cut is artificially high because of the sharp corner; the melting material would not form such a sharp corner so the stress

maximum stress reported at the corners of the ligament and the razor cut are not as important. If the stress at the crack tip is examined it is only 53.5 MPa which is still significantly below the stress at the crack tip in the unhealed specimen. The displacement to force the stress at the crack tip to be the same as in the unhealed samples would have to be 69.9 mm (2.75 in) which would correlate to a 57.1 percent increase in displacement to failure.

This amount of increase would not be likely because it assumes a perfect bond between the original crack surface and the melted material that flowed into the crack and bonded with the original surface. Additionally the perfect bonding would have to be across the entire width of the crack, so the ultrasonic treatment would have to be perfect the entire way across the opening of the crack. This is not likely given the equipment available. The stress based analysis is a way to look past the physical limitations of the bending apparatus and make some predictions about the performance of the samples. The sample would be bent far beyond the curvature used for normal beam theory derivations so more accurate analysis should be done to more accurately model the situation.

FEA Analysis of Short Mode-One Four Point Bend Specimens:

We can quickly modify the previous batch file to model the stress field in the short specimen at the average displacement to failure of the damaged samples and see if the ultimate stress in the samples is similar to what is seen in the long single notch bend samples. The average displacement to failure of the short samples is 6.53 mm. A close

up of the stress concentration at the front of the crack tip is shown in **Figure 36**. The maximum stress at failure is 76.7 MPa which is extremely close to the maximum stress reported in the long single notch bending specimen.

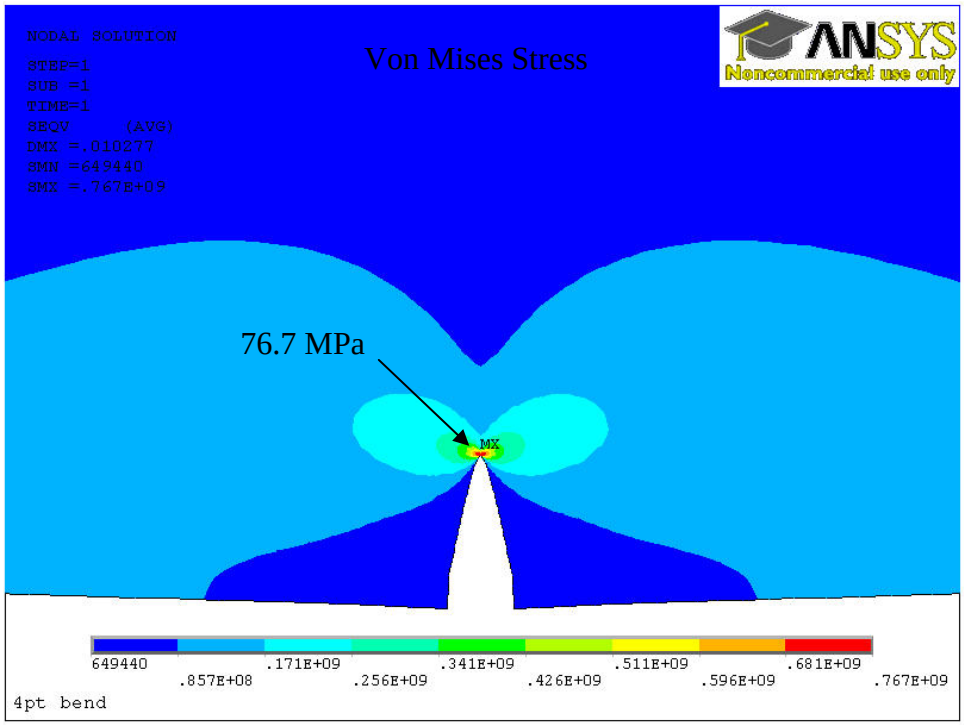

Figure 36: Stress distribution in short single notch bend specimen. Displacement is 6.53 mm which is the average displacement to failure of the damaged samples.

If the ligament is modeled in this short sample length exactly the same as in the long sample case, using a thickness of 0.27 mm the stress at the tip is reduced considerably. For the same displacement of 6.53 mm the stress is reduced from 76.7 MPa to 47.3 MPa which is a reduction of 40 percent. If the healed sample with the maximum displacement to failure is used as a reference for the most healing that can be we have interesting results.

The displacement to failure of the best performing healed sample is 9.6 mm, this can be seen in **Table 11** in Chapter 5. The stress calculated at the crack tip for this case is 70.7 MPa. This is close to the ultimate stress that can be withstood by the polycarbonate. If the lowest of the healed specimens displacement is used to calculate the stress at the crack tip at failure a stress of 61.7 MPa is found. This demonstrates that the adhesion of the melted material to the crack surfaces can be nearly as good as a perfectly bonded sample. The healing process needs to be refined in order to be able to cause melting over the whole crack, and most importantly at the crack tip. Given the equipment available for this thesis it is shown that melting across the damage is a first step to healing the damage.

5. RESULTS OF TESTING

Results of Thermal Experiment

There are a few assumptions that were made about interaction between the ultrasonic probe and the sample that are made when interpreting the information in this section. The first assumption is that the probe is always in contact with the sample, this is likely not entirely true because the probe tip is vibrating, but it is a common assumption made by the ultrasonic welding community when performing analysis of welding processes [47, 48]. The second assumption that is commonly made is that the frequency of the probe is much higher than any significant vibration mode frequency of the test specimen. This assumption is made so that the beam can be considered to be globally stationary which helps in the modeling and interpretation of results.

The temperature profile recorded by the Agilent data logger was quite interesting because the temperature profile did not behave as expected. It was thought that the profile would be that of an exponential decay decreasing in temperature with distance from a thermal source which is the normal profile seen in heat transfer. Instead it was found that the temperature recorded at some of the deeper locations was hotter than the temperature at locations closer to the ultrasonic probe, this can be seen in **Figure 37**. The contact pressure for this trial is 218 kPa, which would be considered light pressure.

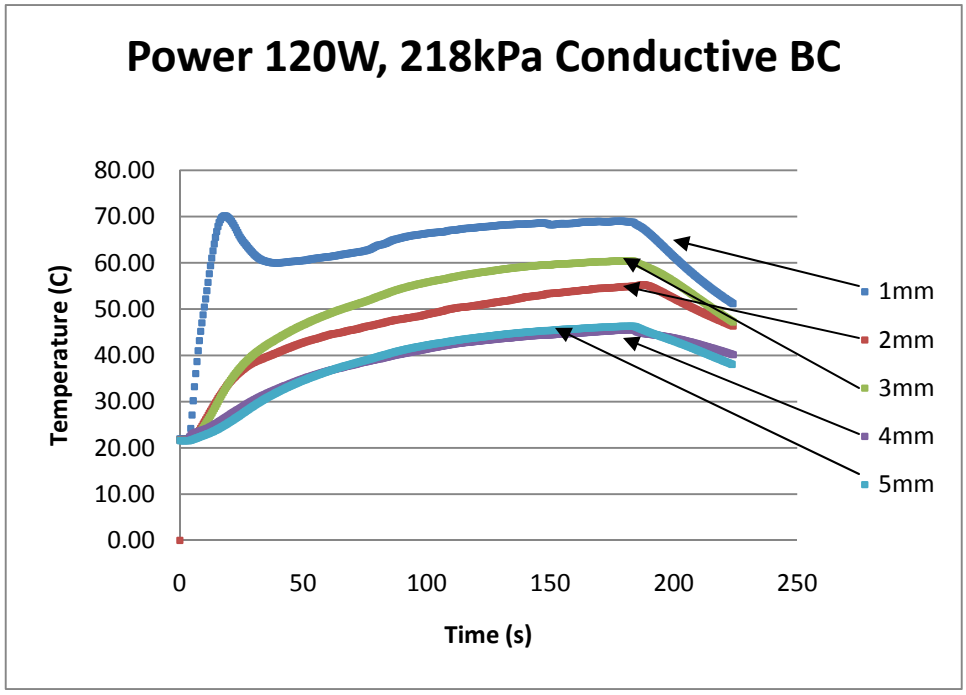

Figure 37: Temperature distribution through the thickness of a nylon sample with conductive back surface.

As can be seen in **Figure 37** the thermocouple located three millimeters deep into the sample records a higher temperature than the thermocouple only two millimeters into the sample. The two thermocouples farthest away from the probe record essentially the same temperature which would be expected near the tail end of an exponential decay when most of the ultrasonic energy has been dissipated the temperature remains mostly constant. The reversal of the temperature recorded at the 2 mm and 3 mm thermocouples; however, was unexpected. There are several plausible explanations for this phenomenon.

The first explanation, which is less likely, is that the probe emits a confocal wave pattern that converges a certain short distance from the end of the ultrasonic probe, this was seen by accident in early experiments on thin materials when an experiment on thin

plastic sheeting was being conducted. The thin plastic needed some backing to help absorb some of the vibration so that the energy did not go straight into the metal ultrasonic stand. One of the backing materials chosen was a pad of post it notes. The ultrasonic energy passed through the thin plastic specimen into the sticky note pad. After a few moments of the application of ultrasonic energy smoke began coming from the sticky note pad, so the experiment was quickly terminated. Upon examination of the sticky note pad it was found that there was only a very small burn on the top most piece of paper. As subsequent pages were examined it was found that the burn area in the paper grew larger up to a maximum diameter then grew smaller to the point where there were no more burn areas on the pages deep into the pad.

A second, and more likely, explanation is that the 51% of the ultrasonic energy reflected by the interface of the plastic and aluminum holder propagates back through the sample and interferes constructively with the forward propagating wave at the location of the 3 mm thermocouple. The latter theory can be tested by changing the boundary condition at the back surface by suspending the sample above the aluminum holder slightly which introduces a convective boundary condition at the back surface. The air interface changes the amount of energy reflected back through the sample to 55% but by going from a material with a higher acoustic impedance to a material of less impedance the reflected wave is inverted when it propagates back through the nylon. The temperature profile of the nylon test specimen with a convective condition on the back surface is shown in **Figure 38**. The contact pressure between the probe and the sample for this trial is 218 kPa, which is on the low end of the range of typical welding pressures.

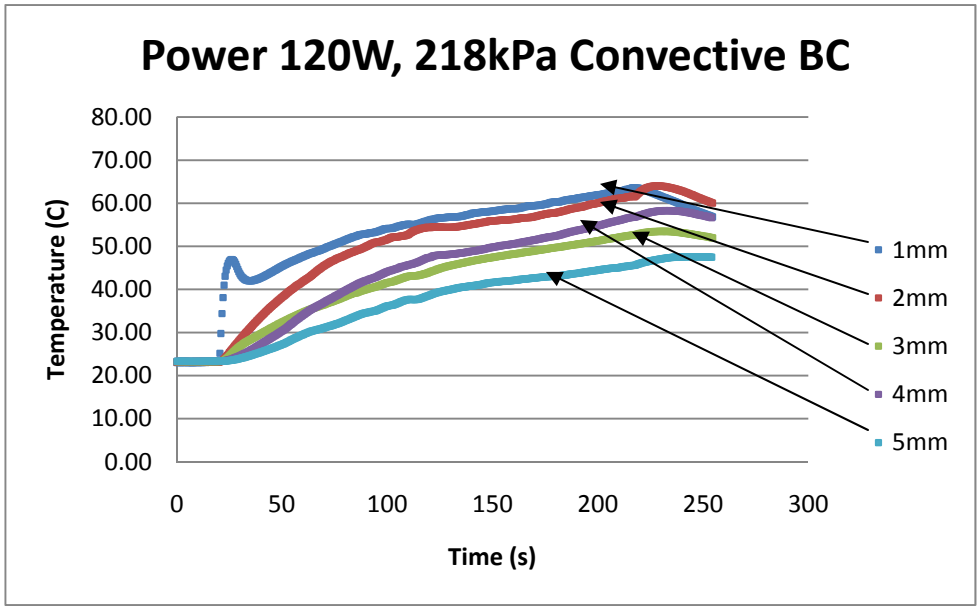

Figure 38: Temperature profile through the thickness of a nylon dog bone specimen with a convective back surface.

The differences between the through thickness temperature profiles between the nylon dog bones with conductive and convective back surfaces (**Figure 37** and **Figure 38** respectively) is negligible when looking at the ultimate temperature achieved; however, it is interesting to note that in the conductive bottom case the thermocouple at 3 mm records the second hottest temperature, while in the convective case it is the 2 mm thermocouple that is the second hottest point. Even though there is little difference in the reflection coefficient between the two trials the reflected wave has been inverted because of the change in material going from an acoustically dense media to a less dense media, this likely causes a change in the points in the sample where the waves constructively interfere which causes a shift in the temperature profile between the two experiments. In the convective trials it is seen that the 2 mm thermocouple is much hotter than the 3mm

thermocouple which is a reversal of the conductive trials, and the 4 mm thermocouple records a higher temperature than the 3 mm thermocouple.

The wavelength of the ultrasonic energy in a given media is simply the speed of sound in the material divided by the frequency of oscillation. It is found that the wavelength in nylon is 0.13 m which is almost exactly twenty times the thickness of the 6.35 mm (0.25 in) samples. The ultrasonic waves propagate through the sample quickly and a portion reflects back through the sample. The point at which the reflected wave interferes constructively with the forward propagating wave depends on the sign of the reflected wave if it is positive they will interfere at a different point than if they were negative. The power dissipated shown in

(1 is an exponential decay that depends on both the distance from the probe and also the amplitude of the wave at any given time and location, so there will be much more energy dissipated as heat where the incoming and reflected waves combine constructively.

The exact modeling and investigation of this scenario is quite complicated and a complete recreation of these phenomena would require modeling of the molecular vibrations and intermolecular interactions of polymers. The modeling and investigation into this area is beyond the scope of this work but the information gained through conducting the thermal process experiment is still useful for determining the appropriate power settings needed to achieve high enough temperatures to heal the polymers. There are several other factors that are extremely important to the healing process.

Contact pressure between the ultrasonic probe and the sample may be the most important factor out of any to the welding process [41]. For investigation purposes

several short sections thick walled sections of pipe that could be stacked on top of the probe were used to increase the contact pressure. The weight of the probe and the two sections of pipe are listed in **Table 2** in Chapter 3, and the pressure applied to the sample through half of the 9.53 mm (0.375 in) diameter tip are calculated.

It was found that the contact pressure does indeed have a significant impact on the temperature seen in the Nylon specimen. With only the first extra weight added the temperature recorded at the 1mm thermocouple nearly doubled. And with both weights added to the ultrasonic probe the temperature rose to the melting point of the nylon (250^{o}C) quickly and destroyed the sample. The conductive Boundary condition trial with the ultrasonic probe set at power level 3 and one weight added is shown in **Figure 39**, it highlights the massive increase in temperature seen by increasing the contact pressure to 348 kPa. The contact pressure was increased by approximately 60% and it resulted in doubling the temperature in the sample.

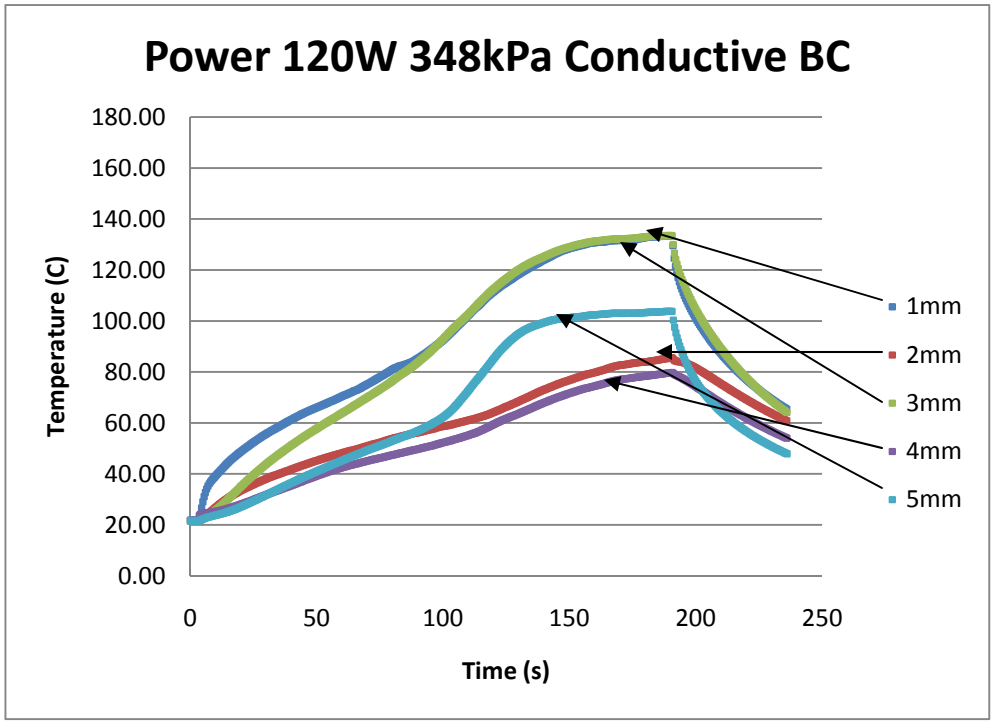

Figure 39: Temperature distribution in a nylon dog bone specimen with a 0.847Kg weight added to the ultrasonic probe to increase the contact pressure between the probe and the specimen. The bottom surface of the dog bone is subjected to a conductive boundary condition because it is in contact with the aluminum holder.

Note that the temperature profile in the trials with the weight added is consistent with the trials conducted with no additional weight. This trial has smooth temperature curves, but there are a few points where the curves definitely change curvature indicating a change in energy transfer to the sample. This change in the amount of energy coupled into the sample could be due to the probe shifting on the sample changing the area that the probe is resting on which changes the contact pressure and also the area through which the flux of energy is flowing.

Another explanation could be a change in the mechanical properties of nylon as it heats; the surface will become softer and possibly allow for better coupling of the probe

tip to the surface of the specimen. **Table 5** lists a few more important thermal properties of nylon that can help to explain the change in slope of the temperature curves.

Table 5: Working temperature limits of plastics taken from various sources

Material	Glass Transition Temp ^{o}C	Vicat A Softening Point ^{o}C	Lower Working Temp. ^{o}C	Upper Working temp. ^{o}C
Nylon 6/6	50	75	-30	80-180
Acrylic	100	85	-40	50-90
Polycarbonate	150	135	-40	115-130
PVC	80	92	-30	50-75

The definition of the temperature limit is where the plastic will no longer function properly. This indicates that there is a change in the material properties of the plastic, at the lower temperature limit the plastic molecules are no longer able to slide past each other and the polymer will fail in a brittle manner rather than having a great deal of plastic deformation before failure. At the upper working limit the plastic has passed the glass transition temperature by a significant margin and is now behaving in a rubbery manner. In the case of the nylon the upper working limit of 80 Celsius degrees is well beyond the glass transition point so the plastic will be almost entirely in the rubbery response region so the probe tip will be allowed to sag into the plastic and result in a much more efficient energy transfer to the plastic. This is the most likely cause of the change in slope of the temperature curves seen in the trials.

Another standard by which to measure a temperature at which there is a change in mechanical properties of plastics is the Vicat softening test. There method is established in ASTM D1525, a flat-ended needle with a square cross sectional area of 1mm is

pressed into a plastic as it is being slowly heated. The needle is pressed into the plastic with 10 N of force, and the temperature at which the needle penetrates 1 mm into the sample is the Vicat softening temperature. This temperature also closely aligns with the temperature where the change in slope of the temperature curves occurs.

With the change in slope of the temperature lines explained we can continue to look at the effects of pressure on the temperature distribution we can look at the effects of increasing the contact pressure between the probe and the specimen to 480 kPa. A graph of the temperature distribution for the high contact pressure model can be seen in **Figure 40.**

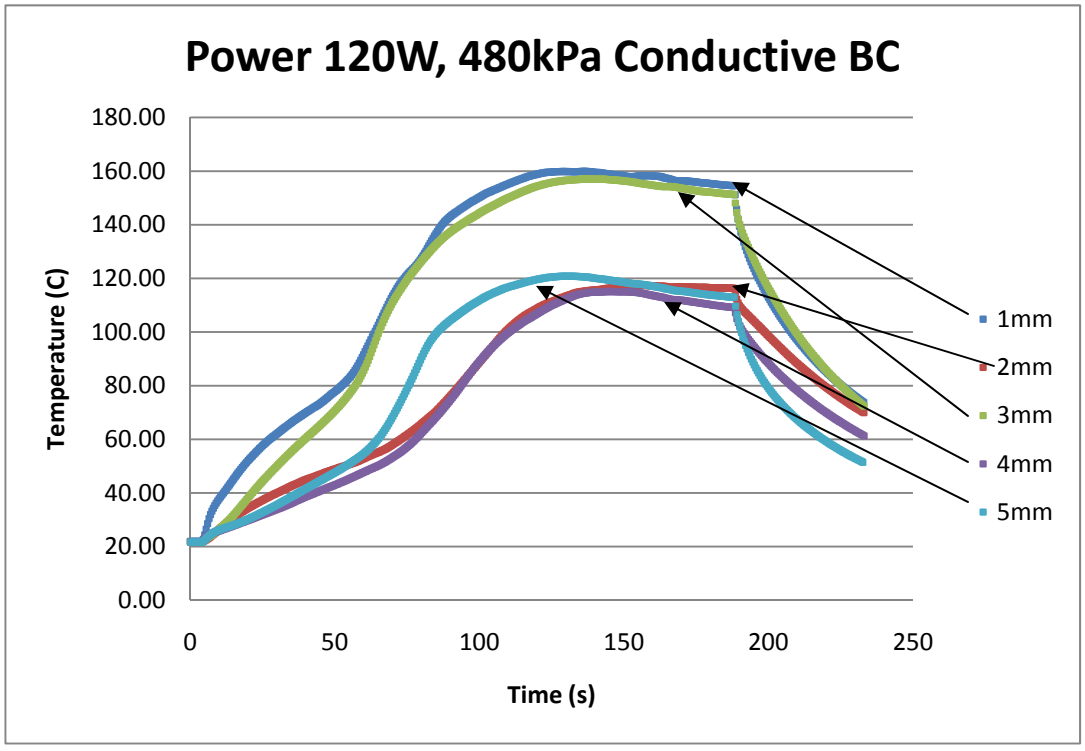

Figure 40: Temperature distribution in a nylon dog bone specimen a contact pressure of 480 kPa. Again, the bottom surface of the dog bone is subjected to a conductive boundary condition.

This same trend showed appeared in each of the three rounds of testing so it is not caused by imperfect bonding of the thermocouples to the nylon such as air pockets surrounding the thermocouples. It is not because of bad thermocouple beads because new beads were welded for each round of testing and the channels on the Agillent data logger were changed between rounds of testing. There could be some influence from where the probe was situated over the thermocouples; care was taken to make sure that the probe was in the exact same location at the start of each test. It also is not a function of the thermocouples shielding one another but because there is a difference in the thermal profiles between the conductive and convective boundary conditions we can rule out that possibility.

It is important to highlight some of the problems that can occur during the experiment and show what problems with the experiment look like. The main problem is probe shifting during the experiment; this can be seen in **Figure 41** by the abrupt change in the top thermocouple. The probe will sometimes shift to contact the samples with a very small area. At approximately the two minute mark the probe shifts and the coupling between the probe and the surface becomes much more efficient raising the temperature rapidly.

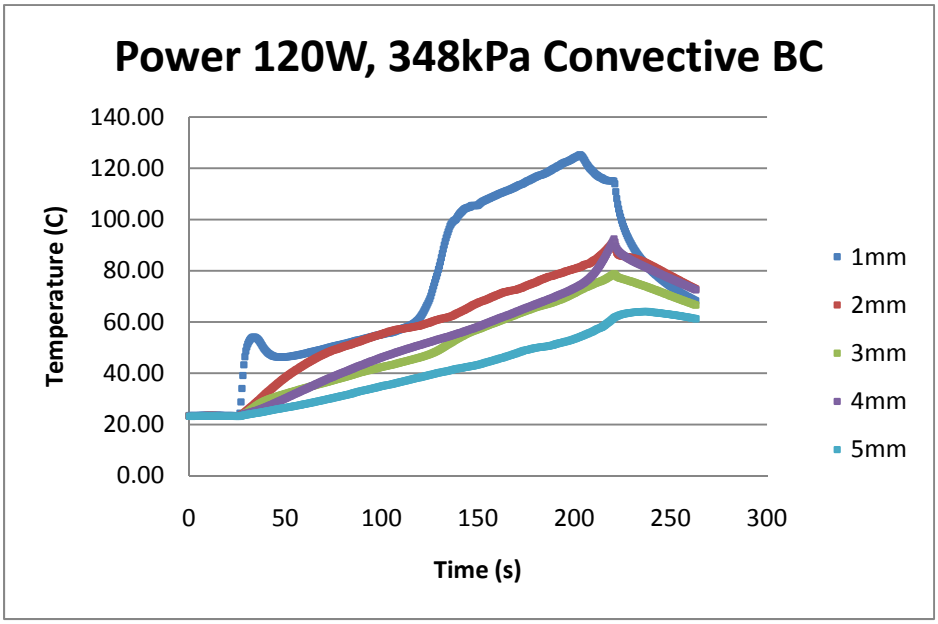

Figure 41: Temperature distribution in a nylon dog bone specimen with a 1.25 Kg weight added to the ultrasonic probe to increase the contact pressure between the probe and the specimen. The bottom surface of the dog bone is subjected to a convective boundary condition because it is suspended above the aluminum holder.

Another explanation for this change in coupling is because the sample is suspended above the aluminum holder and the sample is being heated beyond is glass transition temperature. When this happens the sample will begin to soften and possibly even sag allowing the probe to couple much more energy into the sample. The Convective boundary condition trials were performed to see if there was any significant difference between in the temperature profile by changing the boundary condition, and it turns out that although there is a change in the temperature distribution through the thickness of the sample there is little change in the overall temperature achieved in the sample between the two boundary conditions. The convective boundary conditions also proved to be much more prone to probe shifting as the sample softened during heating. The convective boundary condition was abandoned as a viable way to hold the samples

during treatment because of the problems obtaining consistent results during the thermal trials.

Then the thermal experimental results were ultimately used to determine the appropriate settings for healing it proved easier to have a hand on the ultrasonic probe to control the wobble and also by having a hand on the probe it could be lifted off as soon as any burning of the sample specimens was observed. It is not ideal to have human intervention in the process because it can introduce variance into the experiment, but working with the equipment available it turned out to be one of the best options. The application time of the ultrasonic energy and the pressure applied was kept as consistent as possible to achieve uniform results. The most important part of having intervention is if the probe suddenly shifts and starts to destroy the sample because as mentioned earlier burning will occur in the sample creating gas pockets inside the sample which will decrease the load carrying area of the sample.

Tensile Specimen Results

A few nylon tensile specimens were treated with the new ultrasonic probe stand in an attempt to achieve a more uniform ultrasonic treatment and corroborate the results obtained from the work of Sarrazin [21]. The samples were damaged with a razor cut 1.905 mm (0.075 in) deep through the thickness of the edge of the dog bone. The healed samples were treated on power level 3 (120 W) at the 480 kPa contact pressure setting for three minutes to make sure that the temperature of the samples reached the maximum temperature found in the thermal experiment. The displacement rate of the Instron was

set to 12.7 mm/min (0.50 in/min) which was the displacement rate used in [21]. The samples showed little external evidence of damage from the treatment, so the temperature achieved from the application of ultrasonic energy seems to be in line with the temperature found in the thermal experiment.

When examining the fracture surfaces of the healed specimens there was little evidence of melting that occurred at the crack tip or bridging the razor cut that would account for an increase in strain to failure or ultimate load, although there is convincing photographic evidence that there is a change in the properties of the nylon in the vicinity of the ultrasonic treatment. The ductile fracture zone in the treated samples is much larger than what is seen in the unhealed samples.

A graph of the tensile specimens is shown below. It can be seen that the tensile specimens that were ultrasonically healed outperform the untreated samples in most instances. There is not a lot of difference in the ultimate stress between the damaged and ultrasonically treated specimens, but the ultrasonically treated samples do seem to have short region where they behave in a perfectly plastic manner just before failure. There are some ultrasonically treated samples that fail early due to internal damage caused by the ultrasonic probe. A graph of the stress strain curves of the tensile samples is shown in **Figure 42**.

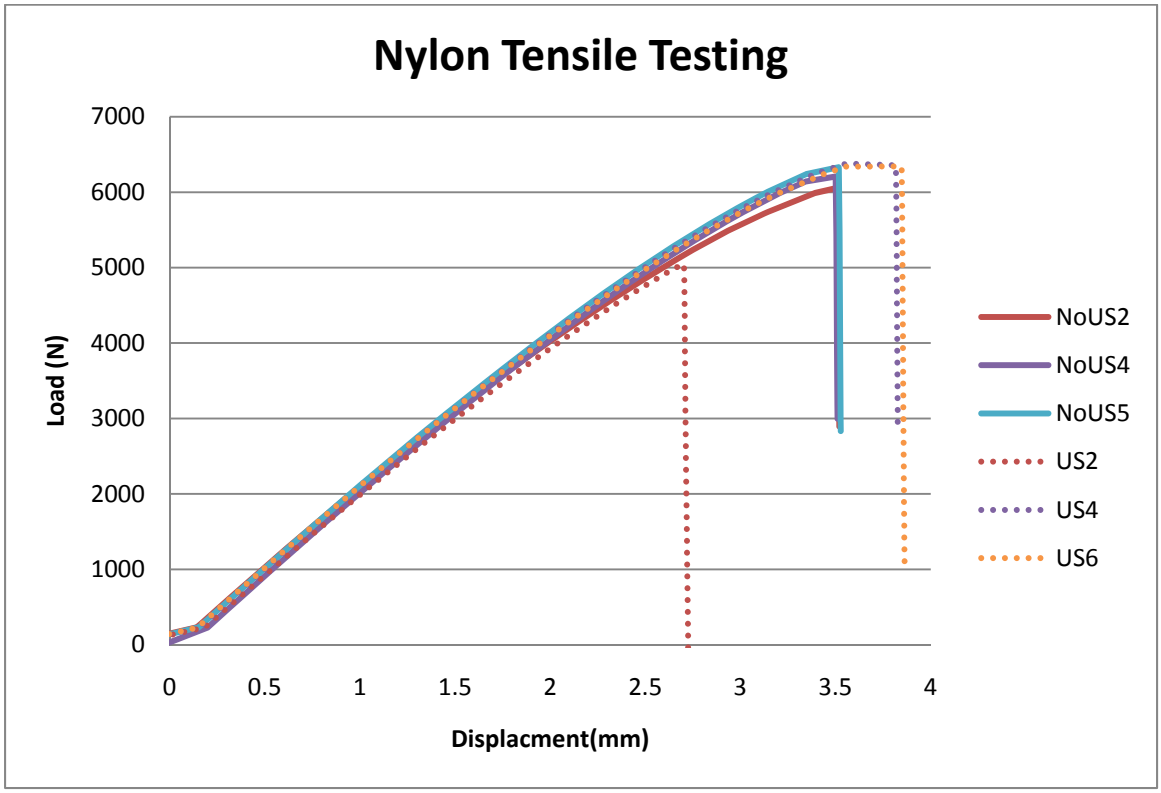

Figure 42: Results of tensile test specimens Two of the ultrasonically treated samples failed early, but the remainder of the ultrasonically treated samples outperformed the damaged samples (from F:Research/Nylon Damaged).

The solid lines in the plot are damaged samples, and the dashed lines are ultrasonically healed specimens. Not all of the samples are presented in the figure above for the sake of clearly presenting results. The first sample that was healed ended up being internally damaged so badly by the probe that it was excluded from the data set because it failed so early that it was not representative of the healing effect of the ultrasonic treatment. The exposure time was decreased to two minutes each to avoid damaging the samples. Two of the samples US2 and US3 had light damage caused by the probe and failed below the threshold of the damaged samples. The performance of all of the samples is compiled in **Table 6.**

Table 6: Comparison of damaged and ultrasonically healed Nylon dog bone tensile samples. The three specimens from each group with the highest strain to failure are chosen as a basis for comparison of average strain to failure between the two groups. F: Research/Nylon Damaged

Sample Name	Displacement to Failure (mm)	Percent improvement	Fracture Energy (J)	Percent Improvement
AVG of NoUS	3.47	--	12.0	--
US2	2.71	-21.9	7.17	-40.0
US4	3.83	10.2	14.2	19.3
US5	3.69	7.17	13.2	10.8
US6	3.86	11.04	14.4	20.5

It is difficult to control the exact length of exposure and the exact pressure applied by the ultrasonic probe because the Branson Sonifier is being used in a way in which it was never intended for. Slight amounts of overexposure of the samples can lead to superheating of the plastic and volatilization of the polymer creating gas pockets inside the specimen and thus canceling any healing effects of the treatment.

The final three ultrasonically healed samples showed significant improvement over the damaged samples. If the performance of these samples is examined, and compared to the average extension to failure of the unhealed samples there is an increase of around 10 percent in maximum extension. Additionally if the area under the curves is calculated using the trapezoid rule the fracture energy of the tests can be calculated and used as a metric to determine the effectiveness of the ultrasonic treatment. The trapezoid rule for discrete data sets is shown in **(5.**

$$\sum_{n=1}^{n-1}(x_{n+1}-x_n)\frac{f(x_n)+f(x_{n+1})}{2} \tag{5}$$

The average fracture energy of all of the unhealed samples is 12.0 J and when comparing this number to the fracture energy of the healed samples there is an even more pronounced improvement. The perfectly plastic behavior of the healed samples near failure increases the area under the curve significantly. This perfectly plastic behavior is likely caused because the prolonged exposure to a strain wave frees some of the polymer chains from one another, and once a critical stress is reached the chains can slide freely for a short time before the sample ultimately fails.

Photographs of the failure surfaces of the unhealed nylon dog bone samples are distinctly different from the damaged and ultrasonically healed surfaces. In the case of the non-treated samples seen in the left hand picture of **Figure 43,** a small ductile failure zone (the white parabolic shape) is seen and the rest of the beam has a failure surface indicative of a brittle fracture. In contrast, the ultrasonically healed samples in the right hand picture of **Figure 43** have a much larger ductile zone. This indicates that there is some change in the material properties of the nylon in the vicinity of the ultrasonic treatment. Note the damage caused by the ultrasonic probe in the healed sample, there is a small bubble along the top of the ductile fracture, if this damage becomes too prevalent the samples will fail early as seen in samples US2 and US3 because a significant load carrying area is removed from the samples.

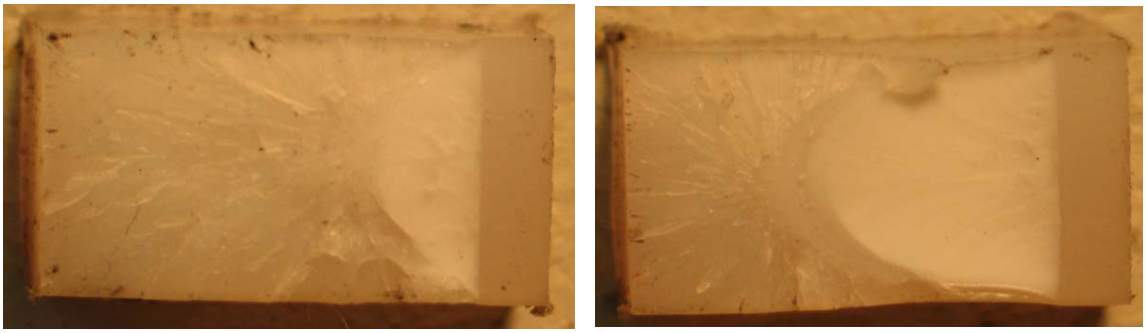

Figure 43: Failure surface of tensile specimens. Left: Untreated specimen, note the razor ct on the left side of the specimen and the plastic failure zone which is the white region. Right: Ultrasonically healed sample, note the large ductile fracture zone compared to the unhealed sample.

These failure surfaces can be correlated to what is seen in the stress-strain graph of the tensile specimens. Once the healed samples hit a critical stress the crack begins to run and the samples ultimately fail. The damaged samples fail immediately, but the healed samples hit a plateau and begin operating in a perfectly plastic manner for a short period of time before they too ultimately fail. This is an interesting and unexpected result that needs to be investigated further once the ultrasonic treatment process is refined to be consistently repeatable.

Note in **Figure 43** above that there is no evidence of any melting that occurred at either the crack tip or any bridging across the two surfaces of the razor cut. If there was some melting would be expected that the razor cut would no longer appear perfectly straight across the sample and or there would be some evidence of material being pulled apart across the two faces of the razor cut either near the tip of the crack or even possibly further back into the razor cut. Obviously there is some impact caused by the ultrasonic probe because there is a distinct change in the size of the ductile fracture zone, but none of these signs of melting are present. It was necessary to change some aspect of the

experiment so that melting across the damage could be observed. The first idea that came to mind was to devise a mechanical test specimen where the strain wave could be applied transverse to the crack direction and where the damage could be located close enough to the surface where the ultrasonic energy was intense enough to be able to cause melting at the depth of the crack and hopefully be able to weld the crack back together.

Transition to Transverse Wave Propagation

As a quick test of the transverse wave theory was conducted using small sections of nylon that were cut from old specimens on a band saw and damaged with a razor blade in the same fashion as the tensile specimens. The razor damage was intentionally placed near the top surface of the sectioned beam with the depth of the damage below the top surface ranging from 1mm (0.039 in) to 3mm (0.118 in). With the razor cut near the top of the sample and the weight of the probe applied across the razor cut as well as the ultrasonic energy propagating transverse to the crack it appeared that the crack was effectively closed and some healing by material bridging the crack surfaces could have occurred.

The amount of crack closure and healing that took place was determined using an optical microscope at various magnification levels to image samples pre and post ultrasonic treatment. The crack was imaged on all 3 sides of the beam and image locations were kept as consistent as possible between pre and post ultrasonic treatment using prominent features from the beam sections to help guide image alignment. Images from the side face one of the beam sections with razor damage 1mm below the surface

were taken with an optical microscope at 200X magnification. The images of the damage pre and post ultrasonic treatment are seen in **Figure 44**.

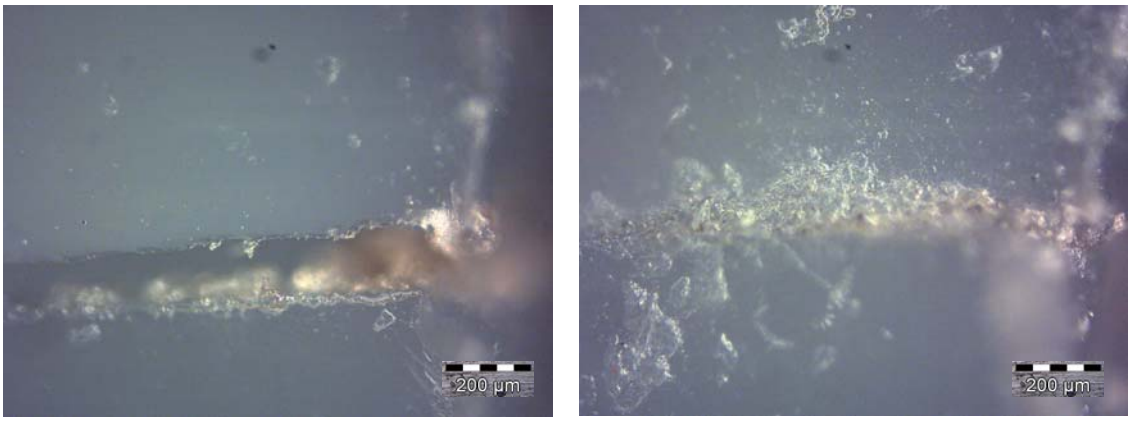

Figure 44: Side of initial Nylon transverse ultrasonic wave specimen. Left: Crack tip before ultrasonic treatment. Right: crack after ultrasonic treatment, note that the crack is closed and it appears some material may have melted and bridged the sample. Picture at 200X magnification.

The image of the sample before treatment is on the left and post treatment is on the right. Note that the crack is closed in the post treatment image and there appears to be some material that has bubbled out of the crack indicating that there may be some melting between the surfaces of the crack that has occurred. Images of the Front surface of the same specimen seen **Figure 45** do not show any signs of flashing or melted material spilling out from between the surfaces of the crack so the amount of melting that occurred across the surfaces of the crack is debatable. The crack is definitely closed in the post treatment picture on the left and the portion of the material between the razor cut and the top of the sample did not want to separate from the bottom part of the sample which indicates that there is some amount of melting occurring. No easy way of separating the top portion of the crack from the bottom was devises so another quick experiment was needed to demonstrate that bridging of the damage was occurring.

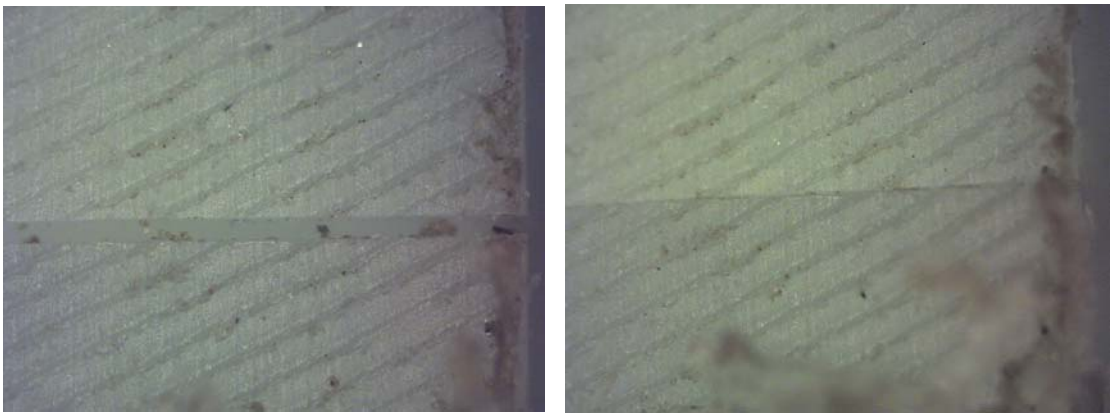

Figure 45: Front of initial Nylon transverse ultrasonic wave specimen. Left: Crack tip before ultrasonic treatment. Right: crack after ultrasonic treatment; note that the crack is closed no apparent flashing due to melted material has exited the razor crack. 50X magnification

Another simple experiment which consisted of welding pieces of plastic cut into various thicknesses onto thick substrate pieces also showed mixed results for the nylon pieces because nylon is a very slippery material and it is hard to achieve good adhesion of nylon to itself using an ultrasonic welding process. Chunks of PVC showed much more promise, the thin strip would become soft and pliable and harden onto the substrate, so it was determined that PVC could be a good candidate for further testing. In addition to its promising response to ultrasonic energy PVC is a common engineering plastic that often sees use in structures.

Results of Four Point Bend Configuration

T-slot Four Point Bend Configuration

The main material used for this set of tests was polyvinyl chloride (PVC). This material was chosen because of its common use in structures and an abundance of scrap material that was available for making test specimens. The test specimens proved to be

remarkably tough and able to withstand up to 7.5 percent strain at the slow strain rate recommended by ASTM 6272-02. So the first step was to see if it was possible to make the material fail within the constraints of the four point bend apparatus. The displacement rate was increased to 50.8mm/min (2 in/min) in an attempt to minimize any viscoelastic effects that may be present.

The samples still did not fail at room temperature even with the increased displacement rate and in fact there was little difference in either the stiffness or the ultimate load carried by the T-slot samples. Hence, a scheme to increase the stiffness in order to reach the ultimate stress and fail the samples was to drop the temperature using a thermal bath first to 0°C, then to -15°C. The load displacement curves for the initial T-slot trials conducted to demonstrate the temperature dependent and rate dependent response of PVC are shown in **Figure 46**.

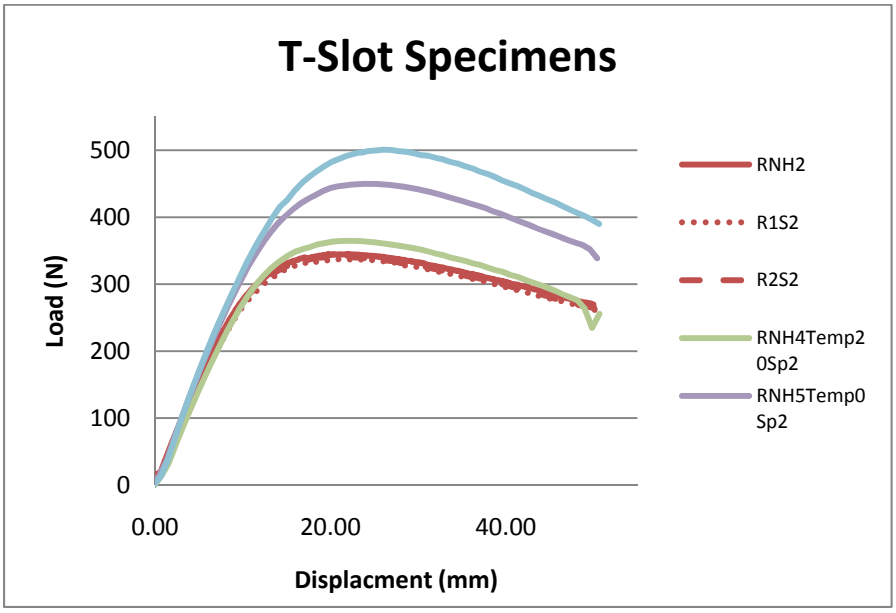

Figure 46: Load displacement curves for PVC T-Slot samples. The ultimate load and thus the stress in the samples increases as the displacement rate increases and the temperature decreases.

Increasing the displacement rate has little effect on the ultimate load experienced by the PVC during the test and the sample still did not fail within the maximum stroke of the four point bend apparatus, that is, 50.8 mm (2 in). (If the tests continue any further the sample will bottom out on the base plate of the four point bender). It can be seen that sample *RNH4Temp20SP2,* which is a sample tested at room temperature at a speed of 50.8mm/min (2 in/min), is barely above the room temperature samples tested at the slow speed recommended by ASTM 6272-02 which is roughly 6mm/min. Decreasing the temperature of the samples by 20 degrees has a much more significant impact on the ultimate load experienced by the samples. A comparison of the percentage increase in ultimate load is summarized in

Table 7.

Table 7: Summary of Rate and Temperature effects on PVC T-slot four point bend specimens

Sample Description	**Ultimate Load (N)**	**Percentage Load Increase to Room Temperature**
Temperature: 20^{o}C Rate: 0.2417 in/min	344.7	--
Temperature: 20^{o}C Rate: 2 in/min	364.8	5.80
Temperature: 0^{o}C Rate: 2 in/min	450.0	30.55
Temperature: -15^{o}C Rate: 2 in/min	500.1	44.15

The PVC still was not at a temperature low enough to cause failure in the test specimens, and the chillers available were not capable of temperatures below -15^{o}C so

dry ice was used to drop the temperature down to -78.5^{o}C. The lower working limit of PVC is shown in **Table 5** is -30^{o}C so the dry ice is significantly below the lower working temperature recommended for PVC and resulted in the material behaving in a brittle manner. As can be seen in **Figure 47** the samples fail at approximately 12.7mm (0.5 in) displacement. One challenge of needing the samples to be at an extremely low temperature is making sure that they remain cold throughout the process of the test. If the slow displacement rate of 6.14 mm/min (0.2417 in/min) was used, the samples would warm up considerably during the test and defeat the purpose of cooling the samples in the first place. So the displacement rate was increased to 25.4 mm/min (1.00 in/min) so that the samples would break before they had a chance to warm up. All of the samples failed within 30 seconds of being removed from the cooler and were still cold to the touch after the test was finished.

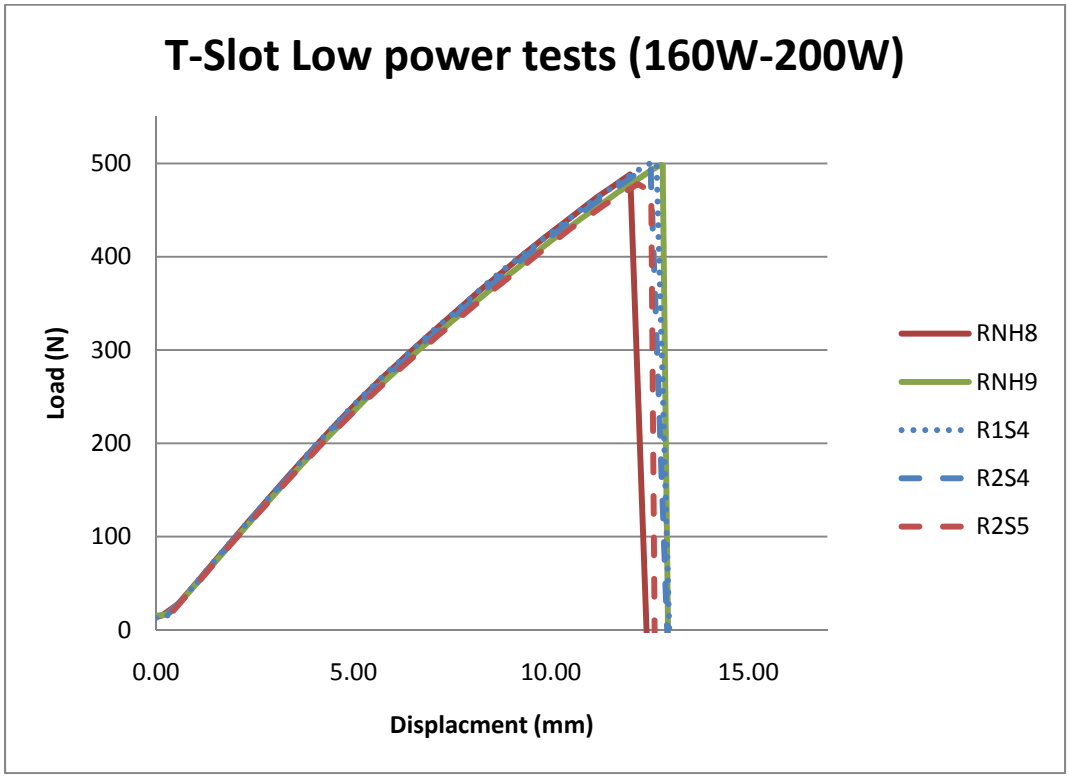

Figure 47: Cold Temperature trials of PVC. Solid lines Indicate damaged but unhealed samples. Dotted lines are samples with healing on only one side at power levels 4 and 5(160W and 200W respectively). Dashed Lines are samples with healing on both sides at power levels 4 and 5.

All of the samples in **Figure 47** have a razor cut on both sides of the specimen and the differences between the groups is the number of the damage sites that are healed. One of the unhealed samples was tested at 50.8mm/min (2 in/min) displacement rate to investigate the effects of rate of displacement but it failed quickly so it was decided that all of the other samples in this group are tested at a slower rate of 25.4mm/min because the slower rate gave a slightly slower failure. All of the samples failed close to the same ultimate displacement so for comparison average displacment to failure and fracture energy of each of the test groups is compared in **Table 8**.

Table 8: Summary of sample maximum strain performance compared to the average maximum strain of the unhealed samples.

Sample Name	Power Level	Displ. to Failure (mm)	Percent improvement	Fracture Energy (J)	Percent Improvement
AVG of NoUS	--	12.43	--	3.46	--
R1S4	4 (160 W)	12.68	2.04	3.63	5.17
R1S5	5 (200 W)	11.74	-5.5	3.13	-9.27
R2S4	4 (160 W)	12.53	0.85	3.54	2.61
R2S5	5 (200 W)	12.53	0.88	3.40	-1.63

The improvement in the average displacement to failure of either of the healed groups is not statistically significant because it is so close to the average strain to failure of the unhealed samples. The power level may not have been high enough in the low power trails to have effective healing of the razor damage site so far below the outer surface of the beam. The majority of the samples showed fracture surfaces starting at the razor damage and propagating across the beam. But we have postulated that crack tip blunting occurs when ultrasonic energy is applied so we want to shift the damage initiation point away from the razor damage and to the secondary stress concentration point, which is the corner of the band saw groove.

In order to see if it was possible to achieve healing at the damage depth the power was increased. The flaps near the surface do not cary any load so it does not matter if substantial burning occurs on the oute lip of the T-slot. The load displacment curves for the high power treatment test specimens are shown in **Figure 48**. Carefull comparison of **Figure 47** to **Figure 48** will reveal a different displacment to failure between the two trials (x-axis), this is because in the first set of trials two large bricks of dry ice were purchased and the samples were sandwitched between the blocks. In the second test only

one block of dry ice was purchases to save money, and the samples were placed ontop of the dry ice and covered by a polystyrene lid that fit closely over the samles. In both cases the samples were allowed to cool on the dry ice for nearly an hour, but there are still some differences between the two trails and it is likely because the samples in the second trial were slightly warmer than the first set. This discrepancy is taken care of because a new set of unhealed samples were tested to insure a baseline for comparison in the high power test samples.

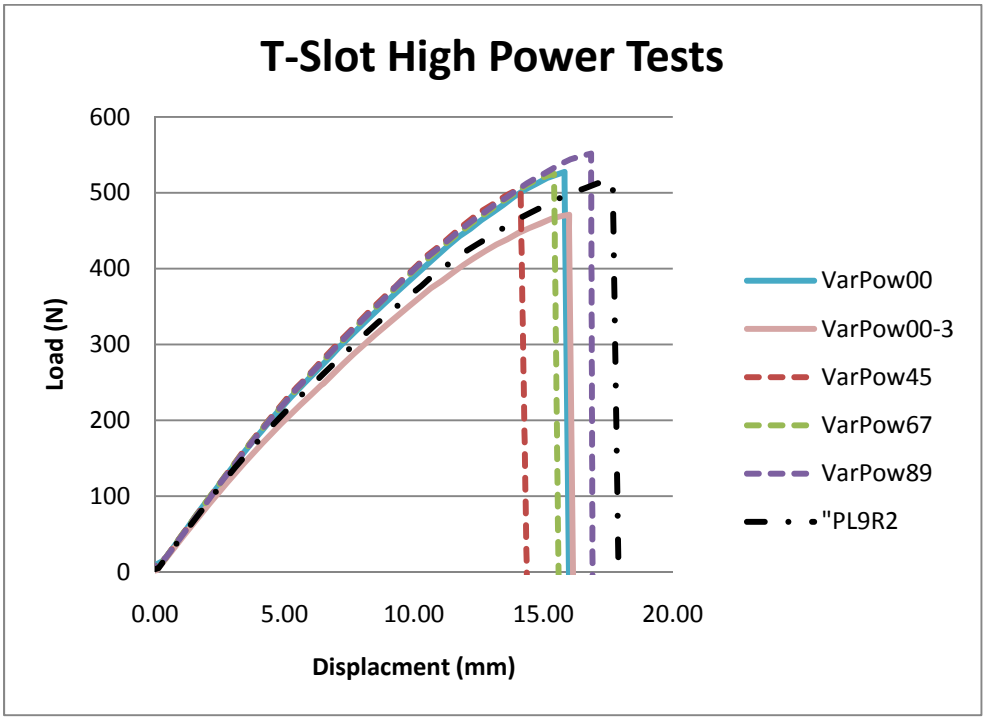

Figure 48: Cold temperature performance of samples treated at high power level settings. Samples with two numbers after the name indicate the two power settings used, one on each of the damage locations.

There is a trend apparent that as the power increases the ultimate strain to failure also increases. The lowest performing healed sample is VarPow45 which had one

damage location treated with power level 4 and the other treated with power level 5. The sample called VarPow67 nearly matches the performance of the unhealed samples, and the samples healed with power levels 8 and 9 outperform the unhealed samples by a significant margin. The performance of each of the healed specimens is recorded in

Table 9, and the maximum displacement is compared to the average maximum displacement of the unhealed samples. In the power level column the two numbers indicate what each of the damage locations were treated with, some have different power settings for the two sides.

Table 9: performance of Healed Cold temperature samples compared to average of unhealed samples.

Sample Name	Power Level	Displ. to Failure (mm)	Percent improvement	Fracture Energy (J)	Percent Improvement
AVG of NoUS	--	15.22	--	4.38	--
VarPow45	4 , 5	14.13	-7.15	4.11	-6.17
VarPow67	6 , 7	15.41	1.30	4.73	7.94
VarPow89	7 , 8	16.84	10.71	5.49	25.33
PL9R2	9 , 9	17.69	16.4	5.72	27.24

It is clear that as the ultrasonic power applied to the test specimens increases the performance of the healed samples also increases. It is not entirely obvious why this occurs because at the higher power settings there is significantly more damage to the outer layer of the sample that is in contact with the ultrasonic probe. In order to try to understand why there was an increase in strain to failure the failure surfaces were examined and the samples were cross-sectioned and polished to try to see how deep the

ultrasonic treatment was penetrating into the samples. Cross sections of some of the low power treated samples were compared to the high power treated samples. Photographic evidence reveals that in the low power settings (160W-200W), there is burning near the surface that was often in localized pockets which were not always over the damage location; in the high power settings (320W-360W), the burning is much more systemic. Pictures of some of the cross sections of the PVC are shown in **Figure 49**.

Figure 49: Damage caused by ultrasonic probe operating at various power levels. Left: Power Level 4 (160 W) generally localized damage not always over crack location. Right: Power Level 8 (320 W), higher power settings cause more wide spread damage.

There did not seem to be any ammount of healing at the low power setting of 4 and 5 because of the generally locallized burning near the surface of the samples. In the high power treatment the burning on the surface is much more wiede spreead but generally not any deaper than in the low power settings. Fortunately the burning on the surface of the T-Slot samples is not detremental to the mechanical performance of the specimen because the small outer portion of the T-slot band saw groove carries no load so if this section incurs significant damage it will not be a problem. Finite element

modeling at the end of this section shows the stress distribution in the samples. Unfortunately, there is little evidence –other than the burned areas—to indicate a thermal process occurred near the crack tip at any ultrasonic power setting.

It is thought that because of the burning that occurs at the surface the majority of the ultrasonic energy is quickly dissipated and very little energy reaches the depth of the damage and cannot heal the samples that are treated at low power settings. All of the samples treated at power level 4 and 5 failed at the razor damage site. Two typical failure surfaces of low power samples as can be seen **Figure 50.**

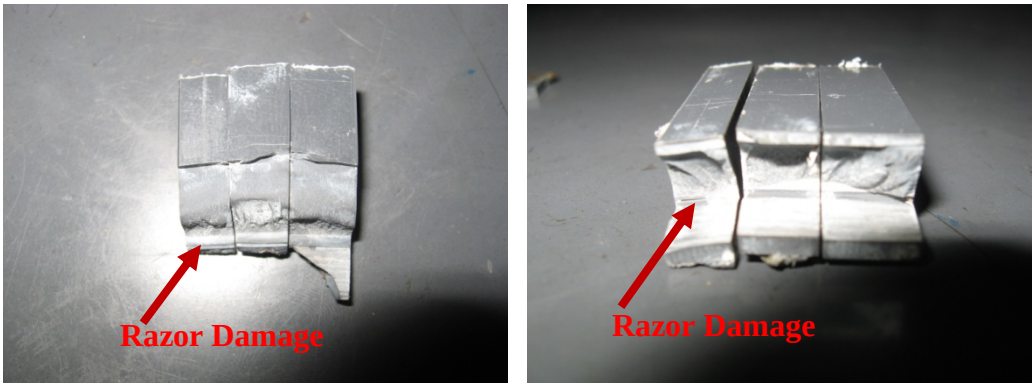

Figure 50: Failure surfaces of low power treatment. Left: power level 4 (160 W), notice that the sample failed at the razor cut which is the flat surface at the bottom of the sample. Right: power level 5 (200 W), also failed at the razor cut location although it is difficult to tell because of the way the failure surface is angled.

At the low power settings, failure occurred that the razor damage site which suggests that there was no blunting of the crack and it is evident from the images that there was no melting whatsoever across the surfaces of the cracks. At the higher power levels there is some evidence to suggest that there is some cross crack melting such as burn marks that penetrated through the top lip onto the bottom of the band saw cut slot,

the problem was the areas that showed evidence of deep penetration of the ultrasonic energy were extremely localized and would not be able to adequately weld the upper portion of the T-slot flap to the bottom of the band saw groove. Higher power settings showed that samples tended to fail at the root of the band saw cut rather than at the crack tip. The band saw cut is slightly further toward the center of the sample so it is further away from the ultrasonic energy. **Figure 51** shows the failure surface of sample VarPow67 treated on power level 6 and VarPow89 treated on power level 9. Notice that the power level 9 surface did not fail at the razor cut and the power level 6 surface still failed cleanly at the razor location.

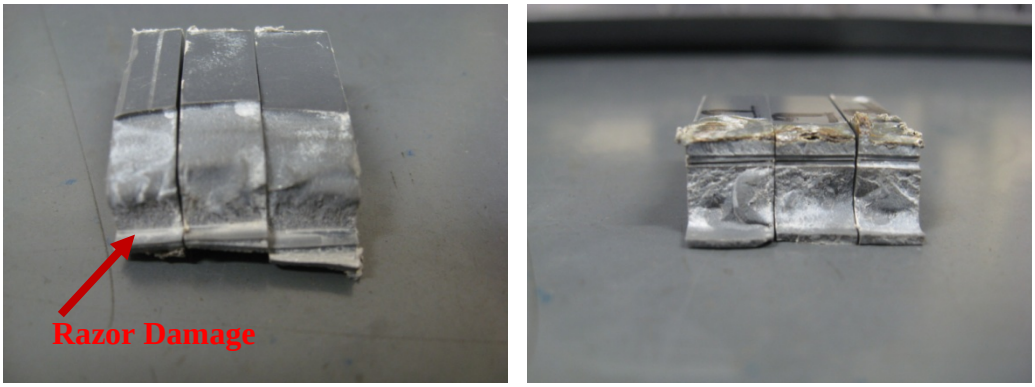

Figure 51: Failure surfaces of high power treatment. Left: power level 6 (240 W), notice that the sample failed at the razor cut which is the flat surface at the bottom of the sample. Right: power level 9 (360 W), did not fail at the razor cut; there may is likely some amount of healing that occurred at the crack tip.

The Instron did not record the best performing sample unfortunately because of a software malfunction but the maximum displacment to failure of sample PL9R1 was recorded by hand as 0.8 in. Both damage locations of this sample were treated at power level nine and the failure surface of the sample are shown in **Figure 52**. It should be

noted that the samples failed at both damage locations, one is side is where the primary failure occurs, and the other side is a secondary failure likely caused by a brittle spring back of the material.

Figure 52: Failure surfaces of PL9R1(360 W). Left: original failure side, notice the ductile failure zone above the razor cut, the failure does not start at the razor. Right, secondary failure side cause by brittleness of material. Notice that the secondary failure does not follow the razor cut the whole way across.

The T-slot samples did not fail entirely as designed, they failed on one side at the razor cut then at the root of the band saw cut on the other side when they bounced off of the bending apparatus after the initial failure. It was hard to predict the failure pattern of these samples and the plastic was too tough for the crack to propagate in mode two at room temperature. The samples were not ideal because there were two significant stress concentrations near the same spot and at cold temperatures when the material was brittle the failure surface could jump from one stress concentration point to the other part way through the beam as can be seen in **Figure 52**.

Scanning Eelectron Microscopy (SEM) images of the crack tip obtained by cross sectioning samples and polishing the sectioned surfaces were taken to try to determine if

any crack tip blunting occurred due to the ultrasonic treatment. In **Figure 53** images of the crack tip of an unhealed specimen are shown. In the images the top image is at 1000x magnification, the bottom image is at 3000x magnification. Notice that the crack tip is sharp and well defined in the unhealed samples.

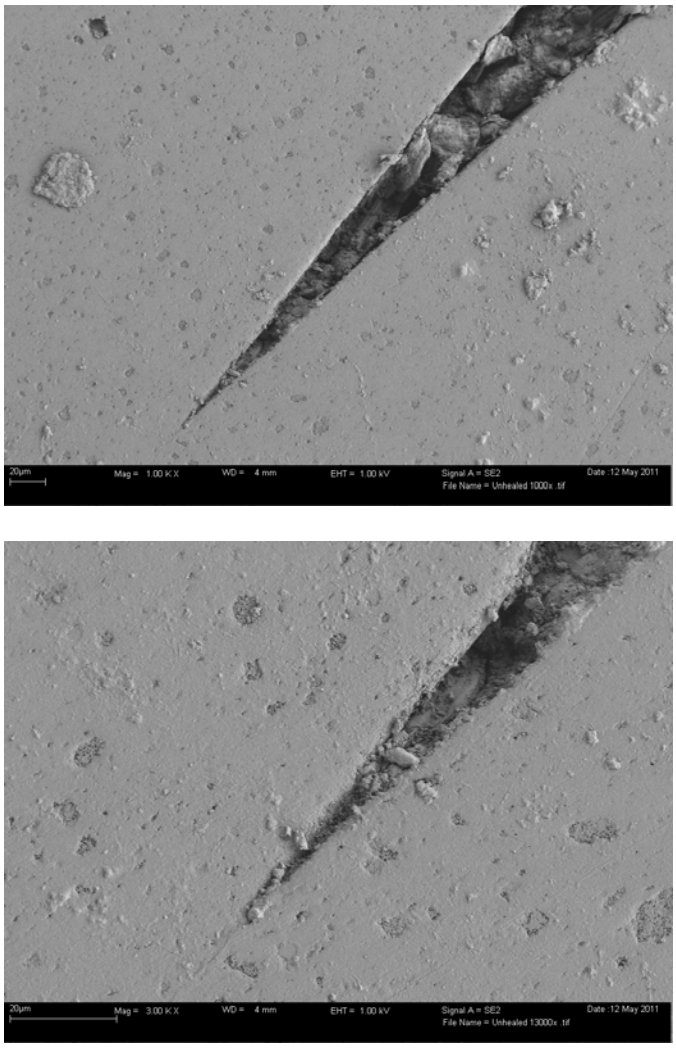

Figure 53: SEM images of an unhealed specimen. Notice the clearly defined Sharp Crack.

It was necessary to compare the unhealed specimens to an ultrasonically treated specimen to determine if there was any crack tip blunting. Images were again taken at 1000x and 3000x magnification. **Figure 54** shows that the crack is closed compared to

the unhealed samples. The crack tip may be blunted slightly, but the more obvious healing is that the crack is closed. Additionally, it looks like there may be some amount of melting across the crack tip because the material that is filling the crack is not nearly as granular as in the unhealed images. It is difficult to say, but it appears that the crack is filled at least partially with continuous material and the crack tip does appear to be slightly rounded when compared to the unhealed samples.

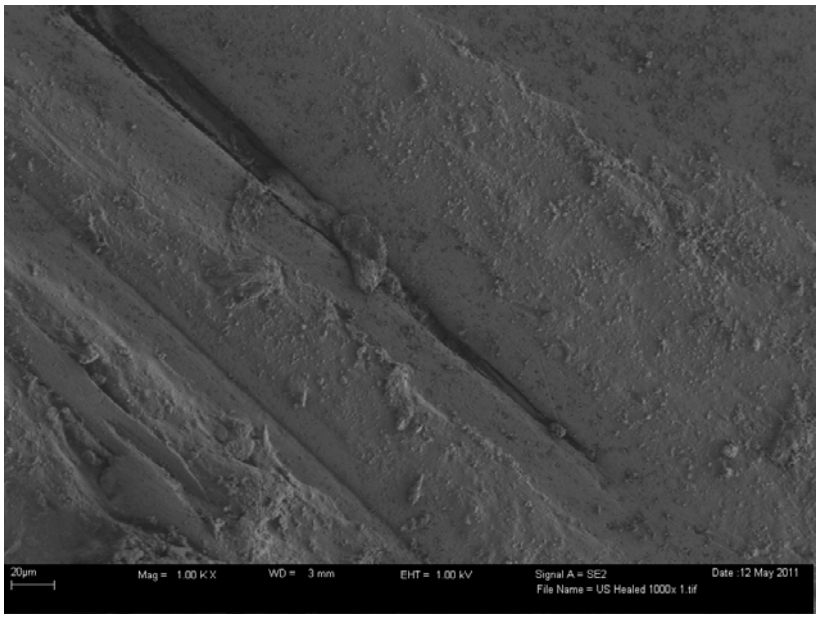

Figure 54: Ultrasonically healed PVC specimen treated with power level 9 (360 W). notice that the crack tip appears to be blunted slightly. The 3000x image (bottom) shows a slightly rounded tip when compared to the unhealed images.

Ultimately, the T-slot samples were difficult to deal with because they needed to be cooled which caused them to behave in a brittle manner. Even with SEM imagery showing a slight amount of crack tip blunting, the performance gains were not what was hoped for. A sample with a more sensitive damage orientation was needed so that cooling the samples could be avoided. Also a more clearly defined stress concentration was needed so that the fracture path was more defined. The samples that resulted are the single notch bend samples presented in the next section.

Results of Single Notch Four Point Bend Specimens

Although the crack configuration in the mod one propagation orientation does not lend itself to transverse wave propagation the crack oriented to open in mode one is much more sensitive to the stress applied in the bending test. Several plastics were investigated

for use in this test including acrylic and polycarbonate. A brittle plastic was desired so that the samples would fail within the stroke of the bending apparatus, and a plastic that did not burn as much as the PVC was also desired.

Acrylic proved to be too brittle to damage with a razor, and any significant penetration of the razor into the sample would cause the polymer to fracture all the way through the beam. The polycarbonate had the best combination of properties sought for the testing. The power level and application time of the ultrasonic probe were experimentally determined with scrap material. The best combination of parameters that allowed operating the probe for a significant length of time without causing burning to the samples was determined to be as follows. A contact pressure of 480 kPa and a power level of 5 applied for approximately 20 seconds per location proved to be the best combination of parameters. Lower power settings and contact pressure did not show any significant amounts of melting across damage areas. Higher power settings caused the samples to be susceptible to burning.

The bending apparatus was set to a support span of 177.8 mm (7 in) and the displacement rate of the Instron was set to the ASTM recommended 6.14 mm/min. Virgin samples of polycarbonate beams were extremely tough and did not fail in the four point bend test within the 50.8 mm stroke of the bending apparatus. Samples were damaged with a 1.27 mm razor cut in the bottom of the beam. Healed samples did show significant melting across the crack opening. Some samples melted across the crack so completely that the damage location was barely detectable except for some surface

melting over where the crack opening used to be. **Figure 55** shows the test results of the Single notch bend specimens.

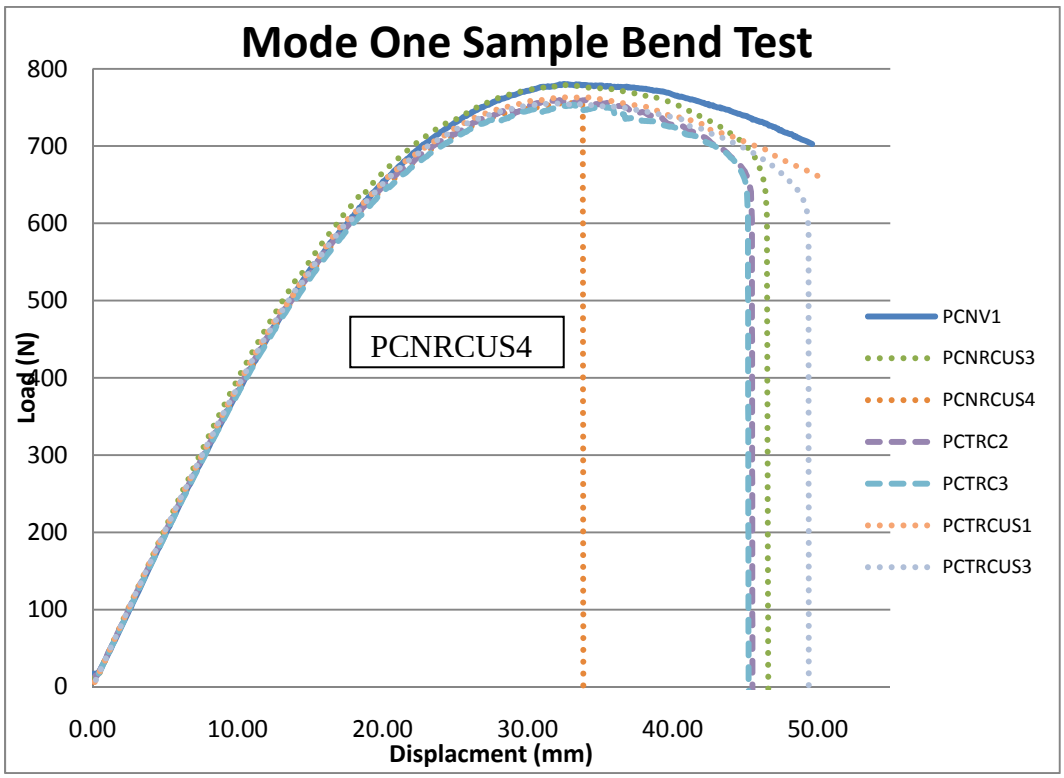

Figure 55: Single notch bend sample test results. Solid lines are virgin specimens with no damage. Dashed lines are damaged samples. Dotted lines are ultrasonically healed samples. The majority of healed samples outperformed the damaged samples.

In **Figure 55** the solid lines are virgin samples which carry the highest load of all the samples tested and show no sign of imminent failure even at the maximum extent of the test. Damaged samples are represented by dashed lines and did not fail until an average of 44.7 mm displacement was reached. This is very close to the maximum displacement of the bending fixture, but the healed samples were tested as well to try to see if the ultrasonically healed samples showed any improvement in mechanical performance. The healed samples are represented as dotted lines and the vast majority of

the samples outperform the damaged samples. There were a few notable exceptions including sample PCNRCUS4 that failed extremely early when compared to the damaged samples. **Table 10** lists the performance of each of the tested specimens including ones omitted from **Figure 55** for clarity.

Table 10: Summary of testing of single notch bend healed samples compared to average performance of unhealed samples.

Sample Name	Max Displ. (mm)	Percent Diff	Energy (J)	Energy Percent diff	Comments
Avg. of NH	44.70 (in)	--	25.17	--	--
PCNRUS2	50.14	12.1	28.96	15.02	No Fail
PCNRUS3	46.51	3.83	27.21	8.10	
PCNRUS4	33.80	-24.04	17.21	-31.65	Light Treatment
PCNRUS5	23.04	-48.45	9.71	-61.44	Light Tratment
PCNRUS6	50.08	12.1	28.54	13.34	No Fail
PCTRUS1	50.15	12.1	29.22	16.08	No Fail
PCTRUS2	49.60	12.1	28.55	13.41	No Fail
PCTRUS3	49.37	9.96	28.45	13.02	

The early failure of the healed samples is due to ineffective ultrasonic treatment where there was not enough melting in the vicinity of the damage to heal the sample. The samples did melt across the crack opening but the layer was extremely thin. When the samples with light treatment were loaded in bending the samples reached a point when the thin ligament that had melted across the crack opening suddenly failed. This sudden rupture caused an abrupt brittle failure of the samples. The brittle failure was caused because the load the the ligament had been carrying was suddenly transferred into

the beam toward the crack tip and the displacement increased suddenly as well transferring a sudden shock to the crack front which quickly propagated across the sample causing brittle failure.

The majority of the samples outperformed the damaged samples in the displacement to failure by at least 12 percent. Further increases were not able to be seen because the samples would bottom out on the bending apparatus. Many of the healed samples did not fail within the available stroke of the test so it is possible that they could have seen additional increases in the maximum displacement. The energy of the healed samples is generally around 1percent more energy to cause failure than the unhealed samples.

Melting across the crack tip is an effective treatment, but given the equipment available the effective melting of the crack front is difficult. The sample melts closer to the ultrasonic probe first then works its way down through the sample forming a ligament that bridges the crack near the surface but does not always get the crack front. This can be seen in **Figure 56**. Eventually the ligament will fail and transfer the load to the crack tip increasing the stress at the crack tip to the failure stress which leads to failure of the samples.

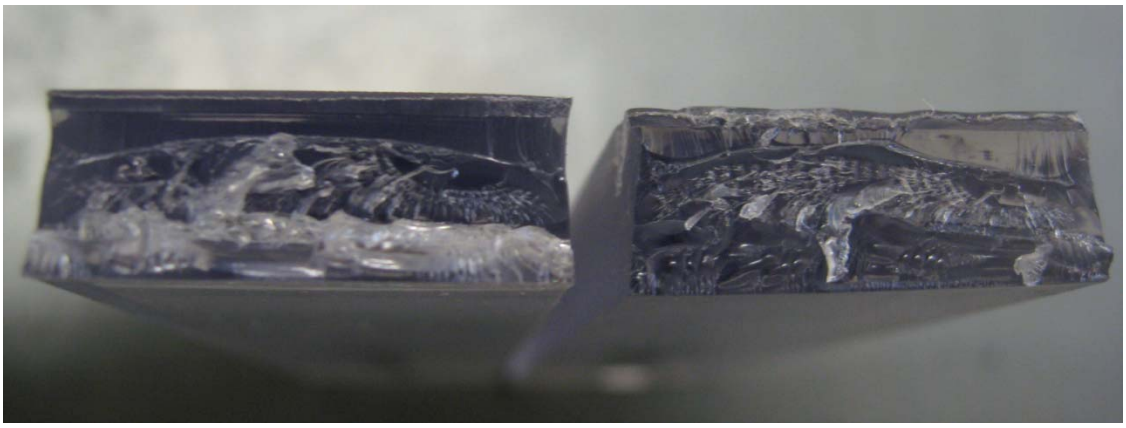

Figure 56: Failure surfaces of polycarbonate specimens. Left: Unhealed specimen with clean razor cut on the top of the sample. Right: Ultrasonically healed specimen, where the razor cut is no longer clean because the material has melted. and bridged the damaged section.

Notice in the picture above that the sample on the left is unhealed and the razor cut is clearly defined at the top of the beam, there is a nice straight line across the top of the beam approximately 1mm down into the beam. In the picture on the right the crack front can clearly be seen in parts of the beam, but the top portion of the razor cut is distorted. This distortion is from a ligament formed on the outer part of the beam due to melting of the material. The ligament eventually pulls apart and leaves a pattern that is due to crazing as the ligament fails.

This healing method is clearly working, but the problem with the long samples is that the bending apparatus runs out of room to break the samples so the full extent of the healing cannot be characterized. A slight modification was done to allow the samples to be broken more effectively. The specimens were shortened to half the length of the original samples to increase their stiffness and allow them to break in a shorter stroke.

Results of Short Single Notch four Point Bend Specimens:

The short specimens were half the length of the original specimens so this series of tests is a significant departure from the recommended thickness to support span ratio recommended by ASTM. The rate was set at 3.05 mm/min so that the displacement rate could be kept within the ASTM recommendation for the displacement rate. The bending fixture was shortened to a support span of 76.2 mm to accommodate the 105.4 mm long beams.

The ultrasonic treatment for the short samples was identical to the longer polycarbonate samples. The power level of the Branson Sonifier was set to 5 and applied to each location along the width of the beam for 20 seconds with a pressure of around 480 kPa. This combination of power level and application pressure and time proved to be an effective treatment for the material. The purpose of the short test is to be able to fail the healed samples within the available stroke of the bending apparatus, so the treatment was kept constant between the two tests.

The shortened samples were much stiffer than the long samples and as a result the healed samples broke well within the available stroke of the bending apparatus. The maximum stroke of the apparatus was 15 mm until the specimen began to hit the side of the support t arms. All but one of the healed samples failed within the limits of the bending apparatus. **Figure 57** shows the load displacement data for the short Single notch bend samples.

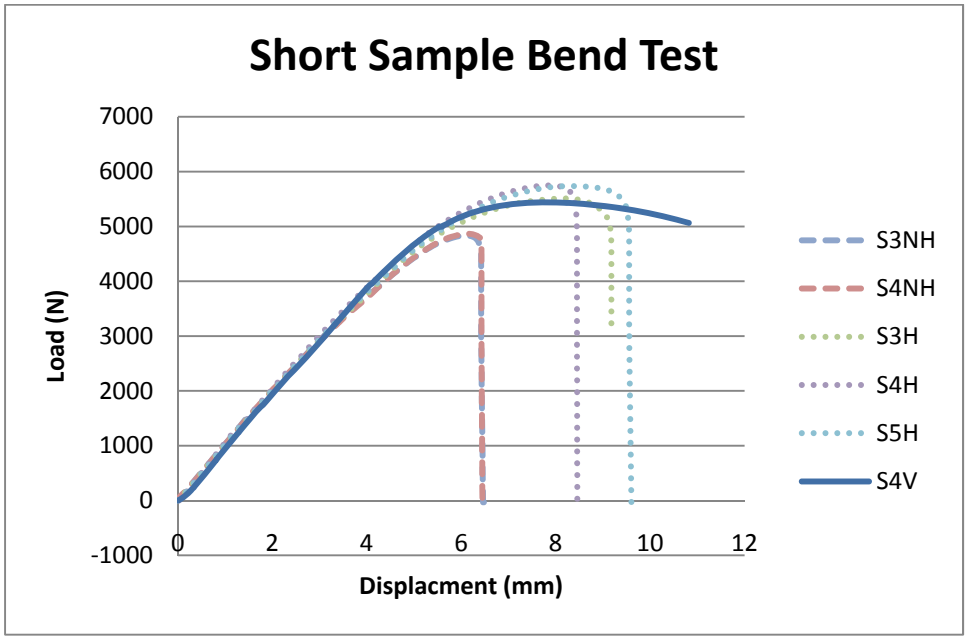

Figure 57: Bend Test results of Short Single notch bend samples. Solid line represents virgin specimens with no damage. Dashed lines are damaged samples with 1.27 mm razor cut in beam. Dotted lines are ultrasonically healed samples.

A number of the samples are removed from **Figure 57** for clarity, the figure accurately represents the trends of the virgin, damaged, and healed samples. The virgin samples once again showed no sign of failing within the limits of the bending apparatus. In fact, one of the samples was run to the limit of the bending frame and the sample made contact with one of the support arms causing failure of the frame because it put a moment on the loading arm and sheared the hardened steel pins that attached the support arms to the base plate of the bending apparatus.

The damaged samples all failed consistently at 6.45 mm displacement. The healed samples all outperformed the damaged samples because an effective treatment method for this material had already been established with the previous round of testing. The performance of all of the short samples tested is listed in **Table 11**.

Table 11: Summary of performance of Short Single notch bend healed samples compared to average performance of unhealed samples.

Sample Name	Max Displ (mm)	Percent Displ. Diff	Energy J	Energy Percent Diff	Comments
Avg. NH	6.44	--	19.73	--	
S1H	8.32	29.1	26.01	31.77	
S2H	10.22	58.65	34.73	76.01	No Fail
S3H	9.18	42.4	33.93	71.92	
S4H	8.45	31.1	30.99	57.03	
S5H	9.56	48.3	36.83	86.58	

The healed samples show a major improvement over the damaged samples consistently in the range of 30 percent improvement because there was plenty displacement available to the bending fixture beyond where the damaged samples failed to test the limits of the healed specimens. The samples were effectively treated with ultrasonic energy, and the outer surface of the samples over the crack opening was melted into the crack to bridge the damage. The energy required to fracture the healed samples is significantly more than that required to fail the damaged samples. Increases in energy were generally more than a 50 percent increase when compared to the average fracture energy of the damaged samples.

Because the bending fixture for this round of testing deviates significantly from the ASTM recommendation s for geometry of the bending fixture in relation to the geometry of the specimen the results may not be able to be directly compared to the longer Single notch bend specimens. There could be end effects caused by the bending fixture that change the response of the samples compared to the fixture with a larger

support span. The finite element modeling did reveal that the ultimate stress at failure at the crack tip between the two models was almost identical, so we can say with some confidence that the short samples is a reasonable representation of the increase in performance that could be expected in some of the longer single notch bend specimens that did not fail within the limits of the bending fixture.

6. CONCLUSIONS

Ultrasonic waves have been shown to effectively be able to heal polymeric materials. The Thermal experiments were done to determine the power level and coupling pressure effects of the temperature profile in nylon-66 dog bone specimens. It was found that higher pressure levels allowed better coupling of ultrasonic energy into the samples. The highest pressure tested was 480 kPa was found to be the best for raising the temperature in the sample close to the melting point of the plastic, and it was used for all mechanical testing performed in the thesis.

The temperature profile in the specimens was quite complex and it proved difficult to model with finite element analysis, but the goal of the thermal experiments was never to model the physical process that occur in the sample and cause the complex temperature state. Instead the Power level and pressure settings were used to try to increase the mechanical performance of the nylon tensile specimens. Power Level 3 (120 W) with an application time of two minutes and a pressure of 480 kPa were used to try to increase the performance. Any weight added to higher power settings melted the samples and tended to cause massive internal damage to the samples because of volatilization of the plastic when it was super heated inside the dog bone specimen.

Even though the temperature seen in the samples is below the 80% of melting temperature recommended for welding applications, the maximum temperature in the sample of 160^{o}C—which is 60% of the melting temperature—was maintained for a period of time much longer than in normal welding applications. This is essentially a form of annealing process that is performed on the beam and there is an increase in the

mechanical performance of the healed samples. Table 12 summarizes the results seen in the mechanical testing.

Table 12: Summary of ultrasonic power settings and percent increase in the mechanical performance of the healed specimens for each test.

Experiment name	material	Power Level	Exposure Time	Displ. Percent increase	Energy Percent Increase
Tensile Test	Nylon-66	3 (120 W)	120 s	~9%	~18%
T-Slot Bend	PVC	9 (360 W)	5 s	~10%	~15%
Mode 1 Bend	Polycarbonate	5 (200 W)	20 s	12% +	%18%
Short bend	Polycarbonate	5 (200 W)	20 s	~30%	50%+

The PVC T-slot samples were difficult to work with because they required cooling below their lower working limit temperature in order to have failure occur. Finite element analysis demonstrated the relative magnitudes of the stress concentrations in the vicinity of the razor cut, and the of healing was hard to characterize other than a shift from the main stress concentration at the razor induced crack tip to a secondary stress concentration at the corner of the band saw groove due to crack tip blunting due to the ultrasonic treatment. Blunting of the crack was modeled by removing the singularity at the crack tip and examining the change in the magnitude of the stresses at the concentration points.

The hypothesis of crack tip blunting was not proved with photographic evidence and rather was proven by a shift of failure initiation away from the crack tip. Due to the brittle nature of the cold samples the failure initiation point did show a trend away from the razor tip, but not exclusively so. There was an increase in the displacement to failure

of the healed samples and also in the fracture energy of the samples that received high power ultrasonic treatments.

The Single notch bending samples were the next evolution in the bending specimen that had a more sensitive damage orientation but got away from the transverse wave propagation. Instead Healing was characterized as melting of the crack surfaces back together. Finite element analysis demonstrated that a ligament of melted material that bridged the razor cut near the outside of the beam significantly reduced the stress at the crack tip and increase the displacement at which the ultimate stress was seen at the crack tip.

Initial testing of the single notch bend samples demonstrated a great potential for healing, but there were limitations in the bending apparatus that limited the amount of healing that could be seen. Nearly all of the healed samples outperformed the damaged samples by at least 12 percent. Many healed samples had not failed by the end of the stroke of the bending apparatus, which was the 12 percent increase in the displacement to failure.

A final test that deviated significantly from ASTM 6272-02 was performed to try to characterize the maximum percent improvement that could be achieved with the ultrasonic treatment. The Single notch bend samples were shortened in order to increase the stiffness of the beam so that the healed samples cold be failed witin the stroke of the bending fixture. Because of the deviation from the ASTM guidelines it is difficult to draw comparisons straight across to the longer samples, but finite element modeling

demonstrated that the stress at the crack tip at failure was the same in both the long and short samples.

The short samples demonstrated that an increase in displacement to failure of at least 30 percent could be achieved, and the fracture energy was increased by at least an extra 50 percent. This demonstrates that ultrasonic energy can be an effective waveform to both detect and heal damage. The equipment available hampered a determination of the ultimate effectiveness of the healing, but even so a substantial proof of concept that ultrasonic energy is a viable method for active healing of polymeric materials has been achieved.

7. FUTURE WORK

The first thing that needs to be done in furthering this research would be to go back and use each material for every mechanical test performed so that the effectiveness of the tests could be determined. Maybe the reason that improvement was not seen on some tests was because the test was not the best design, or maybe it is a material problem. This could be determined by using each material for every test. This is a significant amount of work to accomplish this task but it would be beneficial and one could glean a lot of knowledge from the completion of the test set.

Better finite element models of the bending specimens would be created to better model the crack propagation and fracture sequence for the bending specimens. Either cohesive zone elements with softening characteristics built in or XFEM models could better model the failure sequence. Cohesive zone models would be especially helpful in modeling the thin layer of material that closed the razor opening in the Mode-One model. Some higher order elements and possible more investigation into mesh refinement could also better the finite element results.

As was discussed earlier in this paper the premise of this thesis is a proof of concept that ultrasonic waves can be used for healing of a remotely deployed structure. It would be desirable to implement a time reversed acoustic system that could be able to direct energy at a damage location instead of needing to apply the ultrasonic probe directly to the damage site. The time reversed acoustics would mitigate the need to machine complex sample geometries in order to achieve transverse wave propagation as well as be able to target the energy to any location on the specimen.

REFERENCES CITED

[1] Kumar, A., Poddar, B., Kulkarni, G., Mitra, M., and Mujumdar, P. M., 2010, "Time Reversibility of Lamb Wave for Damage Detection in Isotropic Plate," 51st AIAA/ASME/ASCE/AHS/ASC Structures, Structural Dynamics, and Materials Conference 18th, American Institute of Meronautics and Astronautics, 12 - 15 April 2010, Orlando, Florida.

[2] Lee, B. C., and Staszewski, W. J., 2007, "Lamb wave propagation modelling for damage detection: I. Two-dimensional analysis," Smart Materials & Structures, 16(2), pp. 249-259.

[3] Fink, M., 1999, "Time-reversed acoustics," Scientific American, 281(5), p. 91(97).

[4] Dowling, N. E., 2007, Mechanical Behavior of Materials, Pearson Prentice Hall, Upper Saddle River, NJ.

[5] 2000, "Brittle-Like Cracking in Plastic Pipe for Gas Service," N. T. a. S. Board, ed., NTSB, Washington D.C., p. 49.

[6] Jeon, K. W., and Jeon, M. S., 1975, "CYTOPLASMIC FILAMENTS AND CELLULAR WOUND-HEALING IN AMOEBA-PROTEUS," J. Cell Biol., 67(1), pp. 243-249.

[7] Harrington, M., 2009, "How to grow a new limb.(NEWSFRONTS)(Brief article)," Lab Animal, 38(8), p. 250(251).

[8] Morison, M., Moffatt, C., Bridel-Nixon, J., and Bale, S., 1997, A Colour Guide to the Nursing Management of Chronic Wounds, Mosby.

[9] Tanaka, E. M., 2009, "Unravelling the cellular and molecular basis of salamander limb and tail regeneration," Mechanisms of Development, 126, pp. S46-S46.

[10] Kikuchi, K., Holdway, J., Wills, A., and Poss, K., 2009, "Cardiac regeneration in the zebrafish model system," Mechanisms of Development, 126, pp. S46-S46.

[11] Net, M., 2000, "MedTerms Online Medical Dictionary A-Z List."

[12] Vachon, D., 2009, "Composition and Methods for Promoting the HEaling of Tissue of Multicellular Organisms,"Spokane, WA.

[13] Haggstrom, M., 2010, "Wound Healing Phases.png."

[14] P.W.Garrett, A. L. S., 1976, "Selecting Trees for Their Response to Wounding," Metropolitan Tree Improvement Alliance (METRIA), F. S. Santamour, ed.Lanham, Maryland, pp. 69-72.

[15] Blaiszik, B. J., Caruso, M. M., McIlroy, D. A., Moore, J. S., White, S. R., and Sottos, N. R., 2009, "Microcapsules filled with reactive solutions for self-healing materials," Polymer, 50(4), pp. 990-997.

[16] Caruso, M. M., Blaiszik, B. J., White, S. R., Sottos, N. R., and Moore, J. S., 2008, "Full recovery of fracture toughness using a nontoxic solvent-based self-healing system," Advanced Functional Materials, 18(13), pp. 1898-1904.

[17] White, S. R., Sottos, N. R., Geubelle, P. H., Moore, J. S., Kessler, M. R., Sriram, S. R., Brown, E. N., and Viswanathan, S., 2001, "Autonomic healing of polymer composites," Nature, 409(6822), pp. 794-797.

[18] Trask, R. S., Williams, G. J., and Bond, I. P., 2007, "Bioinspired self-healing of advanced composite structures using hollow glass fibres," Journal of the Royal Society Interface, 4(13), pp. 363-371.

[19] Trask, R. S., and Bond, I. P., 2010, "Bioinspired engineering study of Plantae vascules for self-healing composite structures," Journal of the Royal Society Interface, 7(47), pp. 921-931.

[20] White, S. R., and Geubelle, P. H., 2010, "SELF-HEALING MATERIALS Get ready for repair-and-go," Nature Nanotechnology, 5(4), pp. 247-248.

[21] Sarrazin, J. C., 2009, "Ultrasonic repair of polymers fundamentals and modeling for self-healing," pp. xv, 195 leaves.

[22] Larson, B., 2001-2011, "NDT Education Resource Center," http://www.ndt-ed.org/index_flash.htm.

[23] Krautkrämer, J., and Krautkrämer, H., 1993, Ultrasonic testing of materials, Springer-Verlag, Berlin ; New York ; London ; Paris.

[24] 2010, "Fundamentals of Ultrasonic Imaging and Flaw Detection," http://zone.ni.com/devzone/cda/tut/p/id/3368.

[25] Harkins, W., 1999, "Ultrasonic Testing of Aerospace Materials," NASA, ed., p. NASA.

[26] Tanter, M., and Fink, M., 2009, "Time Reversing Waves for Biomedical Applications," Mathematical Modeling in Biomedical Imaging I, Springer-Verlag Berlin, Berlin, pp. 73-97.

[27] Fink, M., 1992, "Time reversal of ultrasonic fields. I. Basic principles," Ultrasonics, Ferroelectrics and Frequency Control, IEEE Transactions on, 39(5), pp. 555-566.

[28] Kreyszig, E., 2006, Advanced Engineering Mathematics, John Wiley and Sons Inc., Hoboken, NJ.

[29] Fink, M., Montaldo, G., and Tanter, M., 2003, "TIME-REVERSAL ACOUSTICS IN BIOMEDICAL ENGINEERING," Annual Review of Biomedical Engineering, 5(1), pp. 465-499.

[30] Zhang, X., Yuan, S., and Hao, T., 2009, "Lamb wave propagation modeling for structure health monitoring," Frontiers of Mechanical Engineering in China, 4(3), pp. 326-331.

[31] Lee, B. C., and Staszewski, W. J., 2007, "Lamb wave propagation modelling for damage detection: II. Damage monitoring strategy," Smart Materials & Structures, 16(2), pp. 260-274.

[32] Sarvazyan, A., Fillinger, L., and Gavrilov, L. R., 2010, "Time-reversal acoustic focusing system as a virtual random phased array," Ultrasonics, Ferroelectrics and Frequency Control, IEEE Transactions on, 57(4), pp. 812-817.

[33] Conza, N., 2005, "Part 7: Ultrasound detection system for musculoskeletal disorders," Experimental Techniques, 29(6), pp. 54-57.

[34] 2006, "Ultrasonic waves approved for broken bones," UPI NewsTrack, p. NA.

[35] Li, J., 2005, "Healing of Stress Fracture in an Animal Model," Indiana University Indianapolis, Defense Technical Information Center, p. 29.

[36] Chen, W. Z., Zhu, H., Zhang, L., Li, K. Q., Su, H. B., Jin, C. B., Zhou, K., Bai, J., Wu, F., and Wang, Z. B., 2010, "Primary Bone Malignancy: Effective Treatment with High-Intensity Focused Ultrasound Ablation," Radiology, 255(3), pp. 967-978.

[37] Liu, H.-L., Hua, M.-Y., Yang, H.-W., Huang, C.-Y., Chu, P.-C., Wu, J.-S., Tseng, I. C., Wang, J.-J., Yen, T.-C., Chen, P.-Y., and Wei, K.-C., "Magnetic resonance monitoring of focused ultrasound/magnetic nanoparticle targeting delivery of therapeutic agents to the brain," Proceedings of the National Academy of Sciences.

[38] Devine, J., 2001, "Ultrasonic Plastics Welding Basics," Welding Journal, pp. 29-33.

[39] Nonhof, C. J., and Luiten, G. A., 1996, "Estimates for process conditions during the ultrasonic welding of thermoplastics," Polymer Engineering and Science, v36(n9), p. p1177(1177).

[40] Benatar, A., Eswaran, R. V., and Nayar, S. K., 1989, "ULTRASONIC WELDING OF THERMOPLASTICS IN THE NEAR-FIELD," Polymer Engineering and Science, 29(23), pp. 1689-1698.

[41] Rani, R. M., Suresh, K. S., Prakasan, K., and Rudramoorthy, R., 2007, "A STATISTICAL STUDY OF PARAMETERS IN ULTRASONIC WELDING OF PLASTICS.(Author abstract)," Experimental Techniques, 31(5), p. 53(56).

[42] Rani, M. R., Prakasan, K., and Rudramoorthy, R., 2009, "STUDY OF DIFFERENT JOINTS FOR ULTRASONIC WELDING OF SEMICRYSTALLINE POLYMERS," Experimental Techniques, 33(4), p. 36(37).

[43] Corporation, L., 2011, "Basic construction of pneumatic ultrasonic welding machine," Lanxess Corporation.

[44] Strong, A. B., 2006, Plastics : materials and processing, Pearson Prentice Hall, Upper Saddle River, N.J.

[45] Ltd., T. T., 2007. www.tttextiles.com

[46] Stokes, V. K., and Hobbs, S. Y., 1989, "STRENGTH AND BONDING MECHANISMS IN VIBRATION-WELDED POLYCARBONATE TO POLYETHERIMIDE JOINTS," Polymer Engineering and Science, 29(23), pp. 1667-1676.

[47] Suresh, K. S., Rani, M. R., Prakasan, K., and Rudramoorthy, R., 2007, "Modeling of temperature distribution in ultrasonic welding of thermoplastics for various joint designs.(Author abstract)," Journal of Materials Processing Tech., 186(1-3), p. 138(139).

[48] Benatar, A., and Cheng, Z., 1989, "ULTRASONIC WELDING OF THERMOPLASTICS IN THE FAR-FIELD," Polymer Engineering and Science, 29(23), pp. 1699-1704.

[49] International, A., 2002, "Standard Test Method for Flexural Properties of Unreinforced and Reinforced Plastics and Electrical Insulating Materials by Four Point Bending," ASTM International.

APPENDICES

APPENDIX A

ANSYS INPUT FILES

4 Point T-Slot

```
!********************
!****PREPROCESSOR****
!********************

/PREP7

! Useful Parameters:  for half symmetry model
        ! Lengths in meters

        beam_w  = 0.20955
        beam_h  = 0.009271
        beam_t  = 0.0254
        razr_t  = 0.0003
        razr_s  = 0.001
        depth = 0.00127
        load_s= 0.04445
        supp_s= 0.1778

        slot_t= 0.0079375
        slot_h= 0.002921
        saw_t= 0.0008128
        saw_w= 0.009525

! Element Definition:
        et,1,plane183,1,,5

! Real Constant Definition:
        r,1, beam_t

! Material Property Definition:
        mp,ex,1, 2.34E9
        mp,prxy,1, 0.28


! Creat Key Points

        k, 1,    0.0,                          0.0
        k, 2,    0.0,                          beam_h
        k, 3,    beam_w/2-slot_t/2,            0.0
        k, 4,    beam_w/2-slot_t/2,            slot_h-saw_t   ! Depth of cut 0.075in
        K, 6,   beam_w/2,                      slot_h
        k, 7,    beam_w/2-slot_t/2-saw_w/2,    slot_h-saw_t   ! Depth of cut 0.075in
```

```
k, 9,    beam_w/2-slot_t/2-saw_w/2,          slot_h
k, 11,   beam_w/2-supp_s/2,                  0.0
k, 12,   beam_w/2-load_s/2,                  beam_h
k, 13,   beam_w/2,                           beam_h
k, 14,   beam_w/2-load_s/2,                  0
k, 15,   beam_w/2-supp_s/2,          beam_h

k, 16,   beam_w/2-slot_t/2-saw_w/2-depth+ razr_s,        slot_h-saw_t
k, 17,   beam_w/2-slot_t/2-saw_w/2-depth+ razr_s,        slot_h-saw_t+razr_t
k, 18,   beam_w/2-slot_t/2-saw_w/2-depth,                slot_h-saw_t+razr_t/2
k, 19,   beam_w/2-slot_t/2-saw_w/2,                      slot_h-saw_t+razr_t
k, 20,   beam_w/2-slot_t/2-saw_w/2,          beam_h
```

! Connect Keypoints with lines

```
L, 1,    11          L, 11,   14          L, 3,    14
L, 3,    4           L, 4,    7           L, 7,    16
L, 16,   18          L, 17,   18          L, 17,   19
L, 9,    19          L, 6,    9           L, 6,    13
L, 13,   20          L, 12,   20          L, 12,   15
L, 2,    15          L, 1,    2           L, 9,    20
L, 12,   14          L, 11, 15            L, 12,17

AL,1,20,16,17
AL,2,19,15,20
AL,11,12,13,18
AL,21,9,10,18,14
AL,3,4,5,6,7,8,21,19
```

! Mesh Definition:

```
kscon,18,0.00005,1,

mshkey,0
! mesh area
amesh,all

arefine,all,,,2
allsel
```

! Define Boundary Conditions:

```
        ! select the top middle keypoint and constrain x-movement
        dk,13,ux,0
        ! select the support span keypoints and constrain y-movement
        dk,11,uy,0
        ! reselect all lines
        allsel
        dl,12,,symm

! Define Loads:
        ! select the load span keypoints
        dk,12,uy,-0.0254*2

        ! reselect all model
        allsel

finish                                  ! exit the pre-preprocessor
save                                    ! save to database

!********************
!******SOLUTION******
!********************

/SOLU                                           ! enter the solution phase

        ksel,,,,18
        cm,crack,kp
        allsel

        CINT,NEW,1
        CINT,CTNC,CRACK
        cint,normal,0,2

        antype,0                        ! 0 = static analysis
        solve                           ! solve the system
finish                                  ! exit the solution phase

!********************
!***POSTPROCESSOR****
!********************

/POST1                                          ! enter the postprocessor
```

4 Point T-slot Blunt

Initial part is identical to above the only difference is the mesh definition

```
! Mesh Definition:

        mshkey,0
        ! mesh area
        amesh,all

        arefine,all,,,2
        krefine,18,,1,3,2
        allsel

! Define Boundary Conditions:

        ! select the top middle keypoint and constrain x-movement
        dk,13,ux,0
        ! select the support span keypoints and constrain y-movement
        dk,11,uy,0
        allsel
        dl,12,,symm

! Define Loads:
        ! select the load span keypoints
        dk,12,uy,-0.0254*2
        allsel
finish                                  ! exit the pre-preprocessor
save                                    ! save to database

!********************
!******SOLUTION******
!********************

/SOLU                                   ! enter the solution phase

        antype,0                        ! 0 = static analysis
        solve                           ! solve the system
finish                                  ! exit the solution phase

!********************
!***POSTPROCESSOR****
!********************

/POST1                                  ! enter the postprocessor
```

4 Pt Bend 1 Crack

```
!********************
!****PREPROCESSOR****
!********************

/PREP7

! Useful Parameters:  for half symmetry model
        ! Lengths in meters

        beam_w  = 0.20955
        beam_h  = 0.009271
        beam_t  = 0.0254
        razr_t  = 0.0003
        razr_s  = 0.001
        depth = 0.00127
        load_s= 0.04445
        supp_s= 0.1778

! Element Definition:
        et,1,plane183,1,,5

! Real Constant Definition:
        r,1, beam_t

! Material Property Definition:
        mp,ex,1, 2.34E9
        mp,prxy,1, 0.28

! Creat Key Points

        k, 1,    0.0,                          0.0
        k, 2,    0.0,                          beam_h
        k, 3,    beam_w,                       0.0
        k, 4,    beam_w,                       beam_h
        k, 5,    beam_w/2-razr_t/2,            0.0
        k, 6,    beam_w/2+razr_t/2,            0.0
        k, 7,    beam_w/2-razr_t/2,            depth-razr_s
        k, 8,    beam_w/2+razr_t/2,            depth-razr_s
        K, 9,   beam_w/2,                      Depth
        k, 10,   beam_w/2-supp_s/2,            0.0
        k, 11,   beam_w/2+supp_s/2,            0.0
        k, 12,   beam_w/2-load_s/2,            beam_h
```

```
k, 13,  beam_w/2+load_s/2,                  beam_h
k, 14,  beam_w/2,                           beam_h

k, 15,  beam_w/2-load_s/2,                  0
k, 16,  beam_w/2+load_s/2,                  0
k, 17,  beam_w/2-supp_s/2,                  beam_h
k, 18,  beam_w/2+supp_s/2,                  beam_h
```

! Connect Keypoints with lines

```
L, 1,   10          L, 10,  15          L, 5,   15
L, 5,   7           L, 7,   9           L, 8,   9
L, 6,   8           L, 6,   16          L, 11,  16
L, 3,   11          L, 3,   4           L, 4,   18
L, 13,  18          L, 13,  14          L, 12,  14
L, 12,  17          L, 2,   17          L, 1,   2
L, 10,  17          L, 12,  15          L, 9,   14
L, 13,  16          L, 11,  18          L, 7,   12
L, 8,   13
```

```
AL, 1,19,17,18
AL, 2,20,16,19
AL, 3,4,24,20
AL, 5,21,15,24
AL, 6,25,14,21
AL, 7,8,22,25
AL, 9,23,13,22
AL, 10,11,12,23
```

```
aglue,all
allsel
```

! Mesh Definition:

```
kscon,9,0.0001,1,

! specify free mesh (this is the default)
mshkey,0
! mesh area
amesh,all

arefine,all,,,2
allsel
```

```
! Define Boundary Conditions:

        ! select the top middle keypoint and constrain x-movement
        dk,14,ux,0
        ! select the support span keypoints and constrain y-movement
        dk,10,uy,0
        dk,11,uy,0
        ! reselect all lines
        allsel

! Define Loads:
        ! select the load span keypoints
        dk,12,uy,-0.0254*1.75
        dk,13,uy,-0.0254*1.75

        ! reselect all model
        allsel

finish                                  ! exit the pre-preprocessor
save                                    ! save to database

!*********************
!******SOLUTION******
!*********************

/SOLU                                           ! enter the solution phase
        ksel,,,,9
        cm,crack,kp
        allsel

        CINT,NEW,1
        CINT,CTNC,CRACK
        cint,normal

        antype,0                        ! 0 = static analysis
        solve                           ! solve the system
finish                                  ! exit the solution phase

!*********************
!***POSTPROCESSOR****
!*********************

/POST1                                          ! enter the postprocessor
```

4 Pt Bend 1 Crack Melt

Everything is the same as above except for two extra line definitions at the end of the line commands, and one extra area command

L, 1, 10
L, 5, 7
L, 6, 8
L, 3, 11
L, 13, 18
L, 12, 17
L, 10, 17
L, 13, 16
L, 8, 13
L, 10, 15
L, 7, 9
L, 6, 16
L, 3, 4
L, 13, 14
L, 2, 17
L, 12, 15
L, 11, 18
L, 5, 15
L, 8, 9
L, 11, 16
L, 4, 18
L, 12, 14
L, 1, 2
L, 9, 14
L, 7, 12

Additional Lines
L, 5, 6
L, 7, 8

AL, 1,19,17,18
AL, 2,20,16,19
AL, 3,4,24,20
AL, 5,21,15,24
AL, 6,25,14,21
AL, 7,8,22,25
AL, 9,23,13,22
AL, 10,11,12,23

Additional Area
AL, 26,7,27,4

The reset of the commands follow the file 4 Pt Bend 1 Crack

To Model the short beam only the length of the beam and the support span parameters need to be modified because the batch files are built parametrically for easy adjustment of loading scenarios.

APPENDIX B

BRANSON POWER LEVEL CALORIMETERY

This experiment was designed to show that the power output of the Branson sonifier is linear. The power dial ranges from 1 to 10 but it does not specify the output power of the probe, so a calorimetric experiment was performed where the probe was used to heat water. The temperature of the water was monitored with a thermocouple that was placed in the calorimeter.

To make the calorimeter 473mL Styrofoam cups were used. The walls of the calorimeter were two cups thick. The top of the calorimeter was also made out of two Styrofoam cups glued together. The top and bottom cups were cut so that they would seal tightly and no heat could escape from the seal. A hole was cut in the top cups so that the probe could be inserted into the chamber.

Calculations were performed to determine the energy added to the system to raise 400 mL of water from the initial temperature to the final temperature recorded over a specific length of time. The Results show that the power transferred to the water is a factor of 4 off but this could be due to the coupling factor between the probe and the water and also not all of the energy from the probe would be dissipated as heat. Some of the energy is likely dissipated as bulk fluid motion where the part that is converted to heat is due to viscous shearing in the water. But the important part of this experiment is demonstrating that the power output of the Branson sonifier is linear with respect to the selected output on the power dial.

rho	0.9982	g/cm^3		Cp	4.1818	J/g-K
Vol	400	mL or cm^3				
power	Ti	Tf	dT	Min	Sec	Time (s)
1	21.5	23.7	2.2	7	17	437
3	16	22	6	5	28	328
5	16.2	27.8	11.6	5	32	332
7	15.7	31.7	16	5	30	330
9	15	35	20	5	36	336
		Q=rho*V*Cp*dT				
		Heat (J)		Power (W)		
	1	3673.36		8.405858		
	3	10018.25		30.54346		
	5	19368.63		58.33923		
	7	26715.35		80.95559		
	9	33394.18		99.38745		

Calculations of thermal energy added to the system

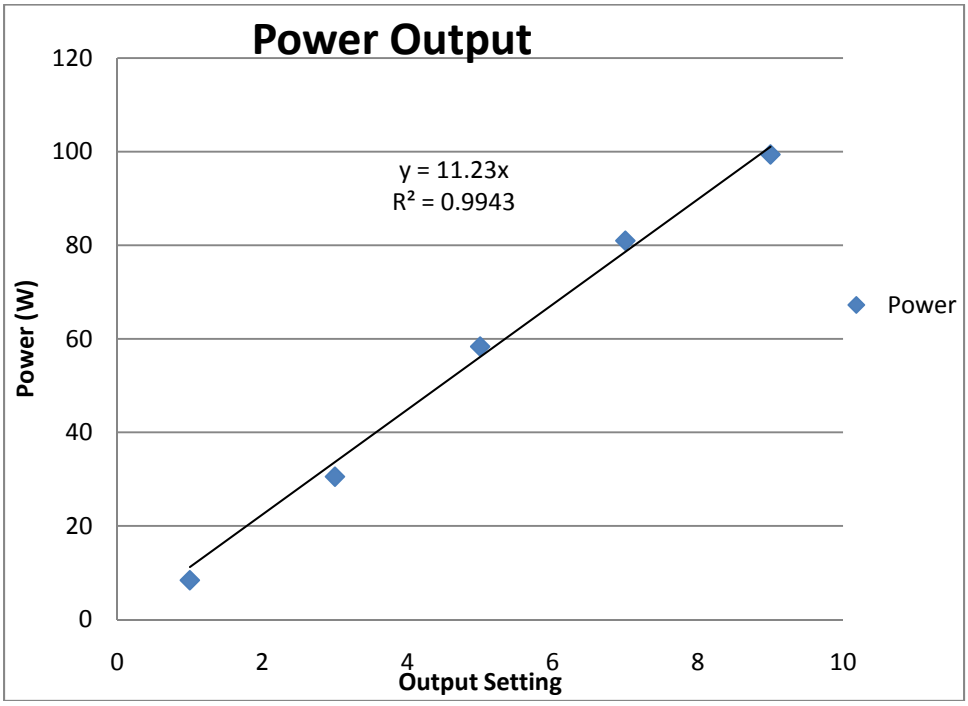

Plot of the thermal Power imparted to the water with respect to the power selection.